First-order correction terms in the weak-field asymptotic theory of tunneling ionization of atoms and molecules in static electric field

Trinh Hoai Vinh

A Dissertation
Presented to the Faculty
of University of Electro-communications
in Candidacy for the Degree
of Doctor of Philosophy

Recommended for Acceptance
by the Department of
Engineering Science
Adviser: Toru Morishita

September 2014

© Copyright by Trinh Hoai Vinh, 2014.

All rights reserved.

Abstract

In this thesis, we study the tunneling ionization of atomic or molecular systems in an external static electric field, which is one of fundamental problems in quantum mechanics. The goal is to analytically incorporate the first-order correction terms into the asymptotic expansions of the tunneling ionization rate and transverse momentum distribution of the ionized electrons. By using the diabatic expansion in parabolic coordinates, we have generalized the early results for hydrogen atom by Damburg *et al.* (1978), and for the first time obtained the corrections for arbitrary atom or molecule treated in single-active-electron and frozen-nuclei approximations. We also extend the theory to many-electron systems where the electron correlation is fully taken into account. The theory is confirmed by exact numerical calculations for atoms and molecules. It is shown that the first-order corrections extend the region of applicability of the weak-field asymptotic theory at the quantitative level toward stronger fields, practically up to the boundary between tunneling and over-the-barrier regimes of ionization.

Acknowledgements

First and foremost I would like to express my special thank to my advisor Professor Toru Morishita. He has constantly provided the vision, support and guidance indispensable for me to proceed through the doctoral program and complete my dissertation. My study has been fostered by motivating instructions. My debt of gratitude must also go to Professor Oleg I. Tolstikhin for staying in close touch with my study. His daily supervision has kept my inexperienced wanderings from going too far. I appreciate his encouragement when things go wrong and excitement when they get done. I would like to thank Professor Shinichi Watanabe for his generosity in providing us with all this stimulating environment. The laboratory is always in full of enthusiasm and inspiration. I wish also to thank the members of my dissertation committee for generously offering time, invaluable comments and feedbacks throughout the preparation and review of this thesis. Last but not least, members of research group and the secretary are deeply acknowledged for kindly assisting me in many different ways.

To my parents.

Contents

List of Tables

List of Figures

List of Abbreviations

The following are significant abbreviations and acronyms, which are frequently used throughout the thesis. More specific context for some of them will be defined explicitly in later chapters when needed.

ADK	**A**mmosov-**D**elone-**K**rainov
MO-ADK	**M**olecular **A**mmosov-**D**elone-**K**rainov
WFAT	**W**eak-**F**ield **A**symptotic **T**heory
WFAT(*n*)	***n***th-order **W**eak-**F**ield **A**symptotic **T**heory
SAEA	**S**ingle-**A**ctive-**E**lectron **A**pproximation
TMD	**T**ransverse **M**omentum **D**istribution
ME-WFAT	**M**any-**E**lectron **W**eak-**F**ield **A**symptotic **T**heory
ME-WFAT(*n*)	***n***th-order **M**any-**E**lectron **W**eak-**F**ield **A**symptotic **T**heory
a.u.	**A**tomic **U**nits
SS	**S**iegert **S**tate
PT	**P**erturbation **T**heory
exact	**exact** numerical calculation

Chapter 1

Introduction

The ionization of atoms and molecules by laser pulses is recognized as a fundamental step in strong-field physics, since it initiates a variety of subsequent phenomena such as the generation of high-order harmonics [1, 2] and high-energy photoelectrons [2, 3]. The two examples are illustrated in Fig. 1.1. After being released from the target, the ionized electron is governed by the oscillating electric field of the laser, and accelerate to high velocities. When the laser field changes sign, it may be driven back to revisit its parent ion. If the driven electron returns to its ground state, high-energy

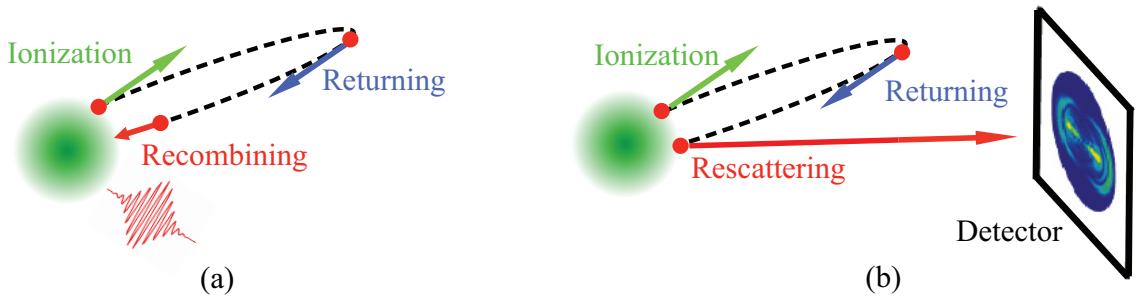

Figure 1.1: Diagram shows a three-step process [1] involved in high-order harmonic generation (a), and emission of photoelectrons (b).

photons will be then emitted with temporal and spatial coherence properties similar to those of driving laser field. This is high-order harmonic generation whose spectrum encodes dynamics of the target. The returning electron may instead undergo an elastic

collision and scatters from the target, resulting in laser-induced photoelectron. The energy measurements of these photoelectrons could provide us with information on the electronic structure of molecules.

The ionization step may fall into three categories as depicted in Fig. 1.2, depending on laser parameter. If the laser has a high frequency but low intensity, the transition from a bound to a continuum state is best modeled by the absorption of discrete photons. This is the multiphoton ionization [4, 5]. In 1965, Keldysh realized an alternative mechanism when the incident field with low frequency is strong enough [6]. In this case, the field modifies the binding potential and allows the electron to tunnel through the barrier into the continuum. This corresponds to the adiabatic regime [7, 8]. Clearly, as the intensity is further increased the gradient becomes more negative. At some moment, the barrier is completely removed, and the state is no longer bound. The ionization now occurs via the over-the-barrier scenario. The boundary between the last two situations naturally separates the weak- and strong-field cases.

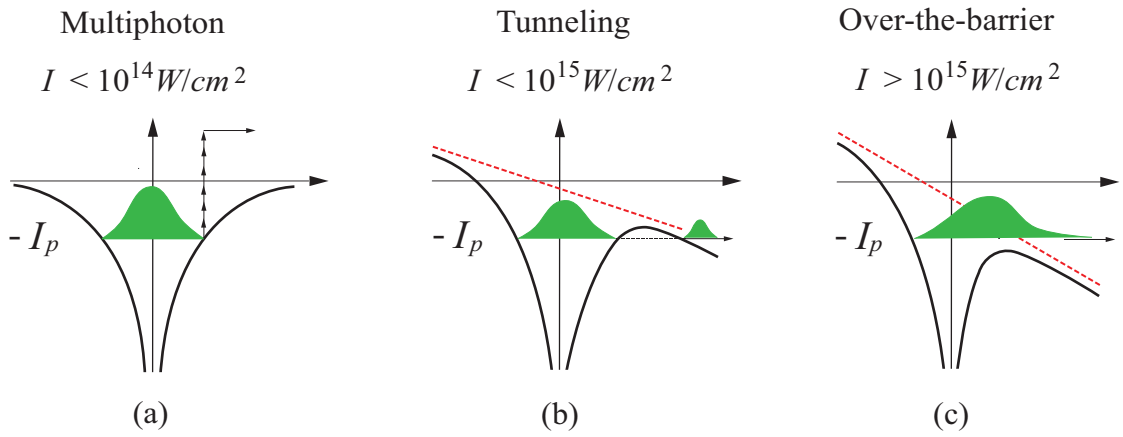

Figure 1.2: Three possible mechanisms for ionization of a typical atomic system. The thick dashed lines: external field. The solid lines: atomic potential modified by the external field. The green areas depict the wave packets, and I_p is the ionization potential.

In the adiabatic regime, when the frequency is sufficiently low at a given intensity, the ionization of an atom or molecule in an *oscillating* laser field $\mathbf{F}(t)$ should proceed

as if in a static field $\mathbf{F}$ equal to the momentary value of $\mathbf{F}(t)$. The underlying idea is that substantial ionization occurs in a fraction of an optical cycle, so that the electric field can be regarded as quasi-static. This highly nonlinear behavior of the tunneling ionization rate was experimentally observed [35], and is sketched in Fig. 1.3. Thus,

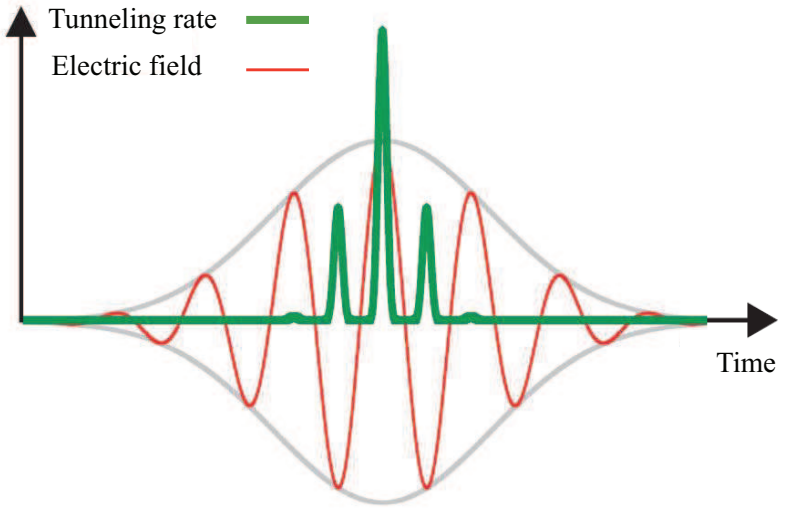

Figure 1.3: The tunneling ionization is confined to very short time intervals near the field oscillation maxima due to the highly nonlinear dependence of the tunneling rate on the width of the potential barrier. In the case of few-cycle near-infrared laser pulse (red line), ionization (green line) is restricted to several intervals of subfemtosecond [35].

the problem of calculating the ionization rate in a laser field reduces to that in a static electric field, and tunneling ionization of atoms and molecules by static electric field is the main focus of this thesis. Tunneling ionization under the time-independent framework has been a topic of considerable interest since the early days of quantum mechanics. It is well known that the standard perturbation theory cannot yield the ionization rate because of its highly nonlinear dependence not only on the width of the potential barrier but also on the field strength. Meanwhile the asymptotic methods can be employed. The asymptotic approach to this problem was pioneered by Oppenheimer [12] and Lanczos [13]. Decades after that the correct weak-field expansion of the ionization rate for the basic system of hydrogen in the ground state was derived [10]. Later, similar results were obtained for a short-range potential

[14], an arbitrary state in a central atomic potential [15, 16], and an arbitrary state of the hydrogen atom [17, 18]. The classical results of Perelomov and co-workers in Ref. [16] were popularized by Ammosov, Delone and Krainov [19], and became known as the ADK theory. These results pertaining to atoms establish the foundation of the asymptotic theory of tunneling ionization. General understanding of atomic ionization has been extrapolated to molecules first for a homonuclear model [20], and very recently for the heteronuclear case [21]. An attempt to extend the atomic results [15, 16] to the general molecular case beyond model treatment was carried out in Ref. [22], and now normally referred to as the MO-ADK theory.

Although commonly utilized by experimentalists to interpret observations, the formulas for the ionization rate presented in the aforesaid MO-ADK theory were constructed by analogy with the atomic case rather than derived from the Schrödinger equation. From the viewpoint of the asymptotic theory, these results contain some inconsistencies. Furthermore, they are lacking a very important physical factor: the molecule possibly possesses a permanent electric dipole moment, which has recently attracted much attention in both experiment and theory [24, 25, 26, 27, 28]. This situation was clarified as the development of the weak-field asymptotic theory (WFAT), which describes the tunneling ionization in a static electric field, was initiated [23]. The theory generalizes the well-known results for hydrogen [10, 11, 18] and an arbitrary atom [15], and also covers the case of an arbitrary molecule. In its formulation, the following approximations are applied. The first is the single-active-electron approximation (SAEA), where the response of the system to the external field is due entirely to one outer electron. An extension of the WFAT to many-electron systems was reported in Ref. [29]. The second regards the nuclei as frozen: How to incorporate into the WFAT the effect of nuclear motion in molecules was discussed elsewhere [30]. Finally, the third approximation, which gives the name to the theory, consists of the assumption that the ionizing field F is much less than a critical field

F_c giving a boundary between tunneling and over-the-barrier regimes of ionization. In other words, the WFAT applies in the deep tunneling regime, and the ionization rate can be obtained as an asymptotic expansion in F. For the ground state of neutral atoms and molecules having ionization potential of ~ 0.5 a.u., $F_c \sim 0.1$ a.u., which corresponds to an intensity $I \sim 3.5 \times 10^{14}$ W/cm^2. Thus, in spite of a seeming contradiction in terminology, the WFAT has a wide range of applications in modern strong-field physics.

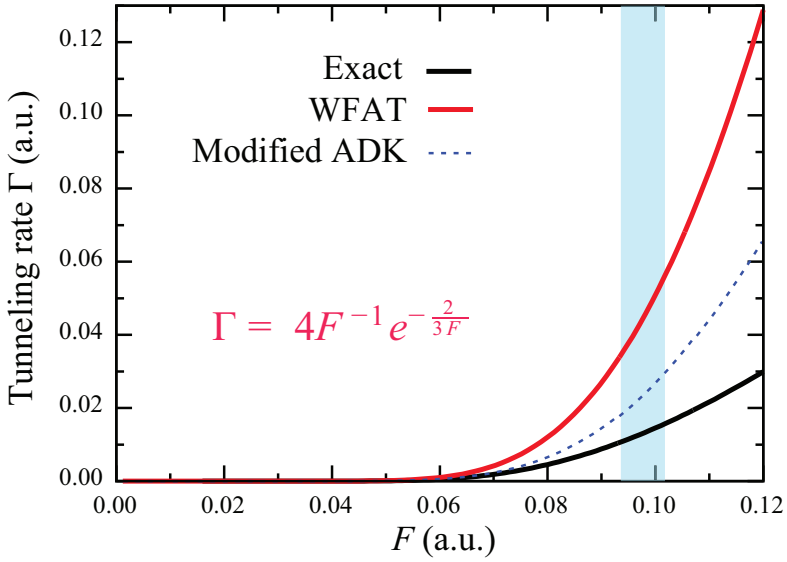

Figure 1.4: The ionization rate of hydrogen atom in ground state as a function of the external electric field F. The theoretical predictions (red and blue lines) are compared with the exact calculation (black line) using procedure described in Appendix C.

Implementing the theory for a variety of systems has shown that the WFAT results of leading-order consistently approach the direct solution to the Schrödinger equation when F goes to zero [23, 29]. This also means at some moderate field F the theoretical predictions suffer from certain error. For simplicity, let consider a much basic system of hydrogen atom in the ground state. The red line in Fig. 1.4 shows the ionization rate Γ for this atom predicted by the WFAT of leading order. At the field strength of current experimental interest, ~ 0.1 a.u., the WFAT result is about three times bigger than the exact value shown by the black line. In this case, the tunneling rate given

by the WFAT coincides with that by the ADK theory, since hydrogen atom has no electric dipole in the ground state. One way to improve the theoretical prediction is to intuitively incorporate the polarizability into the ionization potential, as suggested elsewhere [31, 32]. Such a correction produces a little better result, presented by the dashed line, but still remains a quantitative difference from exact values near $F = 0.1$ a.u., which is typical for many practical situations. For molecular ionization, direct inclusion of polarizability into MO-ADK does not allow one to appropriately predict the angular dependence of ionization rate [37, 38]. On the standing point of the asymptotic theory, a natural step for the WFAT predictions to be enhanced in accuracy is finding the next-order terms in the asymptotic expansion of Γ. Such an improvement is necessary for application, since the detailed analysis of experimentally observable spectra of photoelectrons and ions [33, 34, 35, 36, 37] and harmonics [39, 40, 41] obviously requires an accurate quantitative description of the tunneling process. This problem can be solved numerically. However, numerical calculations of ionization rate are time-consuming and not always feasible, especially for many-electron systems when we have to deal simultaneously with both electron-electron interactions and electron-field couplings. Meanwhile, an analytical formula with good performance could provide convenient solution and allows physical interpretations of the processes under study. Going beyond the leading-order approximation for the tunneling rate is also an interesting exploring in its own right due to the fact that we can account for strong field effect by the new terms, where more properties from the ionizing system would appear. In this way, the WFAT of first order is expected to facilitate many applications in strong-field physics, and to efface the existing discrepancies between the theoretical predictions and experiments, for example, of CO_2 [42, 43], CO [44, 45], and OCS [37].

The content of this thesis is to systematically develop the WFAT to the next order in field under the framework of both one-electron [23] and many-electron [29] treat-

ment. So far, such an extension of the theory was available only for the hydrogen atom. In Ref. [46], the first-order correction to the leading-order term [11, 18] in the asymptotic expansion of the ionization rate for hydrogen in an arbitrary state was derived. In Ref. [47], a procedure to obtain higher-order terms of this series was developed and a number of such terms for a few lowest states were given. In the case of the Coulomb potential, one can separate variables in the Schrödinger equation in parabolic coordinates, which crucially simplifies the analysis. This important advantage of parabolic coordinates is inherited in the general approach of Ref. [23], which applies to arbitrary one-electron potentials. This approach enables us to overcome technical difficulties and generalize the results of Ref. [46] to arbitrary atoms and molecules. We obtain the first-order correction terms in the asymptotic expansions not only for the ionization rate, but also for the transverse momentum distribution (TMD) of the ionized electrons, which defines the photoelectron momentum distribution within the adiabatic theory [8]. For many-electron system, only the tunneling rate was expanded to the first order, the consideration of the TMD is postponed. These results essentially extend the region of applicability of the WFAT at the quantitative level toward stronger fields.

The thesis is organized as follows. In Chapter 2, we summarize main equations of the theory, which describe the Siegert states (SSs) in an electric field [23] for one-electron system, and introduce the basic quantities and concepts. The goal of this chapter is to establish the SS eigenvalue problem, then obtain the decoupled equation, which defines the flux amplitude of the outgoing wave. Following the approach developed in Ref. [23], in Chapter 3 we construct the asymptotic solution of the SS eigenvalue problem for $F \to 0$, extending the results to the next order in F. The main results pertaining to the tunneling rate and TMD are obtained here. The most technically involved part of the derivation is referred to Appendix B. The region of validity for the working formulas is also discussed. The first application of the results

for hydrogen and noble-gas atoms are presented in Chapter 4. The WFAT results are compared with accurate numerical calculations by an original multiple-precision procedure outlined in Appendix C, for H, and by the method developed in Ref. [48], for Ne, Ar, Kr, and Xe. Chapter 5 is for the discussion of molecular systems. The tunneling rate and the TMD for the non-polar linear molecular ion H_2^+, which has different orientations in the external field, are compared with numerical results by the method recently reported in Refs. [49, 50]. The ground $1s\sigma$ state and the excited $2p\pi^{\pm}$ states of this molecular ion are considered. A similar analysis is also performed for polar system of HeH^{2+} in the $2p\sigma$ state aligned along the field. The next part, Chapter 6, is devoted to represent the development beyond the SAEA, where the full correlation between electrons is taken into account. The procedure to treat many-electron system follows the basic steps of that for one-electron system, which are detailed in Chapters 2 and 3. Therefore only principally different points are highlighted. The results for this many-electron problem are then illustrated for He and H^-. Lastly, the summary and outlook are given in Chapter 7.

To facilitate the presentation, and to avoid any confusion with the terminology, it is necessary to adopt some conventions. The term WFAT stands for the asymptotic approach applied within the SAEA [23, 51, 52, 53, 54]. While the asymptotic theory for many-electron systems, in which the frozen nuclei remains the only approximation [29], will be named ME-WFAT. An extension (n) could be attached after notations WFAT or ME-WFAT to particularly point out that the considered asymptotic expansion is truncated up to the order n in field F. In comparison with the asymptotic results, direct solution to the Schrödinger equation obtained by numerical methods [53, 48, 49, 50] is referred to as 'exact'. When data by different numerical procedures are referred to in one comparison, the corresponding author will be decently mentioned. Finally, the atomic units (a.u.), $m_e = e = \hbar = a_0 = 1$, are used throughout this thesis unless otherwise indicated.

Chapter 2

Siegert states in an electric field

In the presence of an external electric field, the bound states of atoms and molecules turn into SSs [48, 49] which are regular eigensolutions to the stationary Schrödinger equation satisfying outgoing-wave boundary conditions [56]. The corresponding SS eigenvalue $E = \mathcal{E} - i\Gamma/2$ exists in complex plane defining the energy $\mathcal{E}$ and ionization rate Γ of the state. Furthermore, the asymptotic behavior of the SS eigenfunction specifies the TMD of the ionized electrons. These are the characteristics of the SS necessary for implementing the adiabatic theory [7, 8]. To calculate SSs, the method of *adiabatic* expansion in parabolic coordinates has been proposed and successfully applied for axially symmetric potentials [48] and recently for a general potential without any symmetry [49, 50]. Nevertheless, as will be presented below, a *diabatic* expansion instead is more suitable for the current purpose.

We consider a molecule (for definiteness, we mention molecules, but our analysis applies also to atoms) treated in the single-active-electron and frozen-nuclei approximations. The stationary Schrödinger equation describing the interaction of the active electron with an external static uniform electric field $\mathbf{F} = F\mathbf{e}_z$, $F \geqslant 0$, reads

$$\left[-\frac{1}{2}\,\Delta + V(\mathbf{r}) + Fz - E\right]\psi(\mathbf{r}) = 0, \tag{2.1}$$

where $V(\mathbf{r})$ is the molecular potential and $\mathbf{r}$ is measured from the center of mass of the nuclei [23]. The potential $V(\mathbf{r})$ implicitly depends on the nuclear configuration and orientation of the molecule with respect to the field. It can be arbitrary, the only assumption is that far away from the nuclei the active electron feels a potential of the form

$$V(\mathbf{r})|_{r\to\infty} = -\frac{Z}{r} - \frac{\mathbf{Dn}}{r^2} + O(r^{-3}). \tag{2.2}$$

This is nothing but a multiple expansion for the charge distribution of molecular ion whose total charge and dipole moment are Z and $\mathbf{D}$, respectively, and $\mathbf{n} = \mathbf{r}/r$. Since the electric field is directed along the z axis as defined, the ionized electron will accelerated to $z \to -\infty$. For this asymptotic region, the problem can be conveniently treated in parabolic coordinates [10],

$$\xi = r + z, \quad 0 \leqslant \xi < \infty, \tag{2.3a}$$

$$\eta = r - z, \quad 0 \leqslant \eta < \infty, \tag{2.3b}$$

$$\varphi = \arctan\frac{y}{x}, \quad 0 \leqslant \varphi < 2\pi. \tag{2.3c}$$

It is well-known [9, 10] that the stationary Schrödinger equation for hydrogen is completely separable in the coordinates (2.3). This is a consequence of $O(4)$ symmetry of Coulomb potential. One would expect that the same applies for considered potential $V(\mathbf{r})$ in the asymptotic regime where the first term on the right side of Eq. (2.2) dominates. To explore this advantage, let start with rewriting Eq. (2.1) in coordinates system (2.3)

$$\left[\frac{\partial}{\partial\eta}\eta\frac{\partial}{\partial\eta} + \mathcal{B}(\eta) + \frac{E\eta}{2} + \frac{F\eta^2}{4}\right]\psi(\mathbf{r}) = 0, \tag{2.4}$$

where the adiabatic Hamiltonian

$$\mathcal{B}(\eta) = \frac{\partial}{\partial\xi}\xi\frac{\partial}{\partial\xi} + \frac{\xi+\eta}{4\xi\eta}\frac{\partial^2}{\partial\varphi^2} - rV(\mathbf{r}) + \frac{E\xi}{2} - \frac{F\xi^2}{4} \tag{2.5}$$

is an operator acting on functions of ξ and φ and depending on η as a parameter. It is easily seen that the limit $z \to -\infty$ corresponds to $\eta \to \infty$, so from Eq. (2.2) the adiabatic Hamiltonian becomes

$$\mathcal{B} \equiv \mathcal{B}(\eta)|_{\eta\to\infty} = \frac{\partial}{\partial\xi}\xi\frac{\partial}{\partial\xi} + \frac{1}{4\xi}\frac{\partial^2}{\partial\varphi^2} + Z + \frac{E\xi}{2} - \frac{F\xi^2}{4}. \tag{2.6}$$

We now construct the *diabatic* basis from the eigenfunctions of $\mathcal{B}$ defined by

$$(\mathcal{B} - \beta_\nu)\Phi_\nu(\xi,\varphi) = 0, \tag{2.7}$$

supplemented by the regularity boundary condition at $\xi = 0$, zero boundary condition at $\xi \to \infty$, and periodic boundary condition in φ. Equation (2.7) allows separation of variables and has solutions of the form

$$\Phi_\nu(\xi,\varphi) = \phi_\nu(\xi)\,\frac{e^{im\varphi}}{\sqrt{2\pi}}, \tag{2.8a}$$

$$\nu = (n_\xi, m), \quad n_\xi = 0, 1, \ldots, \quad m = 0, \pm1, \ldots, \tag{2.8b}$$

where functions $\phi_\nu(\xi)$ and the corresponding eigenvalues β_ν are defined by

$$\left[\frac{d}{d\xi}\xi\frac{d}{d\xi} - \frac{m^2}{4\xi} + Z + \frac{E\xi}{2} - \frac{F\xi^2}{4} - \beta_\nu\right]\phi_\nu(\xi) = 0, \tag{2.9a}$$

$$\phi_\nu(\xi)|_{\xi\to0} \propto \xi^{|m|/2}, \quad \phi_\nu(\xi)|_{\xi\to\infty} = 0, \tag{2.9b}$$

$$\int_0^\infty \phi_{n_\xi m}(\xi)\phi_{n'_\xi m}(\xi)\,d\xi = \delta_{n_\xi n'_\xi}. \tag{2.9c}$$

Here ν is a discrete multiindex enumerating the solutions, m is the azimuthal quantum number, and n_ξ enumerates the different solutions to Eq. (2.9a) for a given m. The eigenfunctions (2.8a) are called *parabolic channel functions*. They are orthonormal

with respect to the inner product

$$\langle \Phi_\nu | \Phi_{\nu'} \rangle \equiv \int_0^\infty \int_0^{2\pi} \phi_{n_\xi m}(\xi) \phi_{n'_\xi m'}(\xi) \frac{e^{i(m'-m)\varphi}}{2\pi} d\xi d\varphi = \delta_{\nu\nu'}, \tag{2.10}$$

where $\nu' = (n'_\xi, m')$. The solution to Eq. (2.4) is sought in the form of diabatic expansion

$$\psi(\mathbf{r}) = \eta^{-1/2} \sum_\nu f_\nu(\eta) \Phi_\nu(\xi, \varphi), \tag{2.11}$$

where the prefactor $\eta^{-1/2}$ will eliminate the first-order derivative in the resulting equations. Substituting this expansion into Eq. (2.4), we obtain a set of ordinary differential equations defining the unknown functions $f_\nu(\eta)$,

$$\left[\frac{d^2}{d\eta^2} + \frac{F\eta}{4} + \frac{E}{2} + \frac{\beta_\nu}{\eta} + \frac{1-m^2}{4\eta^2} \right] f_\nu(\eta) - \frac{1}{\eta} \sum_{\nu'} W_{\nu\nu'}(\eta) f_{\nu'}(\eta) = 0, \tag{2.12}$$

where

$$W_{\nu\nu'}(\eta) = \langle \Phi_\nu \left| [rV(\mathbf{r}) + Z] \right| \Phi_{\nu'} \rangle \tag{2.13}$$

represents the couplings between different channels. The main advantage of parabolic coordinates in treating the SSs stems from the fact that these couplings become diminished in the asymptotic region $\eta \to \infty$. Indeed, from Eq. (2.2) we have

$$[rV(\mathbf{r}) + Z]|_{\eta\to\infty} = \frac{2D_z}{\eta} - 2\left(e^{-i\varphi} D_+ + e^{i\varphi} D_-\right) \frac{\xi^{1/2}}{\eta^{3/2}} + O(\eta^{-2}), \tag{2.14}$$

where $D_\pm = D_x \pm i D_y$. Thus the off diagonal elements of the coupling matrix (2.13) vanishes at $\eta \to \infty$ up to $O(\eta^{-3/2})$ and Eqs. (2.12) become decoupled as

$$\left[\frac{d^2}{d\eta^2} + \frac{F\eta}{4} + \frac{E}{2} + \frac{\beta_\nu}{\eta} + \frac{\gamma_m}{\eta^2} + O(\eta^{-5/2}) \right] f_\nu(\eta) = 0, \tag{2.15}$$

where

$$\gamma_m = \frac{1-m^2}{4} - 2D_z. \tag{2.16}$$

To obtain the leading-order term in the asymptotic solutions of the problem for $F \to 0$, Eq. (2.15) is truncated up to order $O(\eta^{-1})$ as done in Ref. [23]. The goal now is to derive the first-order correction in F, so terms up to order $O(\eta^{-2})$ are also needed. The dominant contribution to the off-diagonal elements of $W_{\nu\nu'}(\eta)$ at $\eta \to \infty$, which couple the different parabolic channels, comes from the second and higher terms in the expansion in Eq. (2.14). Fortunately, these coupling terms vanish faster than those of $O(\eta^{-2})$ needed for the present derivation, and is immaterial for the following discussion. This greatly simplifies the analysis. It is convenient to introduce a boundary of the *coupling* or *core* region η_c such that for $\eta > \eta_c$ the last term in Eq. (2.15) can be neglected within a desired accuracy, and hence these equations for the different ν become decoupled. In the following, we consider only the region $\eta > \eta_c$. The outgoing-wave solution to Eq. (2.15) satisfies the condition

$$f_\nu(\eta)|_{\eta\to\infty} = \frac{2^{1/2} f_\nu}{(F\eta)^{1/4}} \exp\left[\frac{iF^{1/2}\eta^{3/2}}{3} + \frac{iE\eta^{1/2}}{F^{1/2}}\right], \tag{2.17}$$

which describes the outgoing flux into channel ν under consideration. This asymptotic, apart from a constant f_ν, is the same for different channel. The solutions to Eqs. (2.12) satisfying the regularity boundary condition at $\eta = 0$ and the outgoing-wave boundary condition (2.17) at $\eta \to \infty$ exist only for a discrete set of generally complex values of E — this is the SS eigenvalue problem. The real and imaginary parts of the eigenvalue E define the energy $\mathcal{E}$ and ionization rate Γ of the state,

$$E = \mathcal{E} - \frac{i}{2}\Gamma. \tag{2.18}$$

The eigenfunction is normalized by

$$\int \psi^2(\mathbf{r})\, d\mathbf{r} = \frac{1}{4}\int_0^\infty \int_0^\infty \int_0^{2\pi} \psi^2(\mathbf{r})(\xi+\eta)\, d\xi d\eta d\varphi = 1. \tag{2.19}$$

Since eigenvalue E is complex and $\operatorname{Im} E < 0$, the wave function $\psi(\mathbf{r})$ grows exponentially with η in the asymptotic region. As a result, the integrations in Eq. (2.19) do not converge in the usual sense and require a regularization. This can be accomplished by deforming the integration path in η from the real semiaxis into a contour in an appropriate sector of the complex η plane. A more general procedure of normalizing the eigenfunctions of quasi-stationary states was developed in Ref. [58].

The outgoing-wave boundary condition for Eq. (2.1) can also be presented in the form of a Fourier transformation from the momentum space

$$\psi(\mathbf{r})|_{z\to-\infty} = \int A(\mathbf{k}_\perp) e^{i\mathbf{k}_\perp \mathbf{r}_\perp} g(z, k_\perp)\, \frac{d\mathbf{k}_\perp}{(2\pi)^2}, \tag{2.20}$$

where $\mathbf{r}_\perp = (x, y) = (r_\perp \cos\varphi, r_\perp \sin\varphi)$, $\mathbf{k}_\perp = (k_x, k_y) = (k_\perp \cos\varphi_k, k_\perp \sin\varphi_k)$, and

$$g(z, k_\perp) = e^{-i\pi/12} 2\pi^{1/2} (2F)^{-1/6}\, \mathrm{Ai}(\zeta), \tag{2.21a}$$

$$\zeta = \frac{2e^{-i\pi/3}}{(2F)^{2/3}} \left[E - Fz - \frac{k_\perp^2}{2} \right]. \tag{2.21b}$$

Here $\mathrm{Ai}(x)$ is the Airy function [57]. The function $g(z, k_\perp)$ contains only an outgoing wave as $z \to -\infty$. The TMD amplitude $A(\mathbf{k}_\perp)$ can be expressed in terms of the coefficients in Eq. (2.17) and parabolic channel functions (2.8),

$$A(\mathbf{k}_\perp) = \frac{2^{3/2}\pi i}{F^{1/2}} \sum_\nu f_\nu \Phi_\nu \left(\frac{k_\perp^2}{F}, \varphi_k \right). \tag{2.22}$$

The TMD of ionized electrons in the outgoing flux is given by

$$P(\mathbf{k}_\perp) = |A(\mathbf{k}_\perp)|^2. \tag{2.23}$$

Thus the main quantities characterizing a SS and related to observables are the complex eigenvalue E defining its energy and ionization rate, Eq. (2.18), and the asymptotic coefficients f_ν in Eq. (2.17) defining the TMD amplitude (2.22). The procedure to obtain these quantities in the weak-field limit is detailed in the following chapter.

Chapter 3

Weak-field asymptotics

In the weak-field limit, the SS eigenvalue problem established in the previous chapter can be treated analytically. The leading-order asymptotic solution to this problem for

$$F \to 0 \tag{3.1}$$

was obtained [23]. In this chapter, we derive the first-order correction to this solution by following the approach of Ref. [23], and successively extending each of its steps to the next order in F. The goal of this chapter is to construct the asymptotic coefficient f_ν in Eq. (2.17) up to the first order in field, then calculate the ionization rate Γ from the outgoing flux. Meanwhile, the real part of energy $\mathcal{E}$ is found by the standard perturbation theory [10].

3.1 Perturbation theory

Within the standard perturbation theory [10], the solution to Eq. (2.1) for nonzero but small field, which originates from bound state, is given by

$$\mathcal{E} = E_0 - \mu_z F - \frac{1}{2}\,\alpha_{zz} F^2 + O(F^3), \tag{3.2a}$$

$$\psi(\mathbf{r}) = \psi_0(\mathbf{r}) + \psi_1(\mathbf{r})F + O(F^2). \tag{3.2b}$$

Here μ_z and α_{zz} are the components of the electronic dipole moment vector, μ_i, and static dipole polarizability tensor, α_{ij}, $i,j = x,y,z$, in the unperturbed state $\psi_0(\mathbf{r})$, respectively. Importantly, the wave function (3.2b) satisfies the normalization condition (2.19) with an error of order $O(F^2)$. It is noticed, on one hand, that the series (3.2), up to any finite order in F, are real. Thus Eq. (3.2a) defines only the real part of the complex SS eigenvalue (2.18), and cannot account for the ionization rate Γ. On the other hand, Eq. (3.2b) holds only in the region well inside the outer turning point $\eta_t = 2|E_0|/F$, where the field term in Eq. (2.15) can be treated perturbatively. The right-hand side of Eq. (3.2b) exponentially decays in the asymptotic region, where the outgoing wave (2.17) is formed, so this expansion does not allow one to find the coefficients f_ν, which are also exponentially small in F. To calculate f_ν and then Γ one has to connect Eq. (3.2b) with Eq. (2.17) by solving Eq. (2.15). This can be done by asymptotic methods [59, 60] in the limit (3.1). In the following, we assume that all quantities appearing in Eqs. (3.2) are known. They can, for example, be obtained by calculations in a finite volume, where various efficient numerical techniques can be used. The observables related to tunneling ionization will be expressed in terms of these quantities.

The parabolic channels are defined by Eqs. (2.8) and (2.9). One should substitute $\mathcal{E}$ given by Eq. (3.2a) for E into Eq. (2.9a) since Γ is exponentially small when $F \to 0$, then Eq. (2.9a) coincides with Eq. (A.5a). Following Appendix A, we expand the solutions by means of perturbation theory,

$$\beta_\nu = \beta_\nu^{(0)} + \beta_\nu^{(1)}F + O(F^2), \tag{3.3a}$$

$$\phi_\nu(\xi) = \phi_\nu^{(0)}(\xi) + \phi_\nu^{(1)}(\xi)F + O(F^2). \tag{3.3b}$$

In the leading-order approximation, $F = 0$, the solutions are

$$\beta_\nu^{(0)} = Z - \varkappa\left(n_\xi + \frac{|m|+1}{2}\right), \tag{3.4a}$$

$$\phi_\nu^{(0)}(\xi) = \varkappa^{1/2}(\varkappa\xi)^{|m|/2}e^{-\varkappa\xi/2}\sqrt{\frac{n_\xi!}{(n_\xi+|m|)!}}\,L_{n_\xi}^{(|m|)}(\varkappa\xi). \tag{3.4b}$$

When $F \neq 0$, the first-order corrections to the above solutions have the form

$$\beta_\nu^{(1)} = -\frac{\mu_z}{2\varkappa}(2n_\xi+|m|+1) - \frac{1}{4\varkappa^2}\left[6n_\xi(n_\xi+|m|+1)+m^2+3|m|+2\right], \tag{3.5a}$$

$$\begin{aligned}\phi_\nu^{(1)}(\xi) = \frac{1}{8\varkappa^3}\Big\{&c_{n_\xi-2}c_{n_\xi-1}\phi^{(0)}_{n_\xi-2,m}(\xi) - 4c_{n_\xi-1}\left[\varkappa\mu_z+(2n_\xi+|m|)\right]\phi^{(0)}_{n_\xi-1,m}(\xi)\\ &+4c_{n_\xi}\left[\varkappa\mu_z+(2n_\xi+|m|+2)\right]\phi^{(0)}_{n_\xi+1,m}(\xi) - c_{n_\xi}c_{n_\xi+1}\phi^{(0)}_{n_\xi+2,m}(\xi)\Big\},\end{aligned} \tag{3.5b}$$

where

$$c_{n_\xi} = \sqrt{(n_\xi+1)(n_\xi+|m|+1)}. \tag{3.6}$$

It is implied that functions $\phi^{(0)}_{n_\xi m}(\xi)$ with negative n_ξ in Eq. (3.5b) are equal to zero. Substituting Eq. (3.3b) into Eq. (2.8a), we obtain the corresponding expansion for the parabolic channel functions

$$\begin{aligned}\Phi_\nu(\xi,\varphi) &= \phi_\nu^{(0)}(\xi)\frac{e^{im\varphi}}{\sqrt{2\pi}} + \phi_\nu^{(1)}(\xi)\frac{e^{im\varphi}}{\sqrt{2\pi}}F + O(F^2)\\ &= \Phi_\nu^{(0)}(\xi,\varphi) + \Phi_\nu^{(1)}(\xi,\varphi)F + O(F^2),\end{aligned} \tag{3.7}$$

which include the first-order correction as well.

3.2 Ionization rate

In the weak-field limit (3.1), the ionization rate Γ is equal to the total flux of ionized electrons and therefore can be expressed in terms of the coefficients f_ν in Eq. (2.17). So we first find coefficient f_ν in Eq. (2.17). To this end, we need to connect Eq. (3.2b)

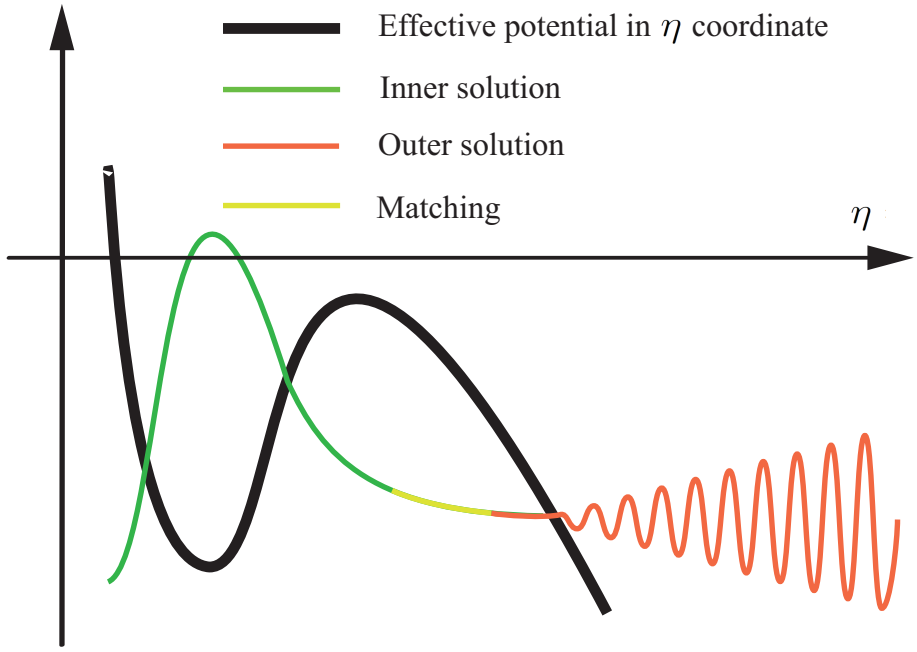

Figure 3.1: Matching procedure for solving Eq. (2.15). The *inner* (PT) solution is combined with the *outer* (WKB-like) solution in the overlap region where they both apply.

with Eq. (2.17) by constructing the asymptotic solution of (2.15). The uncoupled equations (2.15) have the form of one-dimensional Schrödinger equation with the total energy of corresponding particle being taken by $E/4$, and the effective potential generally portrayed in Fig. 3.1. Mathematically, this ordinary differential equation is classified as *singular* problem containing a *physical parameter* $F \to 0$. The difficulty in dealing with this problem stems from the fact that a regular expansion such as PT expansion cannot uniformly describe the solution in the whole domain under consideration. This is the case here, since a PT solution, which exponentially decreases, fails to produce the outgoing wave in the asymptotic region as pointed out in the previous section. The problem, however, can be tackled by *matched asymptotic expansions* [61]. The idea is to partition the domain, guided by the physical properties, into adjacent subdomains in which local solutions can be accurately estimated. These solutions are then combined through *matching* process in such a way that an approx-

imate solution for the whole domain is obtained. Fig. 3.1 shows this procedure for Eq. (2.15), and the detail derivation for a more general equation is given in Appendix B.

To invoke the results obtained in Appendix B, we identify the coefficients E, β, and γ in Eq. (B.1) with $\mathcal{E}$, β_ν, and γ_m given by Eqs. (3.2a), (3.3a), and (2.16), respectively. Substituting Eqs. (3.2a) and (3.3a) into the equations of Appendix B, one should perform an additional expansion in F. In this way, from Eq. (B.13), we obtain the solution to Eq. (2.15) in the inner region $1 \ll \eta \ll F^{-1/2}$ [here we assume that $\eta > \eta_c$, which is always possible to achieve since $\eta_c = O(F^0)$]

$$f_\nu(\eta) = g_\nu \eta^{\beta_\nu^{(0)}/\varkappa} e^{-\varkappa\eta/2} \left\{1 + O(\eta^{-1}) \right.$$
$$\left. + \left[C_2\eta^2 + C_1\eta + C_l \ln\eta + C_0 + a_\nu + O(\eta^{-1}\ln\eta)\right] F + O(F^2)\right\}, \tag{3.8}$$

where

$$C_2 = (8\varkappa)^{-1}, \tag{3.9a}$$
$$C_1 = -\frac{\mu_z}{2\varkappa} + \frac{2-\gamma_m}{8\varkappa^2} + \frac{5\beta_\nu^{(0)}}{8\varkappa^3} - \frac{\beta_\nu^{(0)2}}{8\varkappa^4}, \tag{3.9b}$$
$$C_l = \frac{\beta_\nu^{(1)}}{\varkappa} + \frac{\gamma_m - 2\mu_z\beta_\nu^{(0)}}{2\varkappa^3} + \frac{3\beta_\nu^{(0)2}}{2\varkappa^5}, \tag{3.9c}$$
$$C_0 = \frac{\mu_z}{2\varkappa^2}\left(\gamma_m - \frac{\beta_\nu^{(0)}}{\varkappa} + \frac{\beta_\nu^{(0)2}}{\varkappa^2}\right). \tag{3.9d}$$

Expansion (3.8) contains two unknown field-independent coefficients, g_ν and a_ν, which can be found by comparing with Eq. (3.2b). Indeed, projecting wave function (3.2b) onto the parabolic channel ν in Eq. (3.7) gives us

$$\eta^{-1/2} f_\nu(\eta) = \langle\Phi_\nu|\psi(\mathbf{r})\rangle$$
$$= \langle\Phi_\nu^{(0)}|\psi_0(\mathbf{r})\rangle + \left[\langle\Phi_\nu^{(1)}|\psi_0(\mathbf{r})\rangle + \langle\Phi_\nu^{(0)}|\psi_1(\mathbf{r})\rangle\right] F + O(F^2). \tag{3.10}$$

By comparing this with Eq. (3.8), we find

$$g_\nu = \eta^{1/2-\beta_\nu^{(0)}/\varkappa} e^{\varkappa\eta/2} \langle \Phi_\nu^{(0)} | \psi_0(\mathbf{r}) \rangle_{\eta\to\infty} \tag{3.11}$$

and

$$\begin{aligned} a_\nu = g_\nu^{-1} \eta^{1/2-\beta_\nu^{(0)}/\varkappa} e^{\varkappa\eta/2} \left[\langle \Phi_\nu^{(1)} | \psi_0(\mathbf{r}) \rangle + \langle \Phi_\nu^{(0)} | \psi_1(\mathbf{r}) \rangle \right]_{\eta\to\infty} \\ -(C_2\eta^2 + C_1\eta + C_l \ln\eta + C_0). \end{aligned} \tag{3.12}$$

Extracting the above asymptotic coefficients is requisite for the following, and for that reason the correct asymptotic behavior of wave function up to the first order in field is extremely important. It is noticed that g_ν and a_ν are generally dependent on orientation angle β of the molecule with respect to the field, i.e., $g_\nu = g_\nu(\beta, \eta)$ and $a_\nu = a_\nu(\beta, \eta)$. In practice, they are calculated by considering a polynomial in $1/\eta$ of the form

$$y_\nu(\beta, \eta) = y_\nu(\beta) + \sum_{j=1}^{n} c_j^\nu(\beta) \left(\frac{1}{\eta}\right)^j, \tag{3.13}$$

where

$$y_\nu(\beta) = \lim_{\eta\to\infty} y_\nu(\beta, \eta) \tag{3.14}$$

is the value of desire for a fixed orientation angle β. Appropriate sampling points of g_ν and of a_ν will be picked up in their most stable region to fit with asymptotic expansion (3.13). Having thus obtained g_ν and a_ν, we obtain from Eq. (B.25)

$$f_\nu = f_\nu^{(0)} \left[1 + \frac{1}{2} A_\nu F \ln\frac{F}{4\varkappa^2} + \frac{1}{2}(B_\nu + 2i\,\mathrm{Im}\, a_\nu - i\pi A_\nu)F + O(F^2) \right], \tag{3.15}$$

where the leading-order term is given by

$$f_\nu^{(0)} = \frac{\varkappa^{1/2} g_\nu}{2^{1/2}} \left(\frac{4\varkappa^2}{F}\right)^{\beta_\nu^{(0)}/\varkappa} \exp\left[\frac{i\pi}{4} + \frac{i\pi\beta_\nu^{(0)}}{\varkappa} - \varkappa\mu_z - \frac{\varkappa^3}{3F} \right] \tag{3.16}$$

and the first-order correction coefficients are

$$A_\nu = -\frac{2\beta_\nu^{(1)}}{\varkappa} - \frac{\gamma_m - 2\mu_z\beta_\nu^{(0)}}{\varkappa^3} - \frac{3\beta_\nu^{(0)2}}{\varkappa^5}, \tag{3.17a}$$

$$B_\nu = -\varkappa\alpha_{zz} - \frac{\mu_z^2}{\varkappa} + \frac{\mu_z}{\varkappa^2} + \frac{4\mu_z\beta_\nu^{(0)}}{\varkappa^3} - \frac{10 + 18\gamma_m + 3\gamma_m^2}{24\varkappa^3}$$
$$- \frac{(9 - 6\gamma_m)\beta_\nu^{(0)}}{4\varkappa^4} - \frac{(49 + 2\gamma_m)\beta_\nu^{(0)2}}{8\varkappa^5} + \frac{3\beta_\nu^{(0)3}}{2\varkappa^6} - \frac{\beta_\nu^{(0)4}}{8\varkappa^7} + 2\,\mathrm{Re}\,a_\nu. \tag{3.17b}$$

Note that g_ν and a_ν are generally complex and for real $\psi_0(\mathbf{r})$ and $\psi_1(\mathbf{r})$ they satisfy

$$g_{n_\xi,-m} = g_{n_\xi m}^*, \quad a_{n_\xi,-m} = a_{n_\xi m}^*, \tag{3.18}$$

while A_ν and B_ν are real.

Given the asymptotic coefficient f_ν specifying the outgoing-flux amplitude, we are at position to calculate the ionization rate. From Eqs. (2.1) and (2.18) we have

$$\Gamma|\psi(\mathbf{r})|^2 = \nabla\mathbf{j}(\mathbf{r}), \tag{3.19}$$

where

$$\mathbf{j}(\mathbf{r}) = \frac{-i}{2}\left[\psi^*(\mathbf{r})\nabla\psi(\mathbf{r}) - \psi(\mathbf{r})\nabla\psi^*(\mathbf{r})\right]. \tag{3.20}$$

Integrating both sides of this equation and using the normalization condition (2.19), we obtain

$$\Gamma = \int_{S_\eta} \mathbf{e}_\eta \cdot \mathbf{j}(\mathbf{r})\, dS_\eta \Bigg|_{\eta\to\infty}, \tag{3.21}$$

where S_η is a surface of constant η, $\mathbf{e}_\eta$ is the unit normal vector to S_η pointing toward $\eta \to \infty$, and dS_η is the area element of S_η. We have

$$dS_\eta = \sqrt{\frac{r\eta}{2}}\, d\xi d\varphi, \quad \mathbf{e}_\eta \cdot \nabla = \sqrt{\frac{2\eta}{r}}\,\frac{\partial}{\partial\eta}, \tag{3.22}$$

and hence

$$\Gamma = \frac{-i\eta}{2}\int_0^\infty d\xi \int_0^{2\pi} d\varphi \left[\psi^*(\mathbf{r})\frac{\partial}{\partial\eta}\psi(\mathbf{r}) - \psi(\mathbf{r})\frac{\partial}{\partial\eta}\psi^*(\mathbf{r})\right]_{\eta\to\infty}. \tag{3.23}$$

Substituting here Eq. (2.11), using Eqs. (2.10) and (2.17), and noting that the imaginary part of E is exponentially small in F and can be neglected in Eqs. (2.9a) and (2.17), we obtain

$$\Gamma = \sum_\nu \Gamma_\nu + O(\Gamma^2), \quad \Gamma_\nu = |f_\nu|^2. \tag{3.24}$$

Here Γ_ν is the partial rate corresponding to ionization into parabolic channel ν and the error term $O(\Gamma^2)$ arises from the exponentially small contributions neglected in the derivation. We note that in the same approximation from Eqs. (2.22) and (2.23) we also have

$$\Gamma = \int P(\mathbf{k}_\perp)\,\frac{d\mathbf{k}_\perp}{(2\pi)^2} + O(\Gamma^2), \tag{3.25}$$

which is consistent with the physical meaning of Γ and $P(\mathbf{k}_\perp)$. Substituting Eq. (3.15) into Eq. (3.24), we find

$$\Gamma_\nu = |G_\nu|^2 W_\nu(F)\left[1 + A_\nu F \ln\frac{F}{4\varkappa^2} + B_\nu F + O(F^2\ln^2 F)\right], \tag{3.26}$$

where G_ν and $W_\nu(F)$ are the standard *structure* and *field* factors [51, 52],

$$G_\nu = e^{-\varkappa\mu_z} g_\nu, \tag{3.27}$$

$$W_\nu(F) = \frac{\varkappa}{2}\left(\frac{4\varkappa^2}{F}\right)^{2Z/\varkappa - 2n_\xi - |m| - 1} \exp\left(-\frac{2\varkappa^3}{3F}\right), \tag{3.28}$$

and the *correction* coefficients A_ν and B_ν are defined by Eqs. (3.17).

The partial ionization rates (3.26) for the different channels have the same exponential factor but different powers of F in Eq. (3.28). The power of F grows by 2 and 1 as n_ξ or $|m|$ are increased by unity, respectively. Therefore, in the leading-order ap-

proximation one should retain in the total ionization rate (3.24) only the contribution from the *dominant* channel, the one with the minimum values of n_ξ and $|m|$ for which $g_\nu \neq 0$. However, when we include the first-order correction terms for the dominant channel in Eq. (3.26), the leading-order contributions from the *next-to-the-dominant*, the ones with the same n_ξ and $|m|$ increased by unity, also needs to be retained. The dominant channel is determined by the symmetry of the potential. Three symmetry cases should be distinguished as follows

(a) *Potentials without any symmetry.* This corresponds to arbitrary molecules arbitrarily oriented with respect to the field. In this case, all the coefficients g_ν are generally nonzero, the dominant channel is $\nu = (0, 0)$, and there are two next-to-the-dominant channels $(0, \pm 1)$. From Eqs. (3.24) and (3.26) we obtain

$$\Gamma \approx W_{00}(F) \left[|G_{00}|^2 \left(1 + A_{00} F \ln \frac{F}{4\varkappa^2} + B_{00} F \right) + \frac{F}{2\varkappa^2} |G_{01}|^2 \right]. \tag{3.29}$$

In some specific circumstances, coefficient g_{00} may vanishes due to nodal lines and nodal surfaces of the wave function $\psi(\mathbf{r})$ such that no contribution from channel $\nu = (0, 0)$ shows up. Then the next channels with $\nu = (0, \pm 1)$ become dominate and

$$\Gamma \approx W_{01}(F) \left[2 |G_{01}|^2 \left(1 + A_{01} F \ln \frac{F}{4\varkappa^2} + B_{01} F \right) + \left(2 |G_{02}|^2 + G_{10}^2 \right) \frac{F}{4\varkappa^2} \right]. \tag{3.30}$$

In both cases, the leading-order approximation $\Gamma_{\rm as}$ for tunneling rate can be commonly expressed by

$$\Gamma_{\rm as} = (2 - \delta_{m0}) |G_{0m}|^2 W_{0m}(F), \tag{3.31}$$

where m is the azimuthal quantum number of the dominant ionization channel.

(b) *Axially symmetric potentials.* This corresponds to atoms and linear molecules aligned along the field. In this case, $V(\mathbf{r}) = V(\xi, \eta)$ and Eq. (2.1) has solutions of the form $\psi(\mathbf{r}) = \psi(\xi, \eta) e^{im\varphi}$, for which m is an exact quantum number [48]. For

$m \neq 0$, the solutions $\propto e^{\pm im\varphi}$ are degenerate, so one can switch to another pair of solutions proportional to $\cos m\varphi$ and $\sin m\varphi$. According to our convention, $\psi_0(\mathbf{r})$ is real, which corresponds to the latter representation. Then the sums in Eqs. (2.11) and (3.24) contain only channels with $\nu = (n_\xi, \pm|m|)$. There is one dominant channel $(0,0)$, for $m = 0$, and two dominant channels $(0, \pm|m|)$, for $m \neq 0$, but there are no next-to-the-dominant channels. It can be seen that all the coefficients in Eq. (3.26) in this case depend only on the absolute value of m. Thus for states with a given m we obtain

$$\Gamma \approx \Gamma_{as} \left(1 + A_{0m} F \ln \frac{F}{4\varkappa^2} + B_{0m} F\right). \tag{3.32}$$

For $m = 0$ this formula coincides with Eq. (3.29), taking into account that in the present case $G_{01} = 0$.

(c) *The Coulomb potential.* For a purely Coulomb potential, Eq. (2.1) allows separation of variables in parabolic coordinates, so both quantum numbers n_ξ and m identifying the parabolic channels are exact. In this case, it is convenient to switch to a more conventional representation in which the solutions to Eq. (2.1) depend on φ as $e^{im\varphi}$. Let consider the hydrogen atom in a state with parabolic quantum numbers (n_ξ, n_η, m) ($n_\xi \equiv n_1$ and $n_\eta \equiv n_2$ in the notation of Ref. [10]). Then the sums in Eqs. (2.11) and (3.24) contain only one channel with $\nu = (n_\xi, m)$; this is the dominant channel and there are no next-to-the-dominant channels. For hydrogen $Z = 1$, $\mathbf{D} = \mathbf{0}$, and $\alpha_{ij} = \alpha\delta_{ij}$. The values of E_0, μ_z, and α are well known [10]

$$E_0 = -\frac{1}{2n^2}, \quad \varkappa = \frac{1}{n}, \tag{3.33a}$$

$$\mu_z = -\frac{3}{2}\, n(n_\xi - n_\eta), \tag{3.33b}$$

$$\alpha = \frac{n^4}{8}\left[17n^2 - 3(n_\xi - n_\eta)^2 - 9m^2 + 19\right]. \tag{3.33c}$$

The wave function can also be found analytically

$$\psi_0(\mathbf{r}) = \frac{\sqrt{2}}{n}\,\phi^{(0)}_{n_\eta m}(\eta)\Phi^{(0)}_\nu(\xi,\varphi), \tag{3.34a}$$

$$\psi_1(\mathbf{r}) = \frac{\sqrt{2}}{n}\left[\phi^{(0)}_{n_\eta m}(\eta)\Phi^{(1)}_\nu(\xi,\varphi) - \tilde{\phi}^{(1)}_{n_\eta m}(\eta)\Phi^{(0)}_\nu(\xi,\varphi)\right] + \frac{3}{4}\,n^3(n_\xi - n_\eta)\psi_0(\mathbf{r}), \tag{3.34b}$$

where $n = n_\xi + n_\eta + |m| + 1$ is the principle quantum number and $\tilde{\phi}^{(1)}_{nm}(x)$ coincides with $\phi^{(1)}_{nm}(x)$ defined by Eq. (3.5b) with the sign of μ_z changed to the opposite. Substituting Eq. (3.34a) into Eq. (3.11), we reproduce Eq. (67) from Ref. [23],

$$g_\nu = \frac{(-1)^{n_\eta}\sqrt{2}}{n^{n_\eta+|m|/2+3/2}\sqrt{n_\eta!(n_\eta+|m|)!}}. \tag{3.35}$$

Substituting Eqs. (3.34) into Eq. (3.12) leads to

$$\begin{aligned} a_\nu = \frac{n^3}{16}\big[&n_\eta^4 + (2|m|-10)n_\eta^3 + (m^2 - 15|m| - 11)n_\eta^2 \\ &-(5m^2 + 24n_\xi + 23|m| + 36)n_\eta - 6(2n_\xi + |m| + 3)|m| - 12\big]\,. \end{aligned} \tag{3.36}$$

It is easy to check that coefficient A_ν in Eq. (3.17a) vanishes for hydrogen case, and so does the logarithmic term in Eq. (3.26). Thus

$$\Gamma \approx |G_\nu|^2 W_\nu(F)(1 + B_\nu F). \tag{3.37}$$

With these values of g_ν and a_ν, Eq. (3.37) is *in full agreement* with the result obtained by a different method in Ref. [46]. Notice that the method of Ref. [46] is applicable only to the Coulomb potential, when the variables in Eq. (2.1) can be separated, while the present approach applies to arbitrary potentials. This agreement provides an independent confirmation of the consistency of the present approach and results.

3.3 Transverse momentum distribution

The weak-field asymptotic expansion for the TMD (2.23) can be obtained by substituting Eqs. (3.7) and (3.15) into Eq. (2.22). In calculating the sum in Eq. (2.22), one should again retain all channels whose contributions have the same power of F as the correction terms in Eq. (3.15) for the dominant channel. In this case of dominant channel $\nu = (0,0)$, one should retain in Eq. (2.22) also the contributions from channels $(0,\pm1)$, $(0,\pm2)$, and $(1,0)$. The TMD is thus given by

$$\begin{aligned} P(\mathbf{k}_\perp) \approx \frac{4\pi\varkappa}{F}\, W_{00}(F) e^{-s} \Bigg[G_{00}^2 \Bigg(1 + A_{00} F \ln\frac{F}{4\varkappa^2} \\ + \left\{ B_{00} + \frac{1}{4\varkappa^3}\left[6 + 4\varkappa\mu_z - 4(\varkappa\mu_z + 1)s - s^2 \right] \right\} F \Bigg) \\ - \left\{ (1-s) G_{00} G_{10} - 2s \left[\operatorname{Re}(G_{01} e^{i\varphi_k}) \right]^2 + \sqrt{2} s G_{00} \operatorname{Re}(G_{02} e^{2i\varphi_k}) \right\} \frac{F}{2\varkappa^2} \\ - \sqrt{s} G_{00} (2 \operatorname{Im} a_{00} - \pi A_{00}) \operatorname{Re}(G_{01} e^{i\varphi_k}) \frac{F^{3/2}}{\varkappa} \Bigg], \end{aligned} \tag{3.38}$$

where

$$s = \frac{\varkappa k_\perp^2}{F}, \tag{3.39}$$

and we have explicitly used that $G_{n_\xi,-m} = G^*_{n_\xi m}$, which follows from the first of Eqs. (3.18). For dominant channel $\nu = (0,\pm1)$, the situation is more complicated, and the final formula is

$$\begin{aligned} P(\mathbf{k}_\perp) \approx \frac{4\pi\varkappa}{F}\, W_{01}(F) e^{-s} \Bigg[4s \left[\operatorname{Re}(G_{01} e^{i\varphi_k}) \right]^2 \Bigg(1 + A_{01} F \ln\frac{F}{4\varkappa^2} \\ + \left\{ B_{01} + \frac{1}{4\varkappa^3}\left[2(4\varkappa\mu_z + 9) - 2(2\varkappa\mu_z + 3)s - s^2 \right] \right\} F \Bigg) \\ - 4s \operatorname{Re}(G_{01} e^{i\varphi_k}) \left\{ 24\varkappa^2 \operatorname{Im}(G_{01} e^{i\varphi_k}) \operatorname{Im}(a_{01}) \right. \\ \left. + 3\sqrt{2}(2-s) \operatorname{Re}(G_{11} e^{i\varphi_k}) + \sqrt{6} s \operatorname{Re}(G_{03} e^{3i\varphi_k}) \right\} \frac{F}{12\varkappa^2} \\ + \left\{ (1-s) G_{10} + \sqrt{2} s \operatorname{Re}(G_{02} e^{2i\varphi_k}) \right\}^2 \frac{F}{4\varkappa^2} \end{aligned}$$

$$+2\pi A_{01}\sqrt{s}\,\mathrm{Re}(G_{01}e^{i\varphi_k})\left\{(1-s)G_{10}+\sqrt{2}s\,\mathrm{Re}(G_{02}e^{2i\varphi_k})\right\}\frac{F^{3/2}}{2\varkappa}\Bigg]. \tag{3.40}$$

By using notation Γ_{as}, we can rewrite the leading-order terms in Eqs. (3.38), and (3.40) as

$$P_{\mathrm{as}}(\mathbf{k}_\perp)=(2-\delta_{m0})\Gamma_{\mathrm{as}}\frac{4\pi}{F}\left[\phi^{(0)}_{0m}(s)\right]^2\times\begin{cases}\cos^2(m\varphi_k), & \text{even states,}\\ \sin^2(m\varphi_k), & \text{odd states,}\end{cases} \tag{3.41}$$

where m is the azimuthal quantum number of the dominant ionization channel. For $m=0$, Eq. (3.41) coincides with the well-known result by Perelomov *et al.* [16]. The definition of even and odd state will be given in Chapter 5 when we discuss the molecular systems. In the above equations, we have used that coefficients $G_{n_\xi 0}$ are real, because it is always possible to assume that the unperturbed bound-state wave function is real. Equation (3.38) generalizes Eq. (64) from Ref. [23]. It applies to potentials without any symmetry, but also to states with $m=0$ in axially symmetric potentials, when $G_{01}=G_{02}=0$, and to the ground state of hydrogen, when $G_{01}=G_{02}=G_{10}=0$. In the latter case it reduces to

$$P(\mathbf{k}_\perp)\approx\frac{16\pi}{F^2}\exp\left(-\frac{2}{3F}-s\right)\left[1-\left(\frac{89}{12}+s+\frac{s^2}{4}\right)F\right]. \tag{3.42}$$

The exponential factor e^{-s} in Eqs. (3.38) and (3.42) results in a well-known Gaussian shape of the TMD in the weak-field limit, $P(\mathbf{k}_\perp)\propto\exp(-\varkappa k_\perp^2/F)$. This shape was first obtained within the static limit of the Keldysh theory [62, 16] and later was reproduced by different methods by other authors [63, 64, 23]. The s-dependent part of the correction terms in Eqs. (3.38) and (3.42) accounts for a departure from the Gaussian shape at stronger fields, while the s-independent part accounts for a change of the magnitude of the TMD corresponding to a departure of Γ from the leading-order term in Eq. (3.29), in accordance with Eq. (3.25).

3.4 Region of applicability

Mathematically, the asymptotic solution of the SS eigenvalue problem developed in this chapter applies in the limit (3.1). Physically, the region of applicability of the WFAT can be specified by the condition

$$F \ll F_c, \tag{3.43}$$

where the critical field F_c is a boundary between the tunneling and over-the-barrier ionization regimes. The value of F_c can be estimated as the field for which the two turning points of Eq. (2.15) for the dominant channel coalesce. Substituting for E and β_ν the leading-order terms from Eqs. (3.2a) and (3.3a), we obtain

$$F_c \approx \frac{\varkappa^4}{8|2Z - \varkappa(2n_\xi + |m| + 1)|}, \tag{3.44}$$

where n_ξ and m correspond to the dominant channel. The condition (3.43) ensures that the first-order correction terms in Eqs. (3.15) and (3.26) are much smaller than unity. In practice, we shall see that these corrections remain meaningful, that is, improve the leading-order results, up to $F \sim F_c$.

Chapter 4

Application for atomic systems

The derivation in Chapter 3 of the first-order correction terms in the asymptotic expansions of the ionization rate and TMD within the WFAT is general and covers atomic (spherically symmetric potentials) as well as molecular (arbitrary potentials without any symmetry) cases. In this first illustration of the results obtained we restrict our treatment to the atomic case when accurate calculations of the coefficients required to implement the theory can be performed relatively easily. We consider hydrogen and four noble-gas atoms within the SAEA. In all cases the asymptotic charge seen by the outgoing electron is $Z = 1$, the dipole of the atomic ion is $\mathbf{D} = \mathbf{0}$, see Eq. (2.2), the polarizability tensor reduces to a scalar, $\alpha_{ij} = \alpha\delta_{ij}$, and the TMD (2.23) depends only on the absolute value of the transverse momentum and is denoted by $P(k_\perp)$. We compare the ionization rate and TMD predicted by the WFAT with the results of accurate numerical calculations.

4.1 Hydrogen

Let first consider hydrogen for which earlier theories including higher-order corrections in the field strength for the ionization rate are available [46, 47]. In this case, all the coefficients needed to implement the present theory are known analytically, see

Eqs. (3.35) and (3.36). The exact results for Γ are obtained by the procedure outlined in Appendix C. While the TMD is calculated by procedure developed in Ref. [48].

In Fig. 4.1, we show the ionization rate for the ground state divided by the field factor (3.28) with $\nu = (0, 0)$. This representation facilitates the comparison of different results by eliminating rapid variation of Γ by many orders of magnitude as $F \to 0$. In the convention introduced in Chapter 1, labels WFAT(n) refer to the results obtained by including terms up to order $O(F^n)$ in the asymptotic expansion of Γ. The WFAT(0) and WFAT(1) results are obtained from Eq. (3.37) omitting the linear in F term and including this term with $B_{00} = -107/12$, respectively. The WFAT(2) and WFAT(10) results are obtained by adopting the coefficients of higher powers of F given in Ref. [47]. A good agreement between the WFAT(1) and the exact results at $F \lesssim 0.02$ confirms the second term in Eq. (3.37). Although the value of B_{00} has been known for a long time [46, 47], its unambiguous confirmation by accurate calculations was hindered by extremely small values of Γ at such small F where Eq. (3.37) holds with a sufficient accuracy. To overcome this difficulty, which is needed for validating

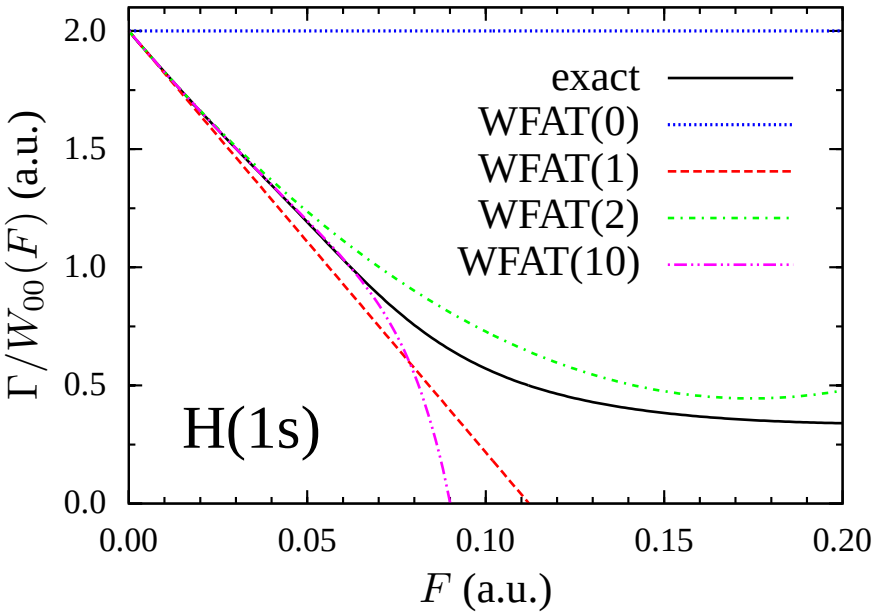

Figure 4.1: Ratio of the ionization rate to the field factor (3.28) as a function of field for hydrogen in the ground state. The WFAT results of different orders are compared with the exact calculations obtained by the method outlined in Appendix C.

the asymptotic results, we have developed a multiple-precision procedure discussed in Appendix C. The departure of the WFAT(1) from the exact results at larger fields is caused by the presence of higher-order terms in the asymptotic expansion. Figure 4.1 illustrates quantitatively how much such higher-order corrections improve the prediction of the WFAT. For any given $F < F_c$, the inclusion of terms up to certain maximum order improves the results, but incorporating further terms makes the results only worse. The smaller F, the larger this maximum order, and the higher accuracy can be achieved. Thus, for example, at $F = 0.05$ the WFAT(10) is closer to the exact results than WFAT(1), but at $F = 0.1$ the opposite is true. Such a behavior reflects a well-known property of divergent asymptotic series; a good illustration of this point on the example of the perturbation-theory series (3.2a) for the real part of the energy of the ground state can be found in Ref. [65]. In contrast to the WFAT(0), which yields at least a positive value of Γ for any field, the WFAT(1) cannot be extended beyond $F_c = -1/B_{00} \approx 0.112$, where the right-hand side of Eq. (3.37) turns zero, which again reflects the asymptotic nature of the expansion. This value of F_c is slightly lower than $F_c = 0.125$ obtained from Eq. (3.44) and gives a better estimate of the boundary for over-the-barrier ionization. The main conclusion to be drawn from Fig. 4.1 is that the first-order correction included in the WFAT(1) significantly improves the prediction for Γ as compared to the WFAT(0), extending the region of applicability of the theory up to $F \sim F_c$, while the higher-order terms can be safely neglected in this region within a tolerable error. For example, the WFAT(1) remains valid within an error of 20% up to $F = 0.076$, while the WFAT(0) is beyond this error already at $F = 0.020$. We will see that this conclusion applies also to other atoms.

The excited states of hydrogen are also of interest to investigate with the present theory. In this case, for states with $n_\xi \neq n_\eta$, there exists a permanent dipole moment $\mu_z = -3n(n_\xi - n_\eta)/2$ which modifies the structure factor (3.27) and also contributes to coefficient B_ν in Eq. (3.37). In Fig. 4.2, we compare the exact results with the

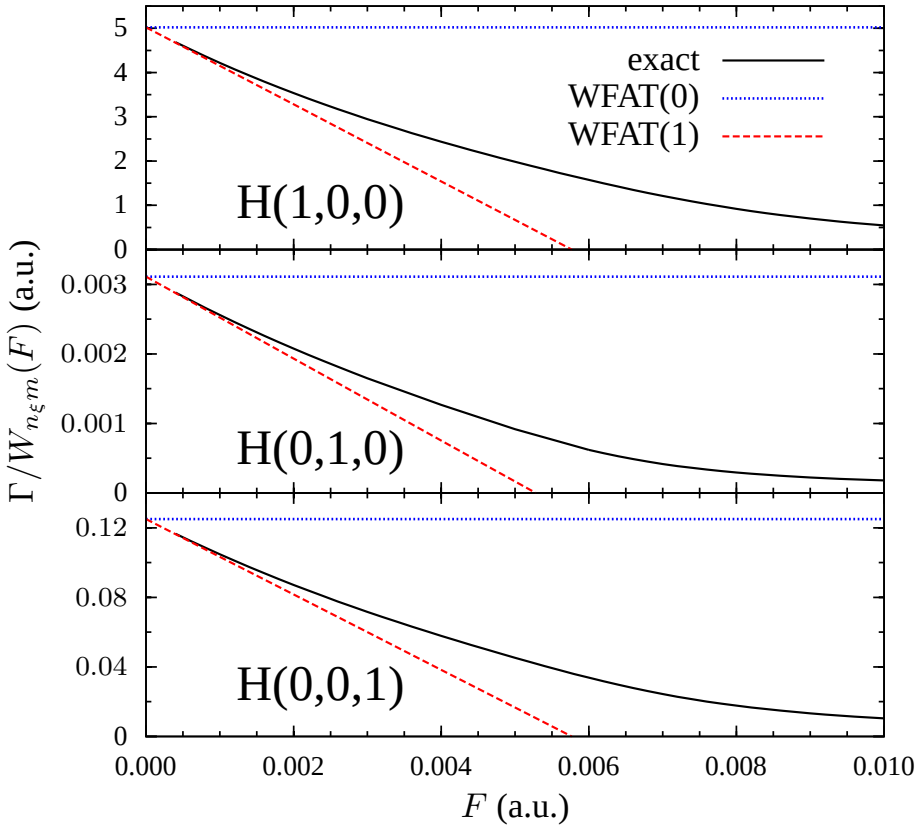

Figure 4.2: Ratio of the ionization rate to the field factor (3.28) as a function of field for hydrogen in states with parabolic quantum numbers (n_ξ, n_η, m) indicated in the parenthesis.

WFAT(0) and WFAT(1), again focusing on the ratio of the rate and the field factor (3.28) which enables one to compare the results quantitatively. We consider the three states with $n = 2$ and $(n_\xi, n_\eta, m) = (1, 0, 0)$, $(0, 1, 0)$, and $(0, 0, 1)$, which are degenerate in the absence of the field. The first two of these states have nonzero dipoles of the same value but different sign. Due to the presence of this dipole in the exponent in Eq. (3.27), and the corresponding polarization of the electron density, there is a large difference in the magnitude of the ionization rates for these states. The third state with $m = 1$ does not have a dipole and its rate takes values between the two other states. Figure 4.2 shows that in all cases a significant improvement on the step from WFAT(0) to WFAT(1) in the agreement with the exact results is achieved. The convergence of the WFAT(1) with the exact results as F decreases confirms the

linear in F term in Eq. (3.37), including the case of states with a permanent dipole. This illustrates that the theory correctly treats polar systems, a typical situation for molecules.

We now turn to a discussion of the accuracy of the WFAT in predicting the TMD. Together with the complex SS eigenvalue (2.18), the TMD (2.23) presents an essential characteristic required for implementing the adiabatic theory [8], so it is instructive to see in which region of the field strengths the WFAT can be used instead of much more time-consuming exact calculations. We consider only the ground state. The results for two representative values of F are shown in Fig. 4.3. The WFAT(0) and WFAT(1) results are obtained from Eq. (3.42) omitting and including the linear in F correction term, respectively. Figure 4.3 shows that the WFAT(1) prediction is in much better agreement with the exact results than the WFAT(0). This is not a surprise, because the field values considered belong to the interval where Eq. (3.37)

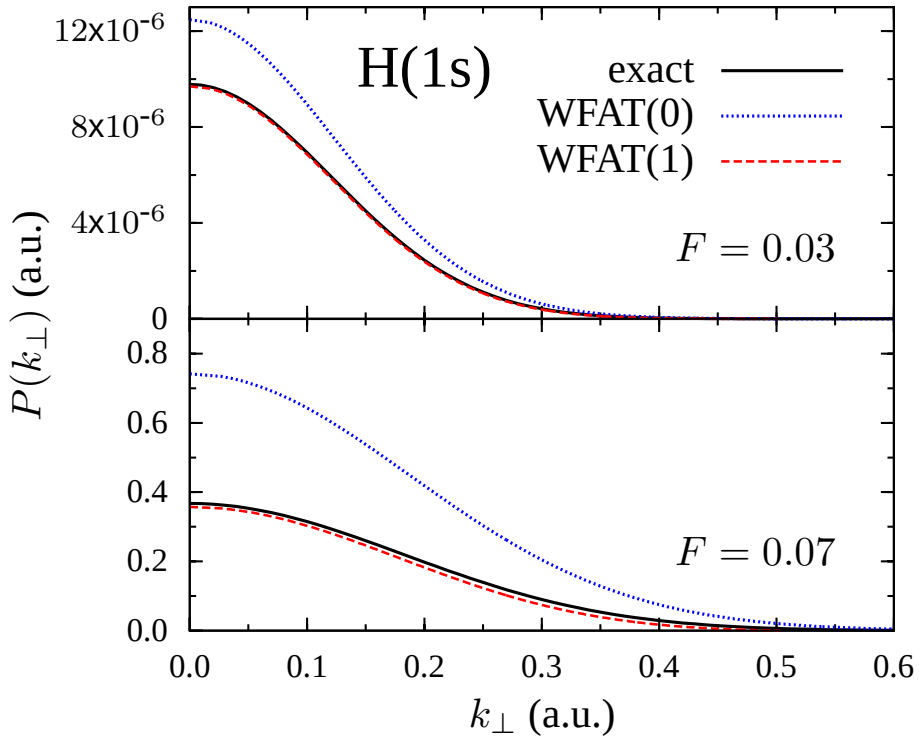

Figure 4.3: Transverse momentum distributions for hydrogen in the ground state at two representative values of the field F.

works well. The improvement of WFAT(1) over WFAT(0) is mainly attributed to the s-independent part of the correction term in Eq. (3.42), see the discussion after that equation. The investigation of a more subtle effect of the departure of the shape of the TMD from the Gaussian, which is accounted for by the s-dependent part of the correction term, is postponed to the end of the next section.

4.2 Nobel gas atoms

We proceed with calculations for the noble gas atoms Ne, Ar, Kr, and Xe. The active electrons in these atoms are described by the $2p$, $3p$, $4p$, and $5p$ states, respectively, with azimuthal quantum number $m = 0$ in all cases, in a local spherically symmetric potential of the form [66, 67]

$$V(r) = -\frac{Z_{\rm eff}(r)}{r}, \tag{4.1}$$

where the effective charge $Z_{\rm eff}(r)$ monotonically decreases from the bare nuclear charge equal to the number of electrons N, at $r = 0$, to 1, at $r \to \infty$, and is given by

$$Z_{\rm eff}(r) = N - (N-1)\{1 - [(v/u)(e^{ur} - 1) + 1]^{-1}\}. \tag{4.2}$$

Equations (4.1) and (4.2) comply with Eq. (2.2). The recommended values of the parameters u and v are given in Table 4.1.

All the atomic characteristics needed to implement the WFAT are also given in Table 4.1. For all atoms, the dominant channel is $\nu = (0, 0)$ and the dipole moment is $\mu_z = 0$. Unperturbed bound-state energy E_0 and wave function $\psi_0(\mathbf{r})$ are obtained using discrete variable representation [68] associated with Laguerre polynomials in parabolic coordinates. The polarizability α and the first-order correction $\psi_1(\mathbf{r})$ to the wave function are then calculated by implementing standard spectral expansions of perturbation theory [10]; a similar procedure using the Legendre basis in a finite box

Table 4.1: Characteristics of noble-gas atoms. The number of electrons N and the parameters u and v define the effective charge (4.2) in the one-electron model potential (4.1). The needed coefficients for implementing Eq. (3.32) are also given.

Atom	N	u	v	E_0	α	g_{00}	g_{10}	a_{00}	A_{00}	B_{00}
Ne($2p$)	10	1.704	2.810	-0.793	0.152	2.1	3.7	-0.8	0.246	$-$ 2.6
Ar($3p$)	18	0.933	3.600	-0.579	1.323	2.7	5.3	-2.1	0.158	$-$ 7.7
Kr($4p$)	36	1.340	4.311	-0.515	2.099	2.3	4.6	-2.8	0.042	-10.5
Xe($5p$)	54	1.048	5.197	-0.446	3.079	2.5	5.2	-4.8	-0.222	-16.4

in spherical coordinates was described in Ref. [49]. The coefficients g_{00}, g_{10}, and a_{00} do not depend on orientation angle β due to the spherical symmetry, and are obtained from Eqs. (3.11) and (3.12). We collect sampling points for the first two coefficients in the range $\eta \in [4; 21]$, and for a_{00} in the range $\eta \in [5; 19]$, then fit with Eq. (3.13) up to $n = 4$. From Eq. (3.27) in the present case we have $G_{00} = g_{00}$ and $G_{10} = g_{10}$. The correction coefficients A_{00} and B_{00} are found from Eqs. (3.17). Note that A_{00} as a function of $\varkappa$ turns zero for $\varkappa = 1$, which corresponds to $E_0 = -0.5$. This explains the small value of this coefficient for Kr($4p$) and its different sign for Xe($5p$). The WFAT results for the ionization rate and TMD are obtained from Eq. (3.32) with $m = 0$ and Eq. (3.38) with $G_{01} = G_{02} = 0$, respectively. For completeness, we also present exact results for the real part of the SS eigenvalue (2.18) and compare them with the perturbation expansion (3.2a). The exact results in all cases are calculated using the method of Ref. [48].

Figure 4.4 shows the energy $\mathcal{E}$, ionization rate Γ, and its ratio to the field factor (3.28) as functions of F for the four atoms. The perturbation theory for $\mathcal{E}$ up to the second order in field, Eq. (3.2a), is accurate up to $F \simeq 0.1$, 0.05, 0.05, and 0.03 for Ne($2p$), Ar($3p$), Kr($4p$), and Xe($5p$), respectively. These values of field correlate with the values of F_c estimated as the field where the WFAT(1) prediction for Γ turns zero and given by $F_c \simeq 0.3$, 0.12, 0.095, and 0.065, respectively. Similar to the case of

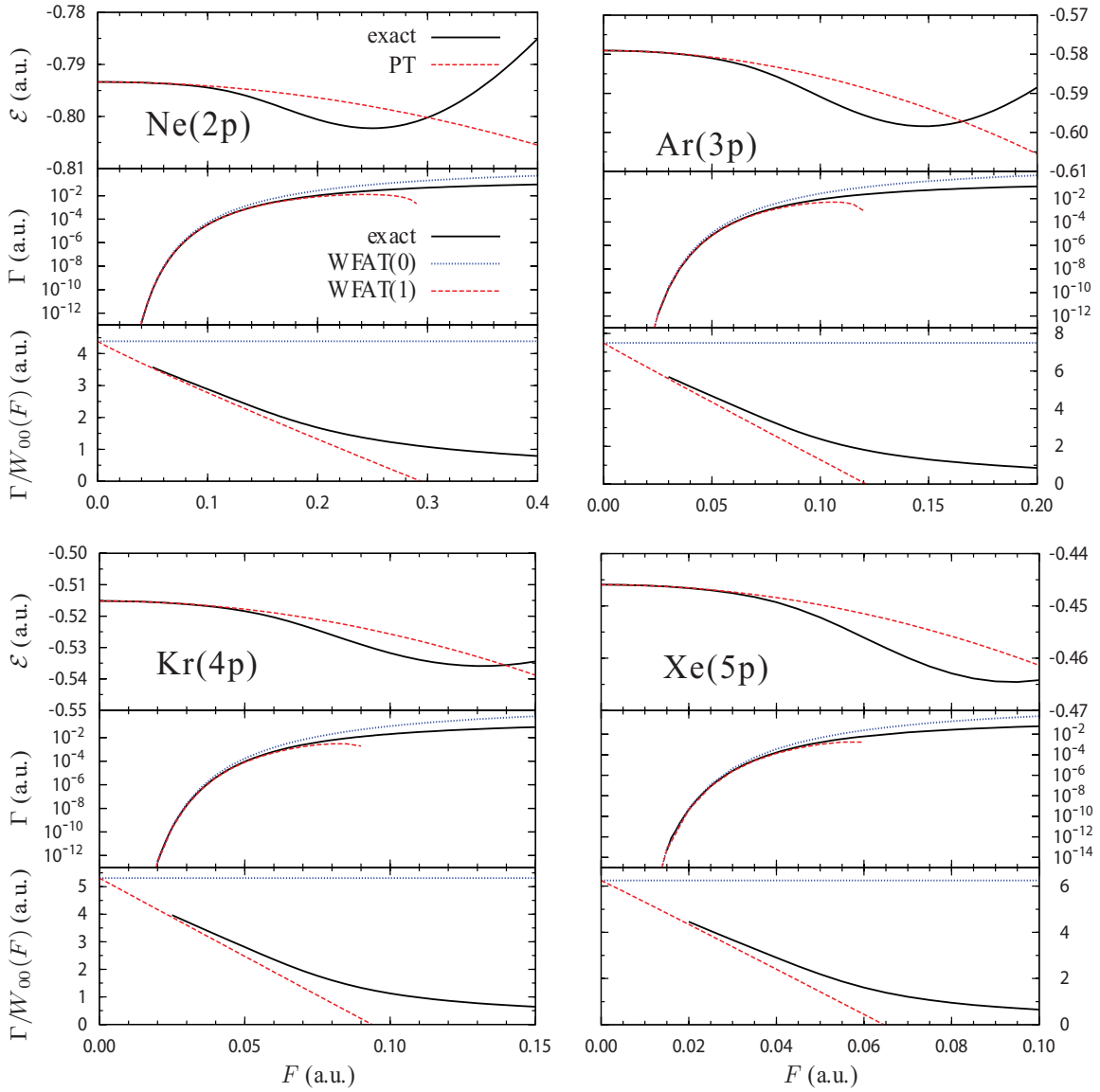

Figure 4.4: Real part of the energy (top panel), ionization rate (middle panel), and its ratio to the field factor (3.28) (bottom panel) as functions of field for Ne($2p$), Ar($3p$), Kr($4p$), and Xe($5p$).

H($1s$), Eq. (3.44) slightly overestimates the critical field giving $F_c \simeq 0.4$, 0.18, 0.13, and 0.09, respectively. The exact results for the ratio shown in the bottom panels cannot be continued to smaller F because of a limitation of double-precision calculations [48] discussed in Appendix C. However, even the available results unambiguously show that the WFAT(1) converges to the exact results as F decreases. This provides a numerical confirmation of Eq. (3.32) for non-Coulomb potentials, when Eqs. (2.12)

are coupled in the core region $\eta < \eta_c$. We again conclude that for all atoms the first-order correction included in WFAT(1) significantly improves the results for Γ as compared to WFAT(0), extending the region of applicability of the theory up to $F \sim F_c$.

The results for the TMDs at two representative values of F for each of the atoms are shown in Fig. 4.5. The WFAT(0) and WFAT(1) results are obtained from Eq. (3.41) with $m = 0$ and Eq. (3.38), respectively. Similar to the case of hydrogen illustrated in Fig. 4.3, the WFAT(1) prediction is always in much better agreement with the exact results than the WFAT(0), provided that the value of F is in the interval where Eq. (3.32) works well. This improvement of WFAT(1) over WFAT(0) is again attributed to the s-independent part of the correction in Eq. (3.38).

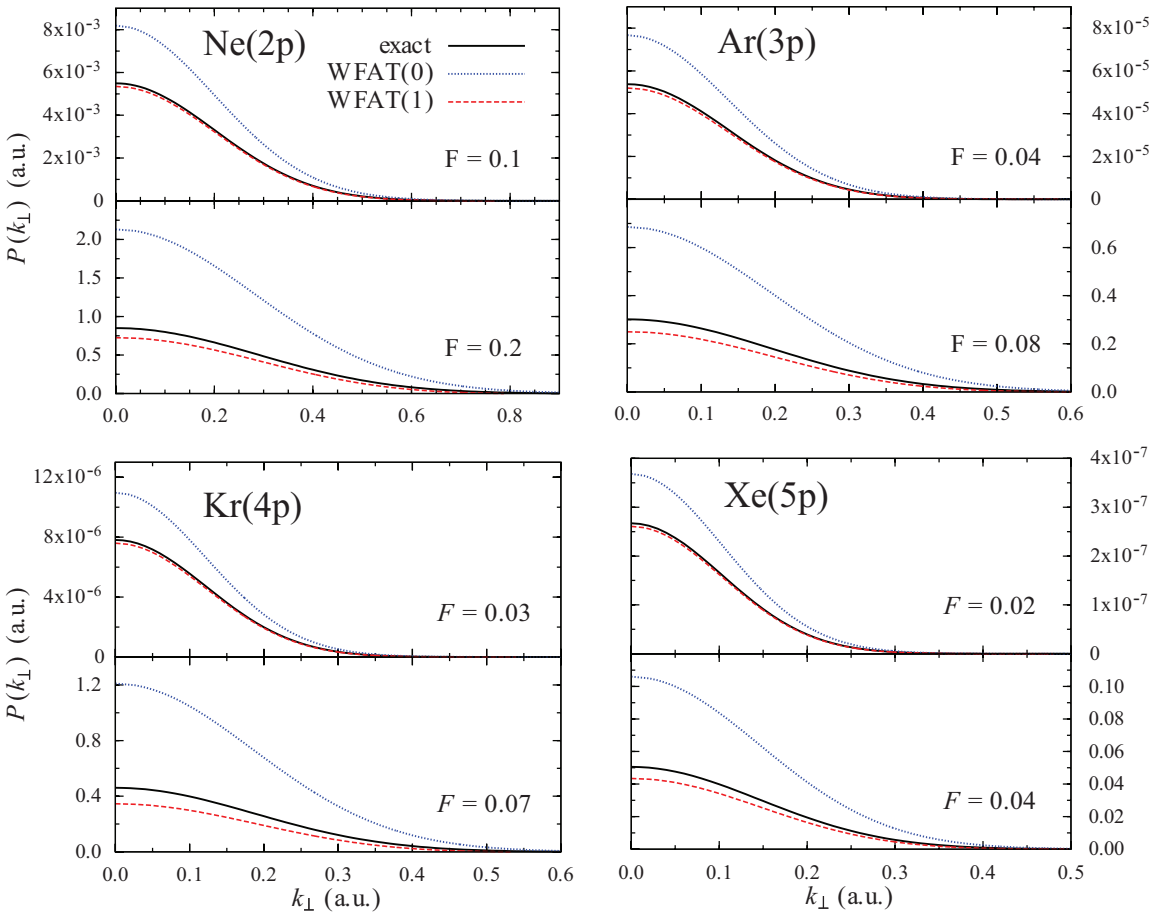

Figure 4.5: Transverse momentum distributions for Ne($2p$), Ar($3p$), Kr($4p$), and Xe($5p$) at two representative field strengths.

Let us illustrate the role of the s-dependent part of the correction in Eq. (3.38), which accounts for the departure of the shape of the TMD from Gaussian, on the example of Ar($3p$). To facilitate the comparison of the different results, we divide the corresponding TMD $P(k_\perp)$ by $P(0)\exp(-\varkappa k_\perp^2/F)$. The results for this ratio as a function of the scaled transverse momentum $k_\perp/F^{1/2}$ are shown in Fig. 4.6. The field of $F = 0.04$ considered coincides with that in the top right panel of Fig. 4.5. The WFAT(1) is in much better agreement with the exact results than the WFAT(0), certainly qualitatively, but also quantitatively up to a certain value of the scaled momentum. For example, for the present case the error of the WFAT(1) does not exceed 10% up to $k_\perp/F^{1/2} = 2$, which corresponds to $k_\perp = 0.4$ in top right panel of Fig. 4.5. This boundary value depends on field and decreases as F grows. Beyond this value the WFAT(1) quickly diverges from the exact results. All this agrees with a typical behavior of asymptotic expansions. As can be seen from Eqs. (2.22) and (2.23), the departure of the shape of the TMD from Gaussian results from two effects: the distortion of the eigenfunction for the dominant parabolic channel $\nu = (0, 0)$ by

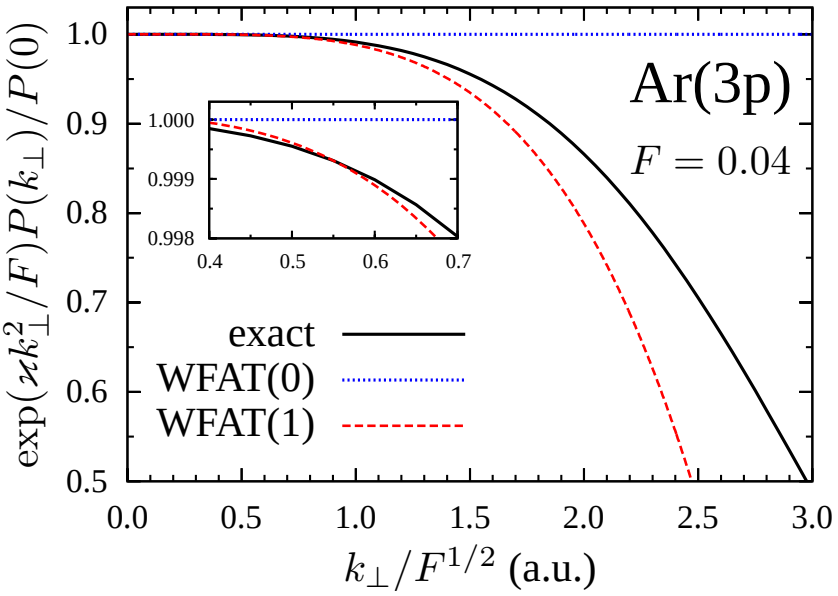

Figure 4.6: Transverse momentum distribution $P(k_\perp)$ for Ar($3p$) at $F = 0.04$ divided by the Gaussian distribution $P(0)\exp(-\varkappa k_\perp^2/F)$ as a function of the scaled transverse momentum.

field and the contribution from higher channels. In the weak-field limit, the first-order account of these effects is given by Eq. (3.38). As the field grows, the role of these effects also grows, and the TMD changes more considerably. In the over-the-barrier ionization regime the shape of the TMD may qualitatively differ from Gaussian [48].

Chapter 5

Application for molecular systems

In this chapter, the application of the WFAT including the first-order correction terms to molecular systems is illustrated. We consider one-electron diatomic molecular ions described by the soft-core potential

$$V(\mathbf{r}) = -\frac{Z_1}{\sqrt{(\mathbf{r}-\mathbf{r}_1)^2+\epsilon}} - \frac{Z_2}{\sqrt{(\mathbf{r}-\mathbf{r}_2)^2+\epsilon}}, \tag{5.1}$$

where Z_i and $\mathbf{r}_i$, $i = 1, 2$, are the charges and positions of the nuclei in the laboratory frame, and ϵ is the softening parameter. This potential satisfies Eq. (2.2) with $Z = Z_1 + Z_2$ and $\mathbf{D} = Z_1\mathbf{r}_1 + Z_2\mathbf{r}_2$. We present calculations of the asymptotic coefficients f_ν, ionization rate Γ, and TMD $P(\mathbf{k}_\perp)$ as functions of field F and orientation angle β for three states of different symmetry of non-polar molecule H_2^+ and one state of polar molecule HeH^{2+}.

In contrast to atomic cases, molecular systems possess a desire feature that the observables are orientation dependent, since the spherical symmetry is no longer the case. The situation now requires a more detailed consideration of the geometry. Let $\mathbf{r} = (x, y, z)$ and $\mathbf{r}' = \hat{R}\mathbf{r} = (x', y', z') \equiv (x'_1, x'_2, x'_3)$ denote the Cartesian coordinates of the active electron in the laboratory and molecular frames, respectively, where $\hat{R}$ is the Euler rotation [69] from the laboratory to the molecular frame. By our

convention, the z axis is directed along the electric field, internuclear axis z' lies in the xz plane of the laboratory frame, and the y and y' axes coincide. Then the different orientations of the molecule with respect to the field are described by a single angle β, $0 \leqslant \beta \leqslant \pi$, defining the rotation $\hat{R}$ from z to z' about the $y = y'$ axis. For diatomic molecules the potential $V(\mathbf{r})$ is axially symmetric about the internuclear axis z'. The unperturbed ($F = 0$) solutions to Eq. (2.1) can be characterized by the projection M of the electronic angular momentum onto this axis. Such solutions as functions of spherical coordinates in the molecular frame, $\mathbf{r}' = (r', \theta', \varphi')$, have the form

$$\psi_{nM}(\mathbf{r}') = f_n^{|M|}(r', \theta') \frac{e^{iM\varphi'}}{\sqrt{2\pi}}. \tag{5.2}$$

The states with $M \neq 0$ are doubly degenerate since their energy $E_{n|M|}$ does not depend on the sign of M. The correct zeroth-order wave functions are given by certain linear combinations of the two degenerate states [10]. We choose them to be real. In our geometry, one of them is even (+) and the other is odd (−) with respect to the reflection $y \to -y$,

$$\psi^+_{n|M|}(\mathbf{r}') = \frac{1}{\sqrt{2}} \left[\psi_{n|M|}(\mathbf{r}') + \psi_{n-|M|}(\mathbf{r}')\right] = f_n^{|M|}(r', \theta') \frac{\cos|M|\varphi'}{\sqrt{\pi}}, \tag{5.3a}$$

$$\psi^-_{n|M|}(\mathbf{r}') = \frac{1}{i\sqrt{2}} \left[\psi_{n|M|}(\mathbf{r}') - \psi_{n-|M|}(\mathbf{r}')\right] = f_n^{|M|}(r', \theta') \frac{\sin|M|\varphi'}{\sqrt{\pi}}. \tag{5.3b}$$

In the calculations below, we consider only states with $M = 0$ (σ states) and $|M| = 1$ (π states). The σ states are even and do not have nodes. The even and odd π states are denoted by π^+ and π^-, respectively; they have nodal planes which for $\beta = 0$ coincide with the yz and xz planes, respectively. The structure of the σ and $\pi^\pm$ states is illustrated below when we discuss the results.

Let E_0 and $\psi_0(\mathbf{r}')$ denote the energy and wave function of the unperturbed initial bound state in the molecular frame. By applying the standard perturbation theory

[10], in the presence of a nonzero field for this state we obtain

$$\mathcal{E} = E_0 - \mu_{z'} \cos\beta F - \frac{1}{2}(\alpha_{x'} \sin^2\beta + \alpha_{z'} \cos^2\beta)F^2 + O(F^3), \tag{5.4a}$$

$$\psi(\mathbf{r}') = \psi_0(\mathbf{r}') + \psi_1(\mathbf{r}')F + O(F^2), \tag{5.4b}$$

where

$$\psi_1(\mathbf{r}') = -\chi_{x'}(\mathbf{r}') \sin\beta + \chi_{z'}(\mathbf{r}') \cos\beta, \tag{5.5}$$

and

$$\mu_{x'_i} = -\langle\psi_0|x'_i|\psi_0\rangle, \tag{5.6a}$$

$$\alpha_{x'_i} = -2 \sum_{nM\neq 0} \frac{|\langle\psi_{nM}|x'_i|\psi_0\rangle|^2}{E_0 - E_{n|M|}}, \tag{5.6b}$$

$$\chi_{x'_i}(\mathbf{r}') = \sum_{nM\neq 0} \frac{\langle\psi_{nM}|x'_i|\psi_0\rangle}{E_0 - E_{n|M|}} \psi_{nM}(\mathbf{r}'). \tag{5.6c}$$

In Eq. (5.4a), we have taken into account that the components of the permanent dipole moment vector perpendicular to the internuclear axis vanish, namely $\mu_{x'} = \mu_{y'} = 0$, and the static dipole polarizability tensor in the molecular frame is diagonal, $\alpha_{x'_i x'_j} = \alpha_{x'_i}\delta_{ij}$, where $\alpha_{x'_i}$ is the polarizability in the direction of the x'_i axis. All terms retained in expansions (5.4) are needed for the implementation of the WFAT of the leading and first order. More specific forms of the above formulas for σ and $\pi^{\pm}$ states and some details of their implementation in the present calculations are given in Appendix D. We are about to compare the WFAT results obtained by implementing general equations of Chapter 3 and particular expansions (5.4) with accurate numerical results obtained by solving Eq. (2.1) using the program developed in Refs. [48, 49, 50] for H_2^+ and HeH^{2+}.

5.1 Nonpolar ion H_2^+

All the calculations for H_2^+ were performed with $Z_1 = Z_2 = 1$, $(z_1, z_2) = (1, -1)$, which corresponds to the equilibrium internuclear distance $R = 2$ for the ground $1s\sigma$ state, and $\epsilon = 0.09$. Because of the symmetry of this potential with respect to the reflection $z' \to -z'$ in the molecular frame, all the observables are invariant under the transformation $\beta \to \pi - \beta$, so it is sufficient to consider orientations in the interval $0° \leqslant \beta \leqslant 90°$. For this potential $Z = 2$, $\mathbf{D} = \mathbf{0}$, and $\mu_z = 0$. Thus A_ν does not depend on β, while the orientation dependence of B_ν manifests itself through α_{zz} and a_ν. The fitting procedure with Eq. (3.13) up to $n = 4$ is applied for ensembles of g_ν and a_ν sampled in the ranges of $\eta \in [4; 20]$ and $[5; 19]$, respectively, to yield their asymptotic values. We will analyze the effects of first-order correction terms for three lowest states of different symmetry $1s\sigma$ and $2p\pi^\pm$ by comparing the WFAT with exact results of asymptotic coefficient f_ν and complex energy E calculated by the Siegert-state approach [49, 50].

5.1.1 Ground $1s\sigma$ state

The field-free energy of the $1s\sigma$ state in the present soft-core model $E_0 = -0.962\,366$ is slightly higher than the corresponding energy of $-1.102\,634$ for the pure Coulomb potential with $\epsilon = 0$. The polarizabilities calculated using Eqs. (D.2a) and (D.2b) are $\alpha_{x'} = 2.8775$ and $\alpha_{z'} = 5.9095$, respectively. At all angles β, the dominant ionization channel is $\nu = (0, 0)$, so the boundary of the over-the-barrier ionization regime estimated from Eq. (3.44) is $F_c = 0.18$. We obtain $A_{00} = -0.715$; the value of B_{00} as a function of β is shown in the top panel of Fig. 5.1.

We first consider the asymptotic coefficients f_ν appearing in Eq. (2.17). Figure 5.2 illustrates the behavior of these coefficients as functions of field F at three representative orientations β. The exact results (solid lines) are compared with the WFAT(1)

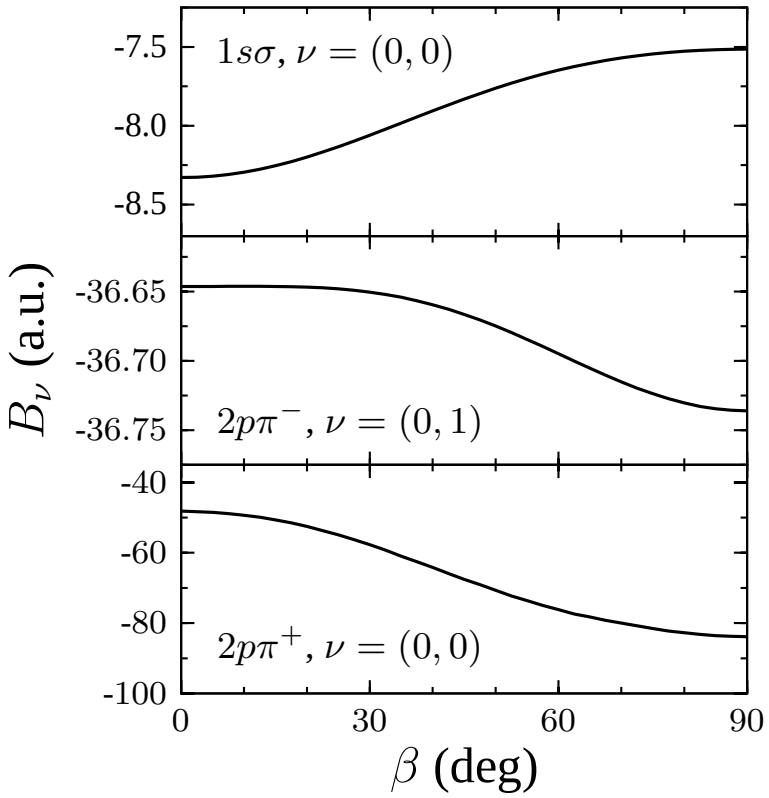

Figure 5.1: Correction coefficients B_ν, Eq. (3.17b), for the dominant ionization channel in each of the three states of H_2^+ as functions of the orientation angle β.

results (dashed lines) obtained from Eq. (3.15). In order to eliminate a rapid variation of f_ν by many orders of magnitude in the interval of F considered, which is caused by the last term in the exponent in Eq. (3.16), and thus to facilitate the comparison, we plot the ratio $f_\nu/f_\nu^{(0)}$. The upper (black lines) and lower (red lines) halves of each panel in Fig. 5.2 show the real and imaginary parts of this ratio, respectively. The results for the dominant channel are shown in the top row of the figure. At all orientations, the ratio obviously approaches 1 as $F \to 0$. For the WFAT(1) results this follows immediately from Eq. (3.15). The exact results stop at some nonzero F, where $\Gamma/\mathcal{E} \sim 10^{-10}$. The present calculations based on double-precision arithmetics cannot be continued to smaller F, where Γ and f_ν become too small, because of the round-off errors. However, by extrapolating the exact results to $F = 0$ one can expect that the ratio approaches unity, which is consistent with the prediction of the WFAT.

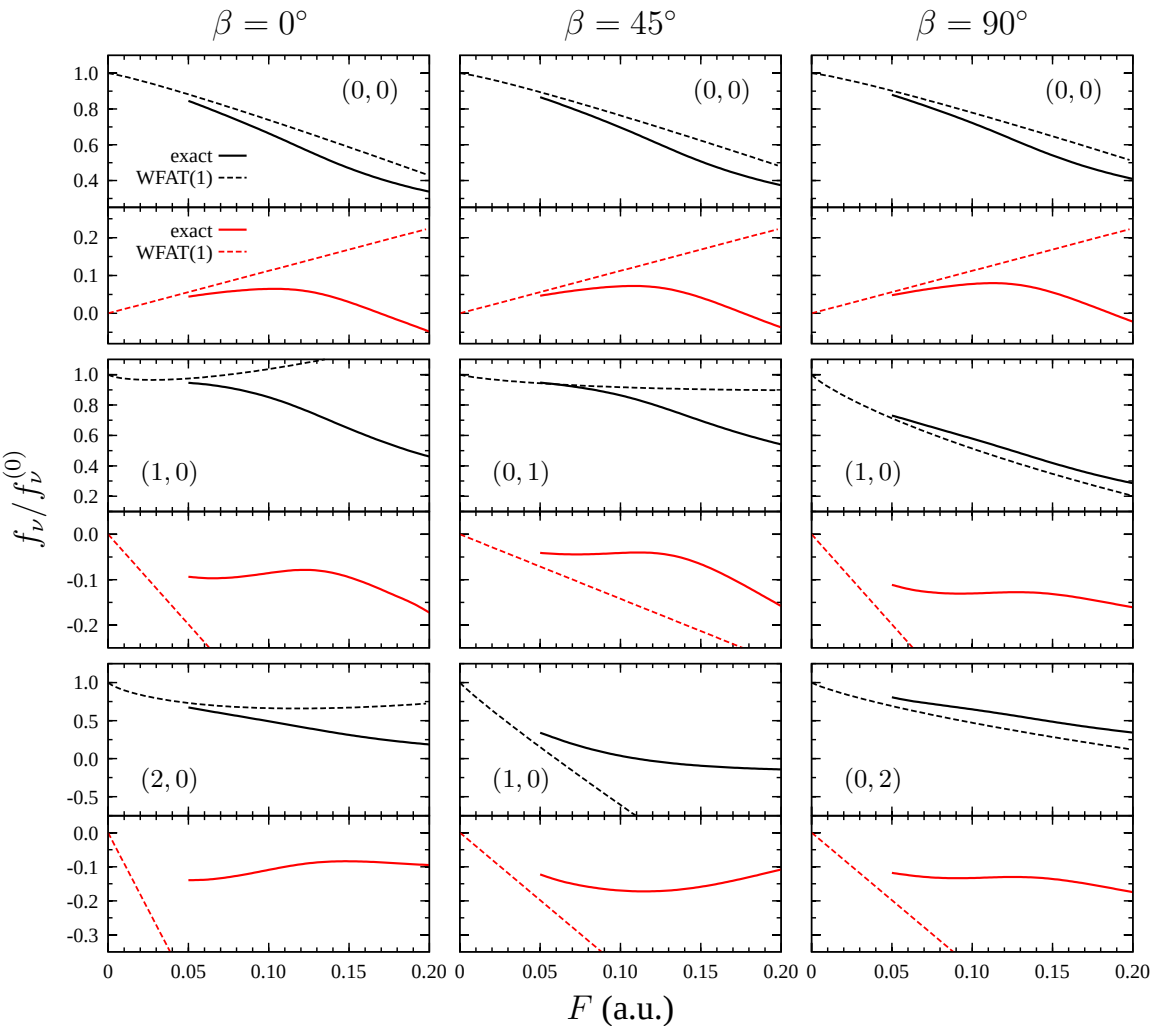

Figure 5.2: Ratios of the first-order WFAT result (dashed lines) and exact calculation (solid lines) for coefficient f_ν to the leading-order approximation $f_\nu^{(0)}$, Eq. (3.16), when the H_2^+ ion is in its ground $1s\sigma$ state.

Moreover, the difference between the exact and WFAT(1) results is seen to decrease $\propto F^2$ as $F \to 0$, as it should be according to Eq. (3.15). Note that this holds for both the real and imaginary parts of the ratio, and hence Eq. (3.15) describes correctly not only the absolute value of f_ν, but also its phase. Because of the symmetry of the $1s\sigma$ state, it depends on β for which of the higher channels $f_\nu \neq 0$. For example, at $\beta = 0°$, the SS eigenfunction is axially symmetric about the z axis, and therefore all f_ν with $m \neq 0$ vanish. At $\beta = 90°$, the eigenfunction is even with respect to the reflection $x \to -x$, and hence f_ν have nonzero values only for channels with even m.

The middle and bottom rows in Fig. 5.2 show the ratio $f_\nu/f_\nu^{(0)}$ for two of the higher channels at each β. These coefficients are more than four orders of magnitude smaller than the coefficient for the dominant channel, so it is more difficult to calculate them accurately. Nevertheless, their behavior also agrees with Eq. (3.15). All this confirms the consistency of the WFAT as well as the high accuracy of our 'exact' results.

Other important characteristics of the SS are energy and ionization rate. The top panels in Fig. 5.3 describe the ground-state energy $\mathcal{E}$ for different configurations. For all cases, the perturbed energy (red line) varies quadratically with F due to the vanishing dipole moment, see Eq. (5.4a). This behavior precisely follows the exact calculation (black line) in the tunneling regime $F < F_c$. In the over-barrier regime

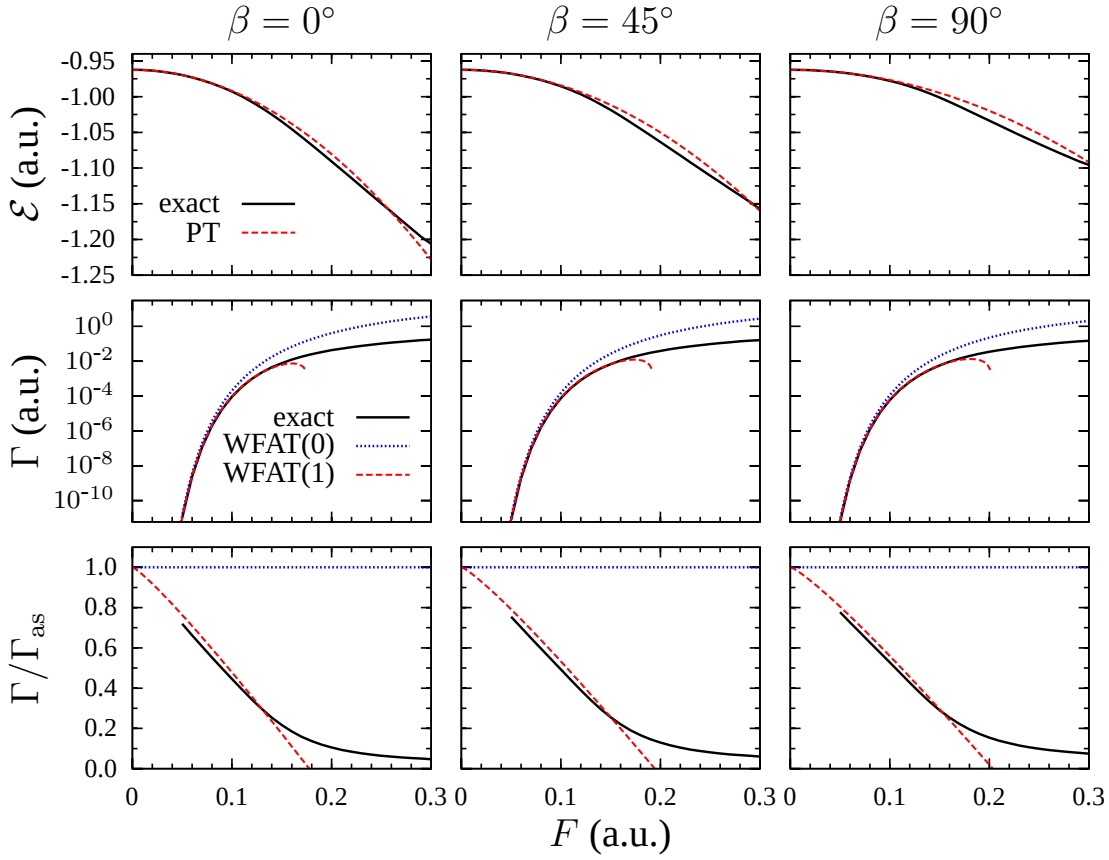

Figure 5.3: The energy $\mathcal{E}$ and ionization rate Γ for the $1s\sigma$ state of the H_2^+ ion as functions of electric field F at three representative orientation angles β. Bottom row: the ratio of the tunneling rate to its leading-order approximation Γ_{as}, Eq. (3.31) with $m = 0$.

$F > F_c$, the energies at different β almost linearly decrease and will depart from their exact values after some accidental crossing point. Generally, energy $\mathcal{E}$ shifts upward as the molecular axis gets far from the parallel orientation, since $\alpha_{x'} < \alpha_{z'}$. We next consider the ionization rate presented in the middle panels of Fig. 5.3. The WFAT results of the leading order and first order are obtained from Eq. (3.31) with $m = 0$ and Eq. (3.29), respectively. The yield at first grows very rapidly, then increases more gently at larger field. This is a typical transition from the tunneling to the over-the-barrier ionization. The WFAT(0) consistently overestimates the rate, while the WFAT(1) is much closer to the exact results up to a field $\approx F_c$, where the right-hand side of Eq. (3.29) becomes negative. To eliminate the variation of the rate by many orders of magnitude and thus facilitate comparison of the different results on a linear scale, in the bottom row of the figure we show the ratio $\Gamma/\Gamma_{\rm as}$. Because of the round-off errors mentioned above, the exact calculations cannot be continued to smaller F. However, even the available results unambiguously confirm Eq. (3.29). The correction terms in this equation, not included in Eq. (3.31), essentially improve the agreement with the exact results throughout the tunneling regime $F < F_c$, where the WFAT is expected to apply. Note that at all β the ratio approaches unity from below as $F \to 0$. This is explained by the fact that the term with B_{00} dominates over the other correction terms in Eq. (3.29) (the term with A_{00} becomes dominant only at very small F), and this term is negative, see the top panel of Fig. 5.1.

The dependence of the ionization rate on orientation angle β for several representative values of F is shown in Fig. 5.4. To bring the results for the different fields to the same scale, we plot the rate divided by the field factor (3.28) for the dominant ionization channel. As follows from Eq. (3.31), within the WFAT(0) the ratio is given by the structure factor G_{00} squared. For the present nonpolar molecule $\mu_z = 0$ and G_{00} coincides with the coefficient g_{00} in the asymptotic tail of the unperturbed bound-state wave function defined by Eq. (3.11). Thus the WFAT(0) results for the

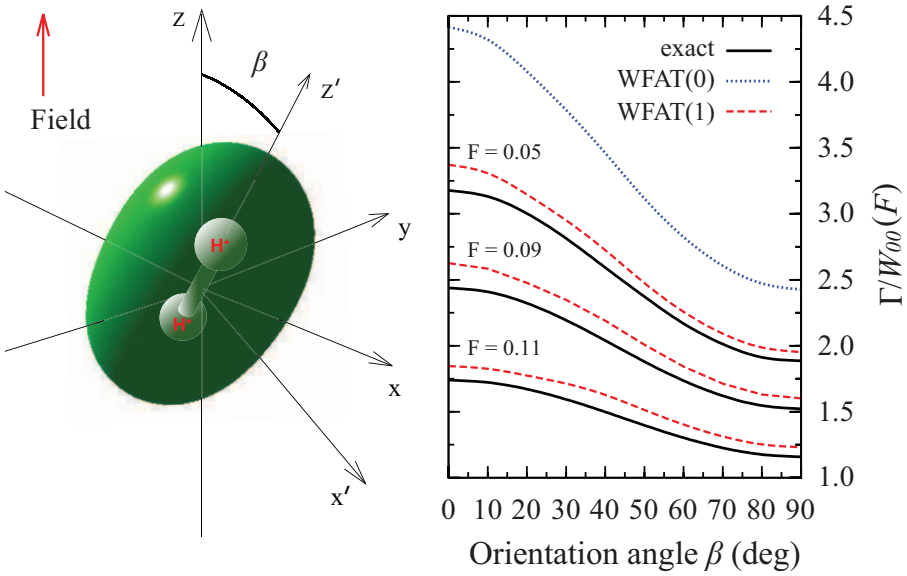

Figure 5.4: Left panel: the unperturbed wave function of H_2^+ in the ground $1s\sigma$ state. Right panel: normalized ionization rate $\Gamma/W_{00}(F)$ for the $1s\sigma$ state as functions of orientation angle β for three representative values of field.

ratio do not depend on F. The exact results should approach the WFAT(0) curve as $F \to 0$. This is indeed the case. The WFAT(1) results do depend on F and are in much better agreement with the exact results. For all values of F considered, the rate maximizes at $\beta = 0°$ and minimizes at $\beta = 90°$, that is the electron is more easily ionized in parallel than in perpendicular orientation. This conclusion agrees with the results of the time-dependent calculations of the ionization yield for $H_2^+(1s\sigma)$ in intense laser fields [71, 70, 72, 73]. The WFAT(0) correctly reproduces the shape of the dependence of Γ on β, and hence this dependence is determined by the asymptotic coefficient g_{00}. This implies that the correction terms in Eq. (3.29) for the present case only weakly depend on β. The WFAT(1) incorporating these terms essentially improves the magnitude of Γ at all orientations.

We now turn to the discussion of the TMD. We consider $P(\mathbf{k}_\perp)$ defined by Eq. (2.23) as a function of polar coordinates $(k_\perp, \varphi_k)$ in the plane of the transverse momentum $\mathbf{k}_\perp$. For the $1s\sigma$ state, the TMD is exactly isotropic (that is, does not depend on φ_k) at $\beta = 0°$. According to the WFAT, it should remain almost isotropic

at $\beta \neq 0°$, because the dominant ionization channel has $m = 0$. Figure 5.5 shows the cuts of the TMD along the ray at $\varphi_k = 0$ for several representative values of β and F. The WFAT(0) and WFAT(1) results are obtained from Eq. (3.41) for even states with $m = 0$ and Eq. (3.38), respectively. As follows from Eq. (3.41), in the weak-field limit the TMD as a function of $k_\perp$ should have a Gaussian shape with the width $\propto F^{1/2}$. This is qualitatively confirmed by the exact results; in particular, the width of the TMD obviously grows with F. However, the magnitudes of the WFAT(0) and exact

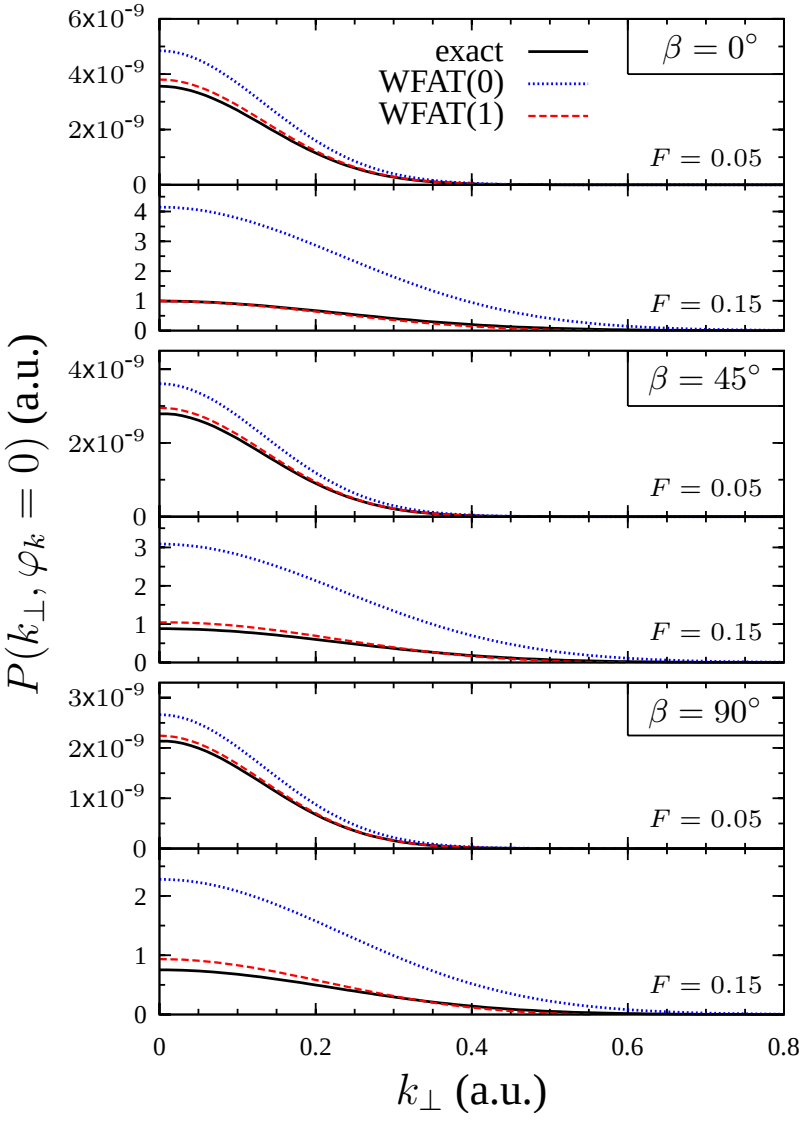

Figure 5.5: Transverse momentum distributions for the $1s\sigma$ state of H_2^+ as functions of $k_\perp$ for three representative orientation angles β and different field strengths F. The cuts are made along the ray $\varphi_k = 0$.

results are different, and this difference grows with F. The correction terms included in Eq. (3.38) make the agreement with the exact results much better.

A more subtle feature is the appearance of an anisotropy of the TMD (that is, its dependence on φ_k) at $\beta \neq 0°$, which is not explained by the leading-order approximation (3.41). To illustrate this feature, we present in Fig. 5.6 the cuts of the TMDs shown in Fig. 5.5 (except for the ones at $\beta = 0°$, which are isotropic) along the circle at $k_\perp = 0.1$. To emphasize the anisotropic part, we subtract from $P(k_\perp, \varphi_k)$ its average over φ_k defined by

$$\bar{P}(k_\perp) = \frac{1}{2\pi} \int_0^{2\pi} P(k_\perp, \varphi_k)\, d\varphi_k. \tag{5.7}$$

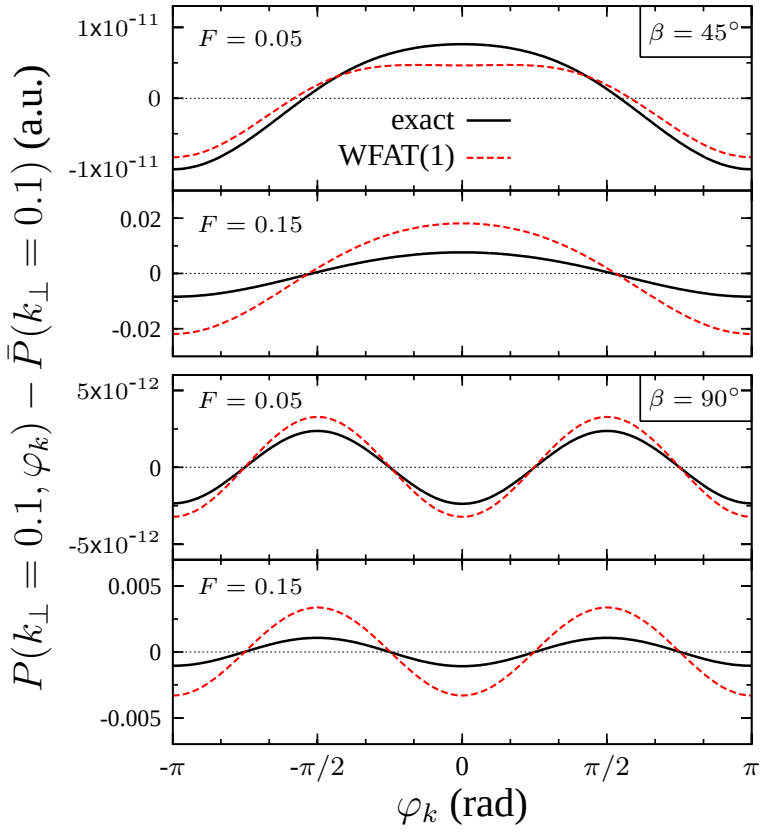

Figure 5.6: Subtraction of the transverse momentum distributions $P(k_\perp, \varphi_k)$ depending on φ_k from their average values $\bar{P}$. The transverse momentum is $k_\perp = 0.1$ in all cases.

Figure 5.6 compares the exact and WFAT(1) results for the difference. At $\beta = 45°$, the dominant correction to Eq. (3.41) at the value of $k_\perp$ considered comes from the last term in Eq. (3.38). This term is $\propto \cos\varphi_k$, which explains the shape of the dependence of $P(k_\perp, \varphi_k)$ on φ_k in this case. However, the coefficient G_{01} in this term vanishes at $\beta = 90°$. All the other corrections in Eq. (3.38) depend on φ_k as $\cos 2\varphi_k$, which is again in accordance with the exact results. Thus Eq. (3.38) correctly describes the shape of the anisotropic part of the TMD and relates it to the symmetry of the state. It also reproduces its magnitude; as expected, the agreement with the exact results becomes worse as F grows.

5.1.2 Excited $2p\pi^-$ state

It is convenient to begin the discussion of states having $M \neq 0$ with the odd $2p\pi^-$ state, because in this case the same ionization channel $\nu = (0, 1)$ remains dominant at all orientation angles β. The field-free energy of this state in the present soft-core model is $E_0 = -0.418\,947$, while in the pure Coulomb potential with $\epsilon = 0$ it is $-0.428\,772$. The polarizabilities calculated using Eqs. (D.4a) and (D.4b) are $\alpha_{x'} = 19.2303$ and $\alpha_{z'} = 23.4056$. The correction coefficients (3.17) were calculated using Eqs. (D.4c) and (D.4d). We have $A_{01} = -1.580$; the dependence of B_{01} on β is shown in the middle panel of Fig. 5.1. The critical field estimated from Eq. (3.44) is $F_c = 0.040$.

We again begin with comparing the exact and WFAT results for the asymptotic coefficients f_ν. Figure 5.7 shows the ratio $f_\nu/f_\nu^{(0)}$ for the dominant channel as a function of F at three representative orientations. The WFAT results are obtained from Eqs. (3.15) and (3.16). The situation is quite similar to that shown in the top row of Fig. 5.2: the ratio approaches 1 as $F \to 0$ and the difference between the exact and WFAT(1) results decreases $\propto F^2$. The results for higher channels also look similar to those in Fig. 5.2.

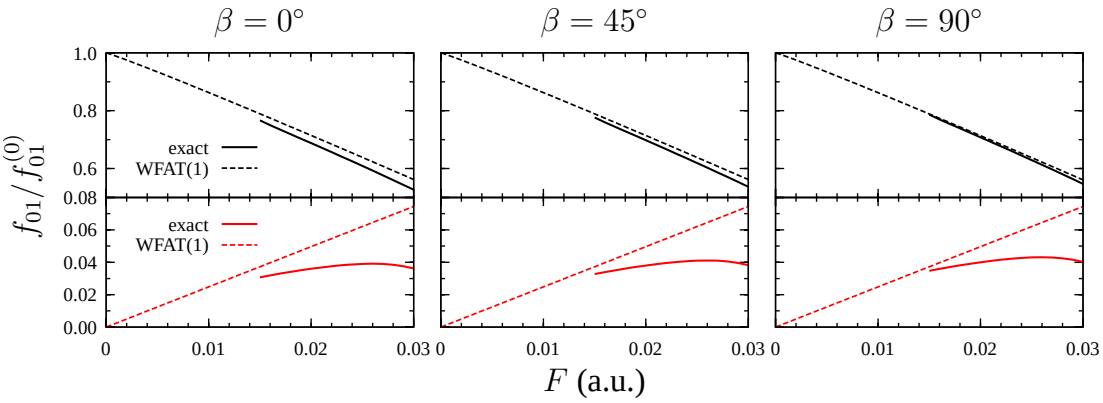

Figure 5.7: Same as in Fig. 5.2, but for the dominant channel $\nu = (0, 1)$ in the odd $2p\pi^-$ state of H_2^+.

Figure 5.8 shows the behavior of perturbed energy $\mathcal{E}$ and ionization rate Γ as functions of F for the same orientations as in Fig. 5.7. The perturbation theory predicts a quadratic dependence of $\mathcal{E}$ when $F \to 0$ due to $\mu_z = 0$. For increasing field, the red curves less agree with the black ones, as expected. Regarding the

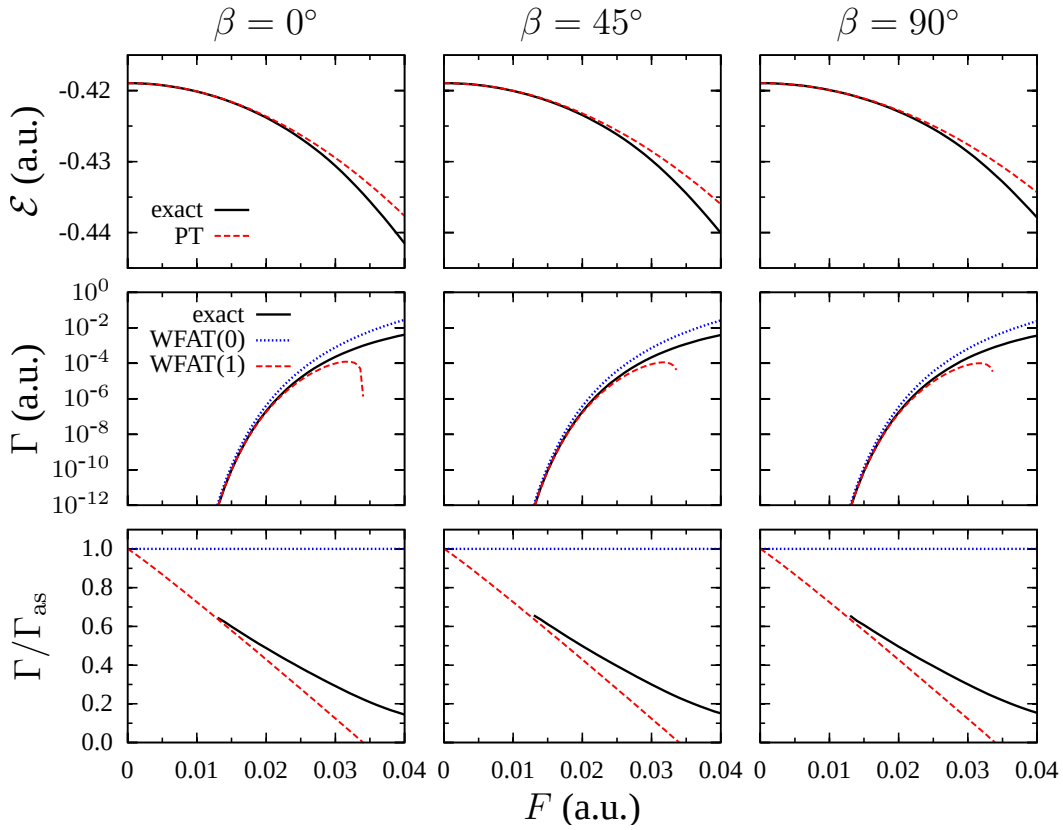

Figure 5.8: Same as in Fig. 5.3, but for the $2p\pi^-$ state of H_2^+.

tunneling rate, the WFAT(0) and WFAT(1) results are obtained from Eq. (3.31) with $m = 1$ and Eq. (3.30), respectively. The results again look quite similar to those in Fig. 5.3. At all orientations, the WFAT(0) overestimates the rate while the WFAT(1) is in much better agreement with the exact results up to a field $\approx F_c$ where the right-hand side of Eq. (3.30) becomes negative. The bottom row of the figure presents the ratio Γ/Γ_{as} on a linear scale. It is clearly seen that the first-order correction terms in Eq. (3.30) essentially improve the WFAT results.

The full dependence of the ionization rate of the $2\,p\pi^-$ state on angle β is presented in Fig. 5.9 for several field strengths. The left panel of this figure illustrates how this state is oriented in the external field. Unlike the ground $1s\sigma$ state, where the electron cloud concentrates around the nuclei, the probability density of the excited $2\,p\pi^-$ state is localized off the nuclei due to the symmetry restriction. This state has a node in the plane xz, including in the direction of the field. This results in a suppression of tunneling ionization from this state; within the WFAT, this suppression is accounted for by an additional power of F in the field factor (3.28) for the dominant ionization channel. The orientation dependence of the ratio $\Gamma/W_{01}(F)$ is flatter than that for

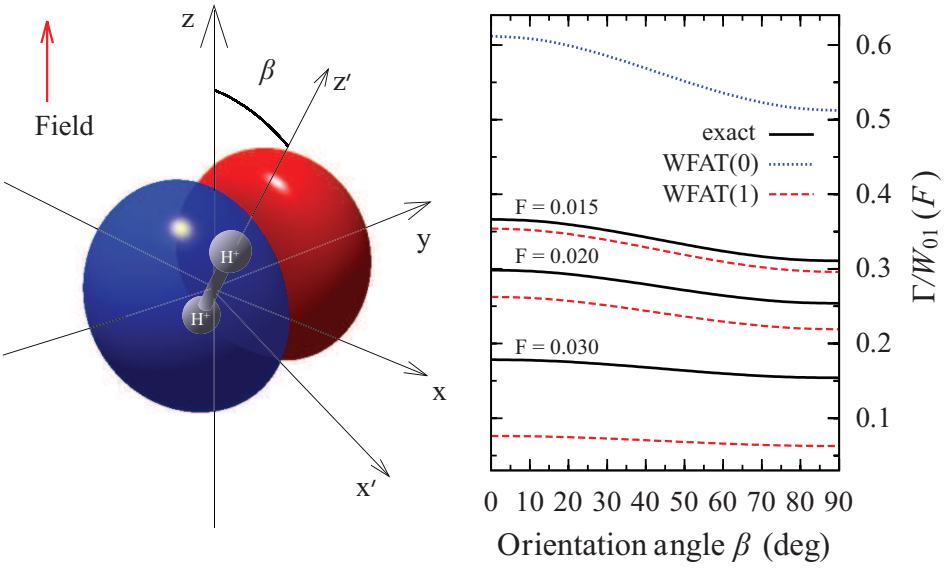

Figure 5.9: Same as in Fig. 5.4, but for the odd $2p\pi^-$ state of H_2^+.

the $1s\sigma$ state (see the right panel in Fig. 5.4). This is explained by the fact that the unperturbed $2p\pi^-$ wave function is almost axially symmetric about the y axis, and therefore all the coefficients in Eq. (3.30) only weakly depend on β. The WFAT(1) results more rapidly depart from the exact results as F grows, but still give more accurate predictions for the ionization rate than the WFAT(0) results.

For the present state, $P(k_\perp, \varphi_k)$ turns to zero at $\varphi_k = 0$ and $\pm\pi$. Figure 5.10 shows the cuts of the TMD along the ray $\varphi_k = \pi/2$ for several values of β and F. The WFAT(0) and WFAT(1) results are obtained from Eq. (3.41) for odd states with $m = 1$ and Eq. (3.40), respectively. Although the shape of the cuts as functions

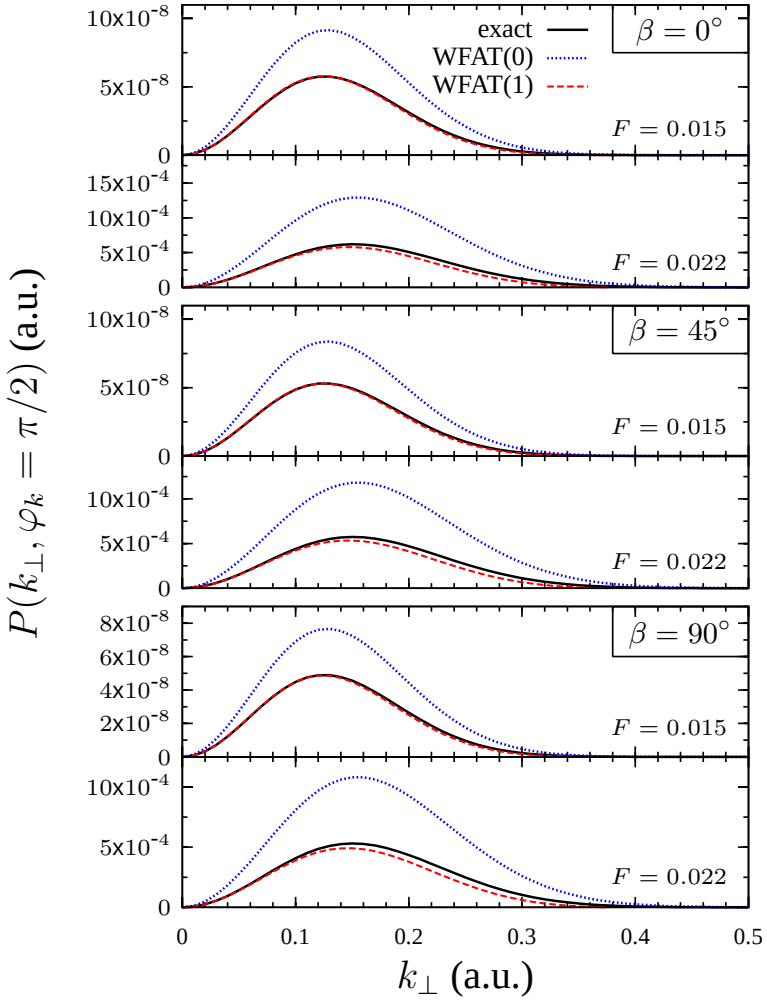

Figure 5.10: Same as in Fig. 5.5, but for the $2p\pi^-$ state of H_2^+. The cuts are made along the ray $\varphi_k = \pi/2$.

of $k_\perp$ is different from that for the $1s\sigma$ state, the situation in Fig. 5.10 is similar to that in Fig. 5.5. At all orientations and fields considered, the WFAT(0) correctly describes the shape but overestimates the magnitude of the TMD, while the WFAT(1) is in much better agreement with the exact results over a wide interval of F. The dependence of $P(k_\perp, \varphi_k)$ on φ_k is illustrated in Fig. 5.11. Here we present the cuts of the TMDs shown in Fig. 5.10 along the circle $k_\perp = 0.2$. As seen from Eq. (3.41), for the present state the TMD is anisotropic even in the leading-order approximation of the WFAT, so there is no need to subtract its average over φ_k as we did above for the $1s\sigma$ state. In all cases, the first-order corrections in Eq. (3.40) essentially improve the agreement between the WFAT and exact results.

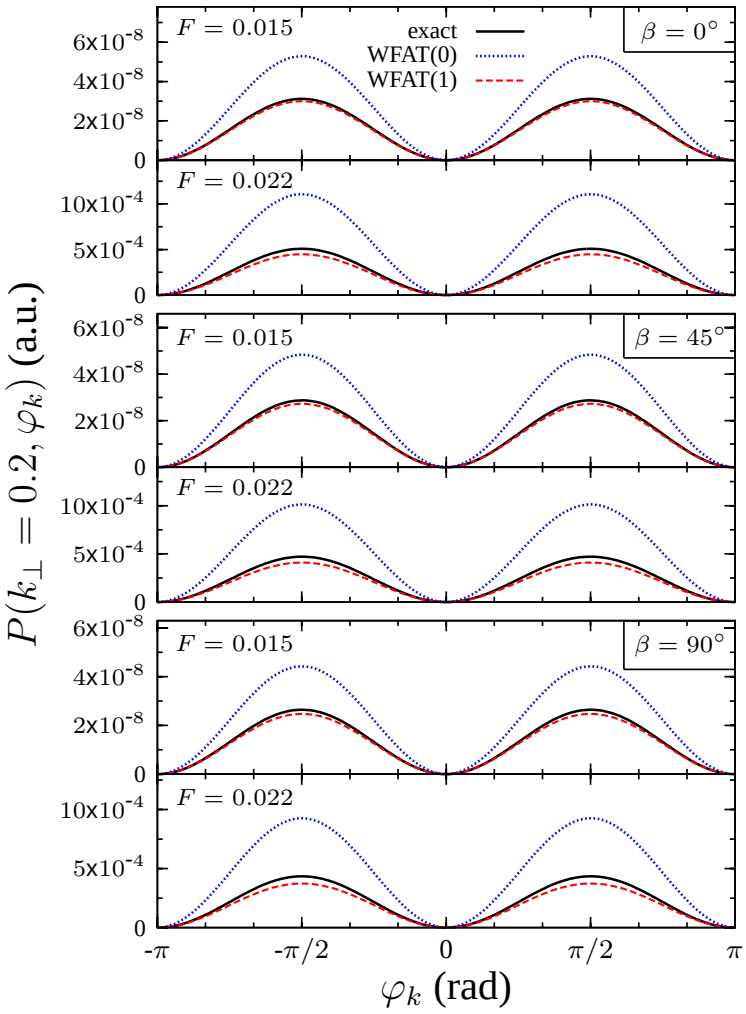

Figure 5.11: Cuts of the TMDs shown in Fig. 5.10 along the circle $k_\perp = 0.2$.

5.1.3 Excited $2p\pi^+$ state

This section is for consideration of the exited $2\,p\pi^+$ state. For $F = 0$ at any β, this state is degenerate with the odd $2p\pi^-$ state discussed above. At $\beta = 0°$ for any F, it coincides with the $2p\pi^-$ state rotated about the z axis by $\pi/2$. In this case the dominant ionization channel is $\nu = (0, 1)$. The rotation does not affect the observables, apart from a shift by $\pi/2$ of the angular argument φ_k of the TMD $P(k_\perp, \varphi_k)$. Thus the results for the $2p\pi^+$ state at $\beta = 0°$ coincide with the corresponding results for the $2p\pi^-$ state, and it is sufficient to consider orientations with $\beta \neq 0°$. In this case the dominant ionization channel is $\nu = (0, 0)$. From Eqs. (D.3a) and (D.3b) we obtain the polarizabilities $\alpha_{x'} = 93.6687$ and $\alpha_{z'} = 23.4056$. Using Eqs. (D.3c) and (D.3d) we find $A_{00} = -10.127$; the dependence of B_{00} on β is shown in the bottom panel of Fig. 5.1. The critical field estimated from Eq. (3.44) is $F_c = 0.028$.

Figure 5.12 shows the ratio $f_\nu/f_\nu^{(0)}$ for the dominant ionization channel, with the WFAT results obtained from Eqs. (3.15) and (3.16). It can be seen, at least at $\beta = 45°$, that the real part of the WFAT(1) results approaches 1 from above as $F \to 0$. This is explained by the fact that the term with A_ν in Eq. (3.15) becomes dominant as $F \to 0$, and this term is positive, because the coefficient A_{00} is negative. In fact, the same applies to all three states considered here at all β, but this behavior

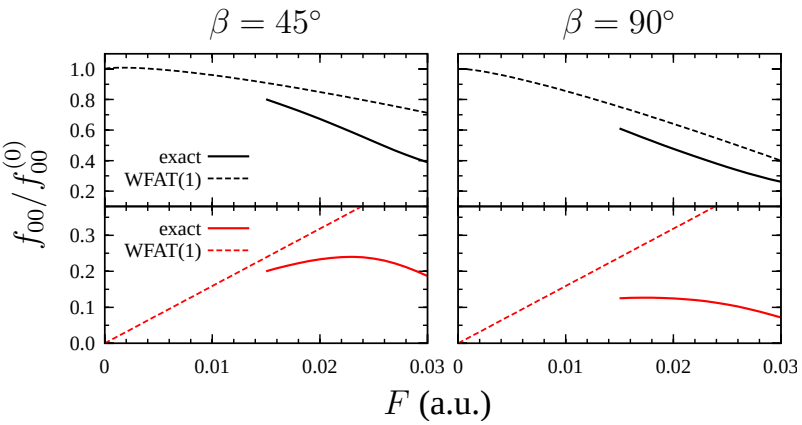

Figure 5.12: Same as in Figs. 5.2 and 5.7, but for the dominant channel $\nu = (0, 0)$ in the even $2p\pi^+$ state of H_2^+.

is not seen in the top row of Fig. 5.2 and in Fig. 5.7 because the coefficients A_ν for the dominant channel in these states have much smaller values than in the present case.

The energies of the current state obtained by the perturbation theory and exact calculation are given in the top panels of Fig. 5.13. The behavior of the red and black curves is normally expected. Unlike the ground and $2p\pi^-$ states, the energy at a fixed field strength now shifts downward with increasing angle β since $\alpha_{x'} > \alpha_{z'}$ in this case. The middle and bottom panels of Fig. 5.13 compares the exact and WFAT results for the ionization rate. Again, the WFAT(1) curve for the ratio $\Gamma/\Gamma_{\rm as}$ at $\beta = 45°$ is seen to approach 1 from above as $F \to 0$. The WFAT(1) is always closer to the exact results than the WFAT(0), but the convergence at weak fields for the present state is somewhat slower than in the previous cases.

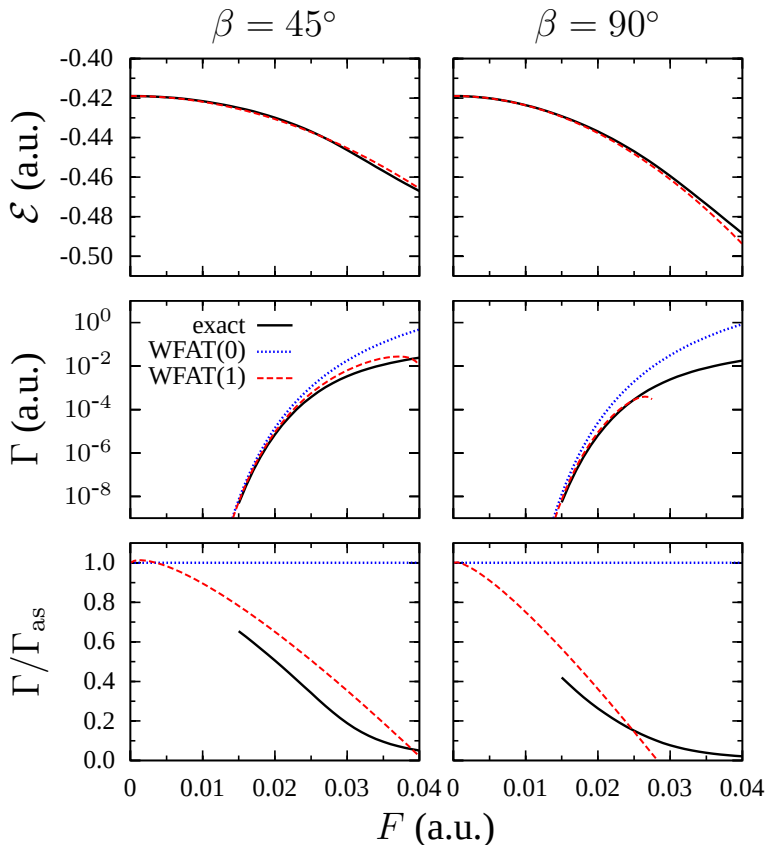

Figure 5.13: Same as in Figs. 5.3 and 5.8, but for the $2p\pi^+$ state of H_2^+.

The dependence of the ionization rate on β for several values of F is shown in Fig. 5.14. There are three main features to be noticed from the figure. First, the exact rates become very small (but remain nonzero) at $\beta = 0°$. Within the WFAT, this is explained by the fact that, on the one hand, the partial ionization rate for the dominant channel $(0, 0)$ vanishes at $\beta = 0°$, because the structure factor G_{00} vanishes. On the other hand, the partial rate for the next-to-the-dominant channel $(0, 1)$, that has a nonzero value at $\beta = 0°$, is suppressed by an additional power of F in the field factor (3.28). The WFAT(1) results from Eq. (3.29) account for the contributions from both these channels and restore nonzero values of the rates. Second, the exact rates have a shallow minimum at $\beta = 90°$ and a maximum at some intermediate β whose position shifts towards 90° as F decreases. Such a maximum in the ionization yield was also found in time-dependent calculations for the present system in an intense laser field [71]. The WFAT(1) results reproduce the position of the maximum of the exact rates and converge to the WFAT(0) curve as $F \to 0$. The third feature is a rapid variation of the shape of the orientation dependence of the rate with F, much more rapid than in the previous cases. This is explained by a large value of the difference between the polarizabilities $\alpha_{x'}$ and $\alpha_{z'}$ in the present case, resulting in a strong dependence of B_{00} on β, see the bottom panel in Fig. 5.1.

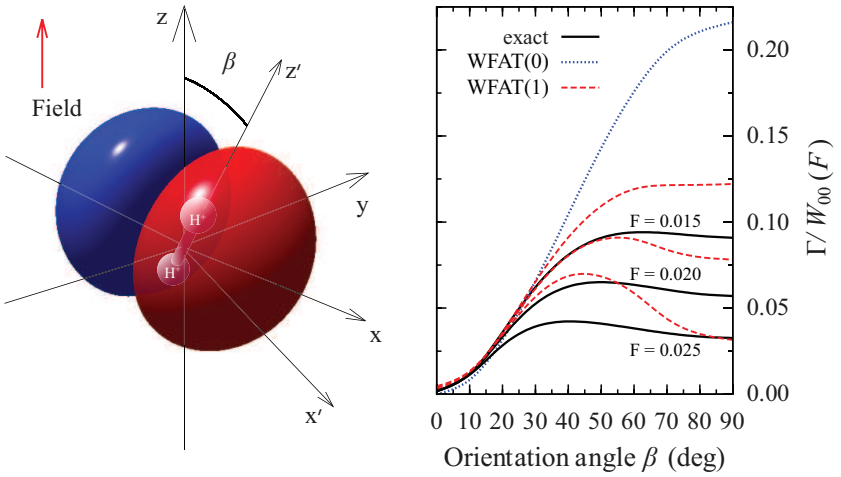

Figure 5.14: Same as in Figs. 5.4 and 5.9, but for the even $2p\pi^+$ state of H_2^+.

A peculiarity of the $2p\pi^+$ state in comparison with the states discussed above is that the structure factor for the dominant channel G_{00} turns to zero at $\beta = 0°$, because of the symmetry of the state. As a consequence, at sufficiently large β for a given F channel $(0,0)$ is dominant, but at small β channel $(0,1)$ becomes dominant. The change of the dominant channel occurs at a critical angle $\beta_c(F) = O(F^{1/2})$ [51, 49], where the contributions from the two channels become comparable. The effect of this interplay on the ionization rate is illustrated in Fig. 5.15. The left panel presents the leading-order contributions to the square brackets in Eq. (3.29) from channels $(0,0)$ and $(0,1)$ as functions of β. The former term does not depend on F; the latter one is shown for a sufficiently weak field $F = 0.02 < F_c$. The two terms become equal at $\beta \approx 6°$, which can be taken as the value of $\beta_c(F)$ for $F = 0.02$. The right panel shows the same ratio $\Gamma/\Gamma_{\rm as}$ as in the bottom row of Fig. 5.13, but at smaller values of β. One can see that in this case the ratio as a function of F behaves very differently. At a given β, it attains a maximum and then approaches 1 from above as F decreases. The WFAT(1) curve for $\beta = 6°$ passes through the value of 2 at $F \approx 0.02$, which

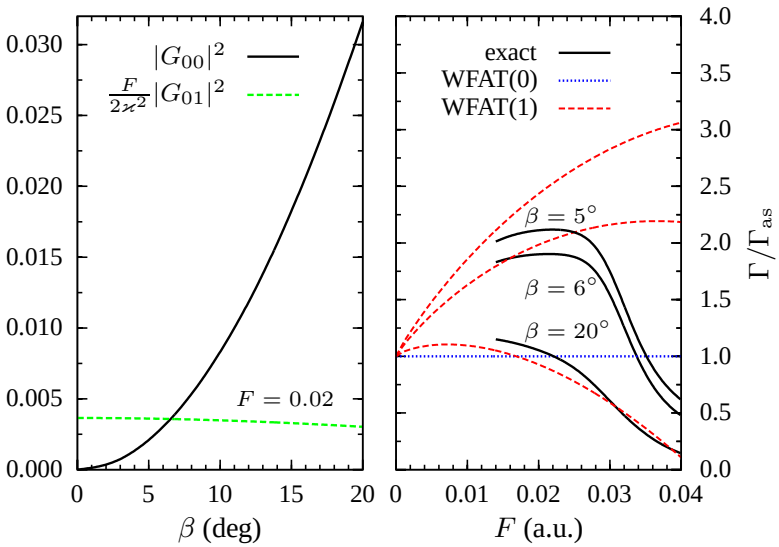

Figure 5.15: Left panel: leading-order contributions to the square brackets in Eq. (3.29) for the ionization rate of the $2p\pi^+$ state of H_2^+ from channels $\nu = (0,0)$ (solid black line) and $\nu = (0,1)$ for $F = 0.02$ (dashed green line) as functions of β. Right panel: ratio of the rate to its leading-order WFAT value $\Gamma_{\rm as}$ (as in the bottom row of Fig. 5.13, but at smaller β).

agrees with the point where the two curves in the left panel cross. This means that at this β the leading-order contribution from channel $(0,1)$ in Eq. (3.29) dominates over the first-order corrections to the contribution from channel $(0,0)$. As β grows, the relative role of the last term in Eq. (3.29) decreases, and we return to the situation where the term with B_{00} dominates and the ratio approaches 1 from below, as in Fig. 5.13. The exact results in Figs. 5.13 and 5.15 confirm this prediction of the WFAT. We emphasize that such an agreement between the exact and WFAT results would not be possible if one retained only the leading-order terms for each of the two channels in Eq. (3.29), omitting the correction terms with A_{00} and B_{00}.

We finally consider the TMD for the present state at sufficiently large β, where channel $(0,0)$ is dominant. In this case, the TMD is almost isotropic, as for the $1s\sigma$ state. Figure 5.16 presents the cuts of the TMD along the ray $\varphi_k = 0$. To make the

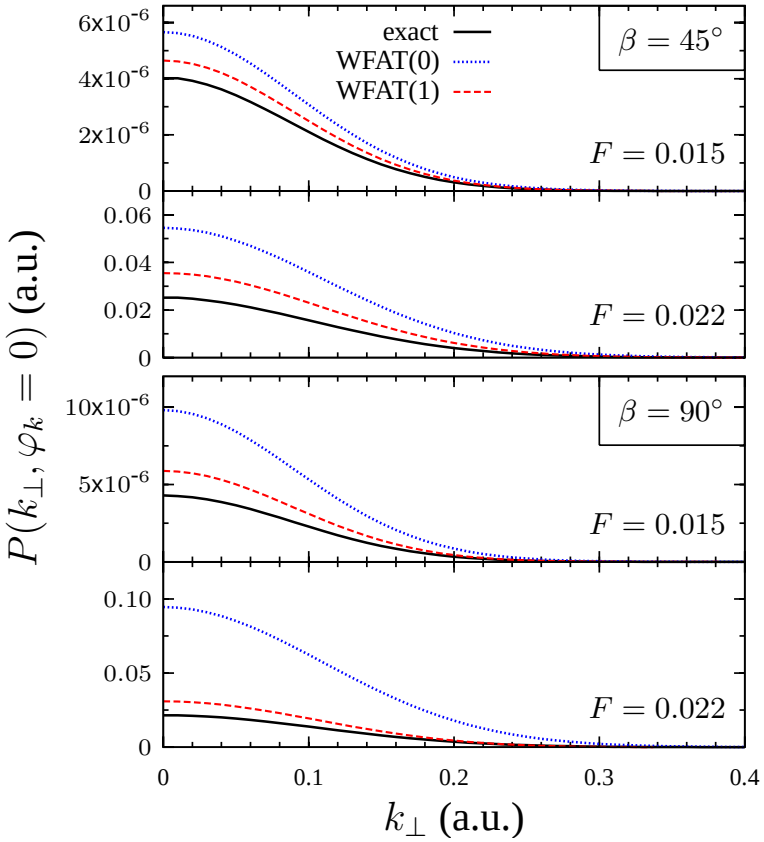

Figure 5.16: Same as in Figs. 5.5 and 5.10, but for the $2p\pi^+$ state of H_2^+. The cuts are made along the ray $\varphi_k = 0$.

anisotropic part visible, we again subtract from $P(k_\perp, \varphi_k)$ its average $\bar{P}(k_\perp)$ defined by Eq. (5.7). The cuts of the difference along the circle $k_\perp = 0.2$ are shown in Fig. 5.17. These results look similar to those in Figs. 5.5 and 5.6.

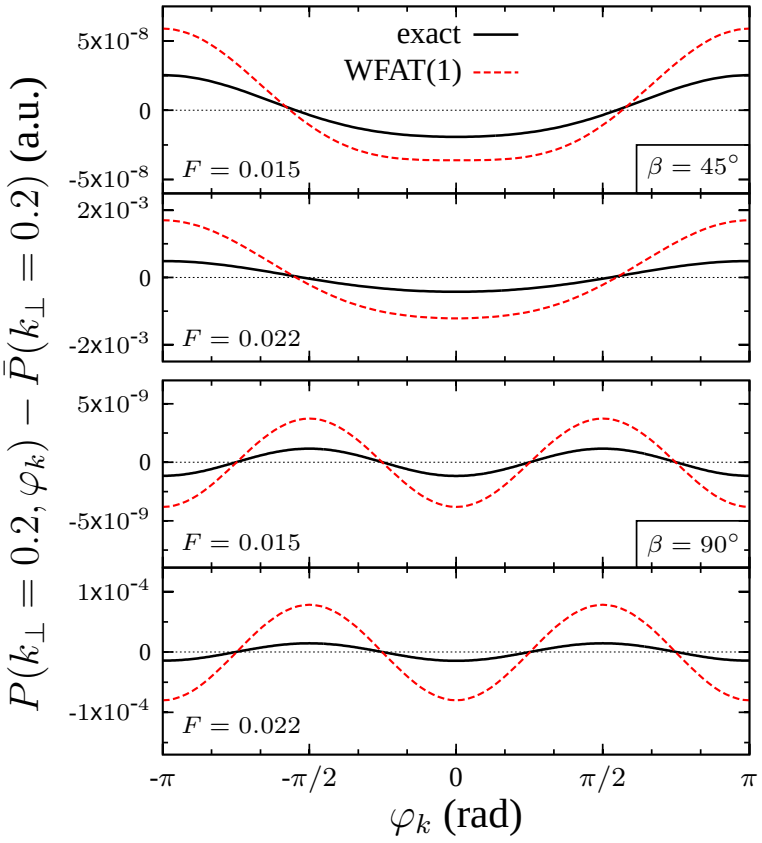

Figure 5.17: Cuts of the TMDs shown in Fig. 5.16 along the circle $k_\perp = 0.2$. To emphasize the anisotropic part of the TMDs, their average $\bar{P}(k_\perp)$ over φ_k, Eq. (5.7), are subtracted.

5.2 Polar ion HeH^{2+} in the $2p\sigma$ state

It is important to demonstrate the performance of the WFAT including the first-order correction terms also for a polar molecule. To this end, we consider the lowest bonding state $2p\sigma$ of HeH^{2+}. Time-dependent calculations for this system in intense laser fields were reported in Ref. [77] and references therein. The equilibrium internuclear distance for the $2p\sigma$ state is $R = 3.89$. The molecule is modeled by the potential (5.1) with $Z_1 = 1$, $Z_2 = 2$, $z_1' = 3.112$, $z_2' = -0.778$, and $\epsilon = 0.1$. In this case $Z = 3$ and

$\mathbf{D} = 1.556\mathbf{e}_{z'}$. The field-free energy in the soft-core model is $E_0 = -0.939\,749$, while for $\epsilon = 0$ it is $-1.045\,349$. The electronic dipole moment in the molecular frame is $\mu_{z'} = -2.202\,070$ and the polarizabilities are $\alpha_{x'} = 5.6887$ and $\alpha_{z'} = 12.4554$. The dominant ionization channel at all β is $(0, 0)$ and the critical field is $F_c = 0.095$.

We restrict our treatment of this molecule to considering the SS eigenvalue (2.18) at the parallel and antiparallel orientations with $\beta = 0°$ and $180°$, respectively, see the left side of Fig. 5.18 for the orientations of this state in the external field. Figure 5.19 compares the exact results with weak-field approximations. In the top row, the energy is compared with the predictions of perturbation theory, Eq. (5.4a). At $\beta = 0°$, the results are in close agreement with each other up to $F \approx 0.07$, where the exact energy rapidly changes its behavior and goes down at stronger fields. This is explained by the fact that the unperturbed state for $F = 0$ is localized on proton in the upper potential well near $\mathbf{r} = z_1'\mathbf{e}_z$. An interatomic barrier potential is created by any nonzero field as portrayed on the right side of Fig. 5.18. As F grows, the energy of this state goes up, while the energy of the lower of the $n = 2$ parabolic states localized on the alpha-particle in the lower potential well near $\mathbf{r} = z_2'\mathbf{e}_z$ goes

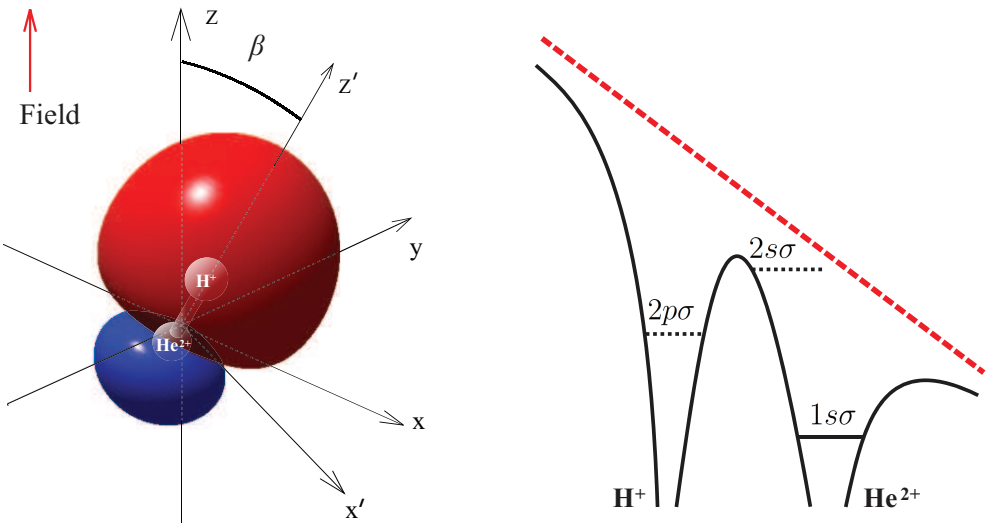

Figure 5.18: Left panel: the unperturbed wave function of HeH^{2+} in the excited $2p\sigma$ state. Right panel: interatomic potential (Solid lines) of HeH^{2+} modified by external field (Dashed line) for $\beta = 0$.

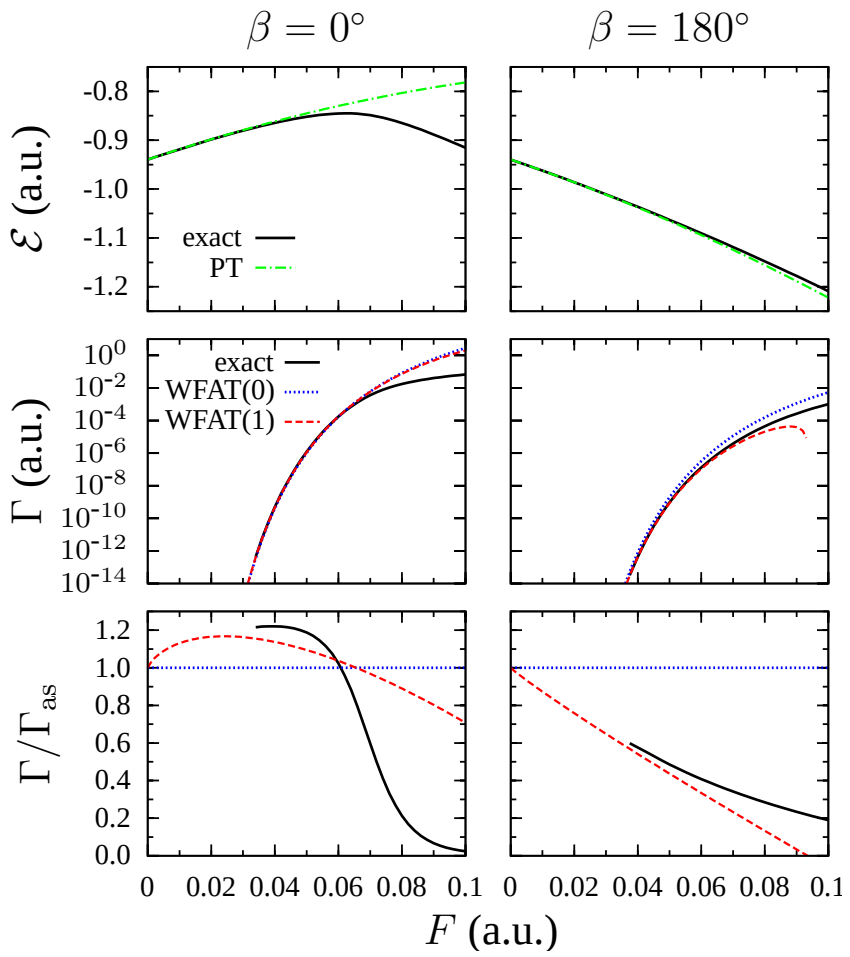

Figure 5.19: Energy $\mathcal{E}$ and ionization rate Γ for the $2p\sigma$ state of ion HeH^{2+} as functions of the electric field F at two representative orientation angles β.

down. The energies of the two states pass through an avoided crossing at $F \approx 0.05$, which is seen in the top left panel in Fig. 5.19. This does not happen if the state is initially localized in the lower well, as is the case at $\beta = 180°$, and perturbation theory in this case works well over the whole interval of F considered. In the middle row, the exact results for the ionization rate are compared with the predictions of the WFAT, Eq. (3.31) with $m = 0$ and Eq. (3.29). To facilitate the comparison, the ratio $\Gamma/\Gamma_{\rm as}$ is shown on a linear scale in the bottom row of the figure. The avoided crossing at $F \approx 0.05$ is seen to manifest itself also in the field dependence of the ionization rate at $\beta = 0°$. At this orientation $A_{00} = -6.9473$. The term with this coefficient in Eq. (3.29) is the dominant correction at small F, which explains why

the WFAT(1) curve in the bottom left panel attains a maximum and approaches 1 from above as $F \to 0$. On the other hand, for $\beta = 180^\circ$ we have $A_{00} = 0.8925$. The positive value of this coefficient explains why the WFAT(1) curve in the bottom right panel approaches 1 from below as F decreases. The exact results confirm this difference in the behavior of the ratio $\Gamma/\Gamma_{\rm as}$ at the two orientations. The difference was noticed already in Ref. [23], but it could not be explained there without having the first-order correction terms in Eq. (3.29).

It should be noted that the $2p\sigma$ state of HeH^{2+} is unstable against a nonadiabatic electronic transition to the $1s\sigma$ state and subsequent dissociation with the lifetime of several nanoseconds [76]. The field ionization rate has the same value at $F \approx 0.045$ and 0.056 at $\beta = 0^\circ$ and 180°, respectively, which corresponds to typical amplitudes of intense laser fields of current interest. This means that theoretical simulations of the interaction of $HeH^{2+}(2p\sigma)$ with such fields must include the nonadiabatic electronic and nuclear dynamics into account.

Chapter 6

The WFAT beyond the SAEA

Until now we have stayed within the SAEA that is one-electron problem. To go beyond this approximation, the electron-electron interaction in the system should be fully taken into account, while leaving the frozen-nuclei approximation intact. This is a many-electron problem. Although the tunneling ionization of such systems was addressed before [78, 79], these considerations are not based on the unique perspective of an asymptotic expansion characterizing the phenomenon in the weak-field limit (3.1). In this chapter, we extend the WFAT presented the Chapter 3 to many-electron systems using the language of Ref. [29]. To avoid an unnecessary repeat of similar steps, only basic equations in the derivation are listed in the next section focusing on introducing new definitions. For a detailed derivation, the reader may have a look at Refs. [29, 55].

6.1 Basic equations

The nonrelativistic Hamiltonian describing the N-electron molecule in a homogeneous electric field $\mathbf{F} = F\mathbf{e}_z$ is

$$H_N = \sum_{i=1}^{N} \left[-\frac{1}{2}\Delta_i - \sum_{a=1}^{A} \frac{Z_a}{|\mathbf{r}_i - \mathbf{N}_a|} + \sum_{j=1}^{i-1} \frac{1}{|\mathbf{r}_i - \mathbf{r}_j|} + Fz_i \right]. \tag{6.1}$$

The molecule under consideration composes of A nuclei treated as fixed in space at positions $\mathbf{N}_a$, which determine the shape of the molecule and its orientation with respect to the external field. This is a consequence of the Born-Oppenheimer approximation applied in the center-of-mass frame. The nucleus-electron and electron-electron interactions represented by the second and the third summations are fully taken into account without making any further assumption. The stationary Schrödinger equation for this system reads

$$(H_N - E)\Psi(Q_N) = 0, \tag{6.2}$$

where $Q_N = (q_1, ..., q_N)$, $q_i = (\mathbf{r}_i, \sigma_i)$, and $\sigma_i = \pm 1/2$ is the spin coordinate of the i-th electron. Among the solutions to Eq. (6.2), we are interested only in *tunneling states* which coincide with a given unperturbed bound state in the absence of electric field, and possess well-defined total spin S and its projection M_S. Such a solution can be expanded in an irreducible representation of the symmetric group $\chi_{\tau S M_s}(\Sigma_N)$ as [29]

$$\Psi(Q_N) = \frac{1}{\sqrt{\tau_{NS}}} \sum_{\tau=1}^{\tau_{NS}} \psi_{\tau S}(\mathbf{R}_N)\chi_{\tau S M_s}(\Sigma_N), \tag{6.3}$$

where $\mathbf{R}_N = (\mathbf{r}_1, ..., \mathbf{r}_N)$, $\Sigma_N = (\sigma_1, ..., \sigma_N)$, and τ_{NS} is the dimension of the representation. The spacial functions $\psi_{\tau S}(\mathbf{R}_N)$ are the degenerate normalized eigenfunctions of Hamiltonian H_N.

Tunneling ionization in the weak-field limit is essentially a single-electron process [29]. In consequence of indistinguishability of the electrons, the wave function $\Psi(Q_N)$

must be antisymmetric with respect to permutations of any two electrons. It is therefore sufficient to consider the tunneling of one, say the N-th electron, whose coordinates are simplified by

$$q \equiv q_N, \quad \mathbf{r} \equiv \mathbf{r}_N, \quad \sigma \equiv \sigma_N. \tag{6.4}$$

We rewrite Hamiltonian (6.1) as follows

$$H_N = H_{N-1} - \frac{1}{2}\Delta + V(\mathbf{r}) + Fz, \tag{6.5}$$

where H_{N-1} is the Hamiltonian of the $(N-1)$-electron subsystem, and the potential felt by the tunneling electron is

$$V(\mathbf{r}) = -\sum_{a=1}^{A} \frac{Z_a}{|\mathbf{r} - \mathbf{N}_a|} + \sum_{i=1}^{N-1} \frac{1}{|\mathbf{r} - \mathbf{r}_i|}. \tag{6.6}$$

This potential asymptotically behaves as

$$V(\mathbf{r})|_{r\to\infty} = -\frac{Z}{r} - \frac{\mathbf{D}_A\mathbf{n}}{r^2} + \sum_{i=1}^{N-1} \frac{\mathbf{r}_i\mathbf{n}}{r^2}, + O(r^{-3}), \tag{6.7a}$$

$$Z = \sum_{a=1}^{A} Z_a - N + 1, \quad \mathbf{D}_A = \sum_{a=1}^{A} Z_a\mathbf{N}_a, \quad \mathbf{n} = \mathbf{r}/r, \tag{6.7b}$$

with Z and $\mathbf{D}_A$ being the total charge of the parent ion and the nuclear dipole moment. The next important step is to introduce the *ionization channels*, which are defined by

$$(\mathcal{B} - \beta_\nu)\,\Phi_{\nu M_S'}(Q_{N-1}, \xi, \varphi, \sigma) = 0, \tag{6.8a}$$

$$\Phi_{\nu M_S'}(Q_{N-1}, \xi, \varphi, \sigma) = \Psi_{nM_S'}(Q_{N-1})\phi_\nu(\xi)\frac{e^{im\varphi}}{\sqrt{2\pi}}\chi_{M_S - M_S'}(\sigma), \tag{6.8b}$$

$$\nu = (n, n_\xi, m). \tag{6.8c}$$

Here *diabatic* operator $\mathcal{B}$ coincides with the counterpart in Eq. (2.6) if one replaces the energy E there by operator $(E - H_{N-1})$, and $\chi_{M_S - M'_S}(\sigma)$ is one-electron spin function [29]. Compared to previous chapters, the multiindex ν in this case includes one more parameter, namely n, which characterizes the SS of the $(N-1)$-electron subsystem

$$[H_{N-1} - E_n]\, \Psi_{nM'_S}(Q_{N-1}) = 0. \tag{6.9}$$

In the weak-field limit (3.1), the solutions to Eqs. (6.2) and (6.9) can be found by the perturbation theory. Indeed we find for $N-$electron system

$$E = E_0^{(N)} - \mu_{0z}^{(N)} F - \frac{1}{2}\alpha_{0zz}^{(N)} F^2 + O(F^3), \tag{6.10a}$$

$$\Psi(Q_N) = \Psi_0^{(N)}(Q_N) + \Psi_0'^{(N)}(Q_N) F + O(F^2), \tag{6.10b}$$

and similarly for $(N-1)-$electron subsystem

$$E_n = E_n^{(N-1)} - \mu_{nz}^{(N-1)} F - \frac{1}{2}\alpha_{nzz}^{(N-1)} F^2 + O(F^3), \tag{6.11a}$$

$$\Psi_{nM'_S}(Q_{N-1}) = \Psi_{nM'_S}^{(N-1)}(Q_{N-1}) + \Psi_{nM'_S}'^{(N-1)}(Q_{N-1}) F + O(F^2). \tag{6.11b}$$

We can also expand the ionization channels up to $O(F)$ by the same way

$$\Phi_{\nu M'_S}(Q_{N-1}, \xi, \varphi, \sigma) = \Phi_{\nu M'_S}^{(0)}(Q_{N-1}, \xi, \varphi, \sigma) + \Phi_{\nu M'_S}^{(1)}(Q_{N-1}, \xi, \varphi, \sigma) F + O(F^2), \tag{6.12}$$

where

$$\Phi_{\nu M'_S}^{(0)}(Q_{N-1}, \xi, \varphi) = \Psi_{nM'_S}^{(N-1)}(Q_{N-1}) \phi_\nu^{(0)}(\xi) \frac{e^{im\varphi}}{\sqrt{2\pi}} \chi_{M_S - M'_S}(\sigma), \tag{6.13a}$$

$$\Phi_{\nu M'_S}^{(1)}(Q_{N-1}, \xi, \varphi) = \left[\Psi_{nM'_S}^{(N-1)}(Q_{N-1}) \phi_\nu^{(1)}(\xi) + \Psi_{nM'_S}'^{(N-1)}(Q_{N-1}) \phi_\nu^{(0)}(\xi)\right] \times \frac{e^{im\varphi}}{\sqrt{2\pi}} \chi_{M_S - M'_S}(\sigma). \tag{6.13b}$$

The function $\phi_\nu(\xi) = \phi_\nu^{(0)}(\xi) + \phi_\nu^{(1)}(\xi)F$ and corresponding eigenvalues $\beta_\nu = \beta_\nu^{(0)} + \beta_\nu^{(1)}F$ stay in the same forms as in Chapter 3, given that $\varkappa$ and μ_z should be replaced by

$$\varkappa_n = \sqrt{2I_n}, \quad I_n = E_n^{(N-1)} - E_0^{(N)}, \tag{6.14a}$$

$$\mu_n = \mu_{0z}^{(N)} - \mu_{nz}^{(N-1)}, \tag{6.14b}$$

respectively. In one-electron problems, the two unknown coefficients constructing the tunneling rate are g_ν and a_ν. They are to be extracted from the asymptotic tail of the unperturbed wave function and its distortion, see Eqs. (3.11) and (3.12). In many-electron problem, they have counterparts which are extracted from the so-called Dyson orbital $\Upsilon_{\nu M_S'}(q)$ and its first-order expansion $\Upsilon'_{\nu M_S'}(q)$

$$\Upsilon_{\nu M_S'}(q) = \upsilon_n(\mathbf{r})\chi_{S'M_S',SM_S}(\sigma), \tag{6.15a}$$

$$\Upsilon'_{\nu M_S'}(q) = \upsilon'_n(\mathbf{r})\chi_{S'M_S',SM_S}(\sigma), \tag{6.15b}$$

where

$$\upsilon_n(\mathbf{r}) = \sqrt{\frac{N}{\tau_{N-1,S'}\tau_{NS}}} \sum_{\tau=1}^{\tau_{NS}} \delta_{S'S_{N-1}} \int \psi_\tau^{(N-1)}(\mathbf{R}_{N-1})\psi_{\tau S}^{(N)}(\mathbf{R}_N)dV_{N-1}, \tag{6.16a}$$

$$\upsilon'_n(\mathbf{r}) = \sqrt{\frac{N}{\tau_{N-1,S'}\tau_{NS}}} \sum_{\tau=1}^{\tau_{NS}} \delta_{S'S_{N-1}} \int \left[\psi_\tau'^{(N-1)}(\mathbf{R}_{N-1})\psi_{\tau S}^{(N)}(\mathbf{R}_N) + \psi_\tau^{(N-1)}(\mathbf{R}_{N-1})\psi_{\tau S}'^{(N)}(\mathbf{R}_N)\right] dV_{N-1}. \tag{6.16b}$$

In the following, it is assumed that all the quantities characterizing the involved system in Eqs. (6.10) and (6.11) are known, so that the ionization channels and Dyson orbital are available. Using the procedure developed in previous chapters, we

can express the ionization rate in terms of those quantities. The final formula is

$$\Gamma_n \approx W_{n00}(F)\left\{|G_{n00}|^2\left[1+A_{n00}F\ln\frac{F}{4\varkappa_n^2}+B_{n00}F\right]+\frac{F}{2\varkappa_n^2}|G_{n01}|^2\right\}. \tag{6.17}$$

This working formula is applicable for an arbitrary orientation of the molecule with respect to the external field, determining the rate of tunneling ionization into all M_S' components of the final state $\Psi_{nM_S'}^{(N-1)}$. This equation plays the same role as Eq. (3.29) in one-electron case. All the notations here inherit the meaning and the form of their counterparts in Eq. (3.29), where one should use $\varkappa_n$, μ_n, α_n, and γ_{nm} instead of $\varkappa$, μ_z, α_{zz}, and γ_m. For this many-electron case, the last two are defined by

$$\alpha_n = \alpha_{0zz}^{(N)} - \alpha_{nzz}^{(N-1)}, \tag{6.18a}$$

$$\gamma_{nm} = \frac{1-m^2}{4} - 2D_n, \quad D_n = D_{Az} + \mu_{nz}^{(N-1)}. \tag{6.18b}$$

Here D_n is the total dipole moment of the parent ion in a particular state n. The two unknown coefficients mentioned above are to be extracted by

$$g_\nu = \eta^{1/2-\beta_\nu^{(0)}/\varkappa_n} e^{\varkappa_n\eta/2}\int_0^\infty\int_0^{2\pi}\phi_\nu^{(0)}(\xi)\frac{e^{-im\varphi}}{\sqrt{2\pi}}\upsilon_n(\mathbf{r})d\xi d\varphi\Big|_{\eta\to\infty}, \tag{6.19a}$$

$$\begin{aligned} a_\nu = g_\nu^{-1}\eta^{1/2-\beta_\nu^{(0)}/\varkappa_n} e^{\varkappa_n\eta/2}&\int_0^\infty\int_0^{2\pi}\left[\phi_\nu^{(0)}(\xi)\upsilon_n'(\mathbf{r})+\phi_\nu^{(1)}(\xi)\upsilon_n(\mathbf{r})\right]\frac{e^{-im\varphi}}{\sqrt{2\pi}}d\xi d\varphi\Big|_{\eta\to\infty} \\ &-\left(C_2\eta^2+C_1\eta+C_l\ln\eta+C_0\right), \end{aligned} \tag{6.19b}$$

$$g_{nn_\xi,-m} = g_{nn_\xi m}^*, \quad a_{nn_\xi,-m} = a_{nn_\xi m}^*, \tag{6.19c}$$

provided that $g_\nu \neq 0$, and coefficients C_2, C_1, C_l and C_0 remain the same forms as those given in Eqs. (3.9).

6.2 Tunneling ionization of two-electron atoms

The theory is demonstrated for prototypical two-electron systems including He and H^-. The former is the prototype neutral system for studying of electron-electron correlation from both experimental and theoretical viewpoints. The early interest related to the latter was rooted in the astrophysical observations [80, 81]. However, the lack of singlet discrete excited levels and small ionization potential makes it suitable candidate for testing nonresonant multiphoton ionization theory and accurate alternating or static-field-induced ionization experiments [82, 83]. Theoretically, due to the computational difficulty in dealing simultaneously with both electron-electron interactions and electron-field couplings, there exist only few quantum-mechanical calculations on the tunneling ionization for these two systems [84, 87, 88, 89]. They are referred to as test ground to benchmark the theoretical prediction of Eq. (6.17).

For two-electron systems, $N = 2$, two possible values of the total spin are 0 and 1. The corresponding irreducible representations of the symmetry group are one-dimensional, $\tau_{2S} = 1$, and corresponding spin basis functions $\chi_{00}(\sigma_1, \sigma)$ and $\chi_{1M_S}(\sigma_1, \sigma)$ can be found in Ref. [29] and standard textbooks. The first-order perturbed wave functions of the form in Eq. (6.3) for the initial (2-electron) and final states (1-electron) reduce to

$$\Psi(q_1, q) = \left[\psi_S^{(2)}(\mathbf{r}_1, \mathbf{r}) + \psi_S'^{(2)}(\mathbf{r}_1, \mathbf{r})F\right] \chi_{SM_s}(\sigma_1, \sigma), \tag{6.20a}$$

$$\Psi_{nM_S'}(q_1) = \left[\psi_{nM_S'}^{(1)}(\mathbf{r}_1) + \psi_{nM_S'}'^{(1)}(\mathbf{r}_1)F\right] \chi_{M_s'}(\sigma_1). \tag{6.20b}$$

Notice that we have omitted spin $S' = 1/2$ for one-electron system from the notation of Eq. (6.20b). To simplify the Dyson orbital and its expansion in this case, we further omit the superscript and M_S' for the space part of the wave functions and end up with

$$\upsilon_n(\mathbf{r}) = \sqrt{2} \int \psi_n(\mathbf{r}_1)\psi_S(\mathbf{r}_1, \mathbf{r}) d\mathbf{r}_1, \tag{6.21a}$$

$$\upsilon'_n(\mathbf{r}) = \sqrt{2}\int \left[\psi'_n(\mathbf{r}_1)\psi_S(\mathbf{r}_1,\mathbf{r}) + \psi_n(\mathbf{r}_1)\psi'_S(\mathbf{r}_1,\mathbf{r})\right] d\mathbf{r}_1. \tag{6.21b}$$

In this first implementation of the theory, we consider the total rate Γ_{1s} for an electron from the ground $1s^2\,{}^1S^e$ states of He and H^- to tunnel, and leaves the parent ions He^+ and H in the ground $n \equiv 1s$ states. In these two cases, the rate Γ_{1s} is dominated by the channel with $n_\xi = m = 0$. The states involved possess the total orbital angular momentum $L = 0$, the dipole moments $\mu^{(2)}_{0z} = \mu^{(1)}_{1sz} = 0$, and the vanishing ionic dipole moment $D_{1s} = 0$. Because of the rotational invariance of the initial and final states, we have $\upsilon_{1s}(\mathbf{r}) = \upsilon_{1s}(r)$, but $\upsilon'_{1s}(\mathbf{r}) = \upsilon'_{1s}(r,\theta,\varphi)$ due to the couplings with higher angular momentum of the 2-electron perturbed wave functions. In the current tunneling processes with dominant channel $n_\xi = m = 0$, the extraction of coefficient a_{1s00} required only the real part of $\upsilon'_{1s}(\mathbf{r})$, which does not depend on φ and is factorized as $Re[\upsilon'_{1s}(\mathbf{r})] = \upsilon'_{1s}(r)\cos\theta$. For estimating Γ_{1s} of the zeroth order, one needs at hand the total charge of the parent ion Z, Eq. (6.7b), the parameter $\varkappa_{1s}$ defining the ionization potential into the final state $1s$, Eq. (6.14a), and the asymptotic coefficient g_{1s00}, Eq. (6.19a), extracted from the Dyson orbital (6.21a). To go beyond the zeroth-order approximation, it is also required coefficient g_{1s01} for the contribution from the next-to-the dominant channels, the polarizability α_{1s}, Eq. (6.18a), and the asymptotic coefficient a_{1s00}, Eq. (6.19b). The last coefficient is to be extracted from the Dyson orbital and its first-order expansion, Eqs. (6.21).

Since perturbed energies and wave functions of the final state $1s$ in He^+ and H is known analytically [10, 53]

$$E_{1s} = -\frac{Z_c^2}{2} - \frac{9}{4}\frac{F^2}{Z_c^4}, \tag{6.22a}$$

$$\Psi_{1s}(\mathbf{r_1}) = \sqrt{\frac{Z_c^3}{\pi}}e^{-Z_c r_1}\left[1 - F\left(\frac{r_1}{Z_c^2} + \frac{r_1^2}{2Z_c}\right)\cos(\theta_1)\right], \tag{6.22b}$$

with Z_c being the corresponding nuclear charge, the current application is centered at calculating the two-electron wave function and its first-order correction for the initial state. The accurate two-electron wave functions were expanded in hyperspherical coordinates [90]. This approach replaces two three-dimensional vectors $\mathbf{r_1}$ and $\mathbf{r_2}$ representing the two electrons by a single six-dimensional vector (R, Ω), where $\Omega = (\alpha, \theta_1, \phi_1, \theta_2, \phi_2)$ denotes collectively the five angles including hyperangle α, and spherical angles θ_j and ϕ_j, $j = 1, 2$. The coupled adiabatic hyperradial equations are solved utilizing the slow variable discretization method [91]. We constructed the global orthonormal basic functions $\Phi_\lambda^{LM}(\Omega, R_i)$ at each quadrature abscissas R_i by a two-step numerical procedure [92, 93], in which the orthogonal basis set $g_\mu^{l_1 l_2}(\alpha, R_i)$ for each pair of angular momenta (l_1, l_2) are the eigenfunctions of the diagonal part of the adiabatic Hamiltonian. Thus obtained wave functions and energies help one overcome the difficulties faced in a standard scheme of the adiabatic approximation regarding the accuracy and computational labour. In practical calculations, we used 40 eigenfunctions $g_\mu^{l_1 l_2}(\alpha, R_i)$ for each of 10 pairs of angular momenta to construct the basic functions. The total wave functions are expanded over 100 sectors, up to hyperradius $R_{\max} = 70$ and 110 for He and H^-, respectively. The precise wave functions of the latter basically need larger hyperradius compared to those of the former due to the more spreading in space of its electronic density. In both cases, 100 basic functions are used at each sector. The accuracy of the present calculation is demonstrated by comparing the ground-state energies for He and H^- with the variational values listed in Table 6.1. The Dyson orbitals built up with the $1s^2$ wave functions are in consistency with the benchmark results in Ref. [29], they are indistinguishable in Fig. 6.1. We constructed the first-order correction to the two-electron wave function by standard perturbation-theory expansion including transitions to the doubly excited states $^1P^o$. Only this symmetry is reached from the ground state $1s^2\,{}^1S^e$, following the selection rules for electric dipole transitions. The quality of the excited-

Table 6.1: Characteristics of He atom and H^- ion obtained in present calculations, and corresponding variational results reported in [a]Ref. [94] and [b]Ref. [95].

	He		H^-	
	Present	Exact	Present	Exact
$E_0^{(2)}$	-2.903722759	-2.903724377^a	-0.527745235	-0.527751017^a
f_2	0.276292	0.2761957^a	0.000011	
f_3	0.073358	0.0733997^a	0.000315	
f_4	0.029809	0.0298408^a	0.001564	
α_{0zz}	1.383068	1.383^b	206.225416	206.1^b

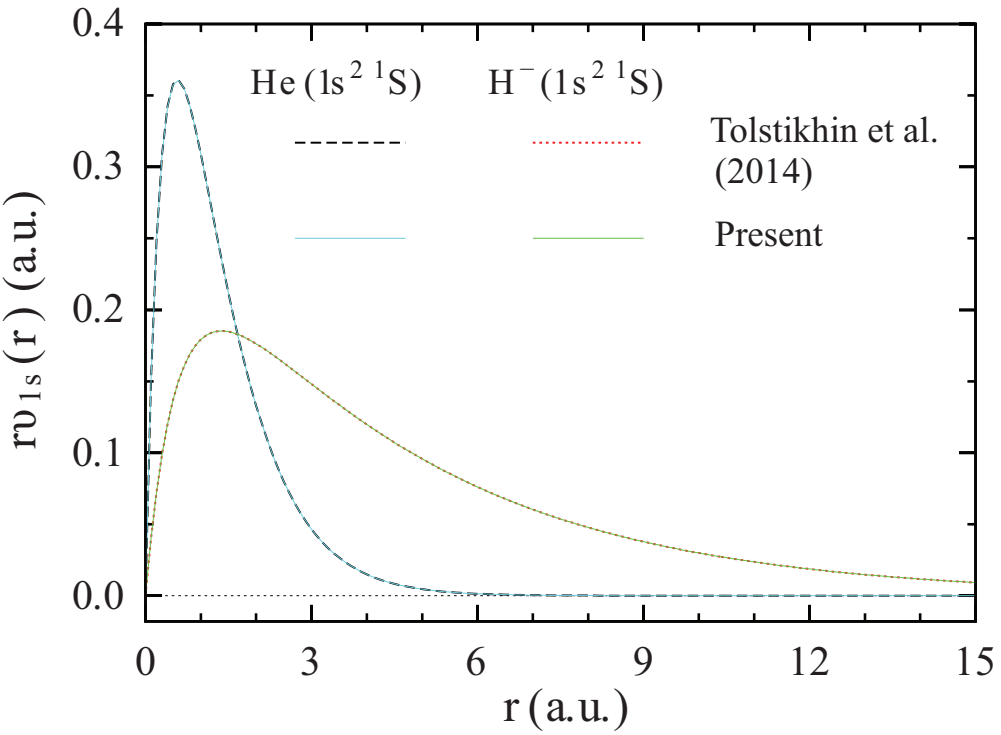

Figure 6.1: Dyson orbitals for He and H^-, Eq. (6.21a), multiplied by the radius r of the ionized electron. The present calculations are compared with benchmark results from Ref. [29].

state wave functions is guaranteed by precise oscillator strength which is defined by [96, 97]

$$f_k = 2\left(E_{1skp\,^1P^o} - E_{1s^2\,^1S^e}\right)\left|\int \Psi_{1skp\,^1P^o}(\mathbf{r}_1,\mathbf{r})(z_1+z)\Psi_{1s^2\,^1S^e}(\mathbf{r}_1,\mathbf{r})dV_2\right|^2. \quad (6.23)$$

The values for the first three transitions, $k = 2, 3, 4$, are given in Table 6.1, to be compared with variational results of Ref. [94]. The relative errors are less than 0.1% in He case. We are not aware of calculations on transitions to discrete states for H^-. However, the present value of its static polarizability agrees with variational value in Ref. [95] by a relative error of 0.06%. For He case, this relative error is even smaller, 0.005%. All of these observations suggest a sufficient assurance of the numerically obtained wave functions, and therefore of the Dyson orbital and its first-order distortion defined by Eqs. (6.21).

Having correct Dyson orbitals facilitates extracting the asymptotic coefficients by Eqs. (6.19a) and (6.19b). Thus obtained coefficients g_{1s00}, g_{1s01}, and a_{1s00}, as well as other needed coefficients are tabulated in Table 6.2. No contribution from higher channels shows up, $g_{1s01} = 0$, due to the independence of the Dyson orbital on variable φ. We now can apply the working formula (6.17) for He atom. The tunneling rates up to zeroth and first order appear as blue and red lines in the upper panel of Fig. 6.2. The exact tunneling rate was obtained by the complex rotation method [87, 88, 89], and shown by different types of symbol. Their ratios to the field factor $W_{1s00}(F)$, which is exponentially small, are presented in the lower panel. It is believed that the numerical data below $F = 0.1$ was not correctly obtained, and could not be properly treated by any method within double-precision calculations because of the singular behavior of Γ when $F \to 0$ [29, 23, 53]. By extrapolating the reliable data from $F > 0.1$ to $F = 0$, one observes a much faster convergence of the ME-WFAT(1) to the exact value than the ME-WFAT(0). For example, at $F = 0.2$, Eq. (6.17) suffers

Table 6.2: Necessary coefficients to apply Eq. (6.17) for tunneling processes $\mathrm{He}(1s^2\,{}^1S^e) \to \mathrm{He}^+(1s)$ and $\mathrm{H}^-(1s^2\,{}^1S^e) \to \mathrm{H}(1s)$ of He atom and H^- ion, respectively. The counterparts calculated under the framework of the WFAT using potential (6.24) are given in the last row.

ME-WFAT	$\varkappa_{1s}$	α_{1s}	g_{1s00}	g_{1s01}	a_{1s00}	A_{1s00}	B_{1s00}
$\mathrm{He}(1s^2\,{}^1S^e)$	1.344413	1.101818	2.935	0	-0.27	0.235254	-2.60
$\mathrm{H}^-(1s^2\,{}^1S^e)$	0.235564	201.725416	3.258	0	10.4	0	-135.10
WFAT	$\varkappa$	α	g_{00}	g_{01}	a_{00}	A_{00}	B_{00}
He	1.344414	0.788115	2.987	0	-0.04	0.235254	-1.72

an relative error of 25%, while the ME-WFAT(0) overestimates the rate by a factor of 2.4. This strongly confirms the consistency of the formulation. The first-order terms essentially extend the region of applicability of the theory up to the onset of over-the-barrier ionization where the ME-WFAT(1) turns to zero.

It is desirable to revise the step from the WFAT to the ME-WFAT. In the SAEA, the active electron of He atom is regarded as moving in an effective potential of the form [86]

$$V_{He}(r) = -\frac{1+\exp(-\alpha r)}{r}. \tag{6.24}$$

When $\alpha = 2.132\,405$, the ground state energy of He is $E_{grnd} = 0.903\,724$ reproducing the exact ionization potential I_n, see Table 6.1 and Eq. (6.22a). The tunneling rate from this state calculated by the method of Ref. [48] and multiplied by two is included in Fig. 6.2. The factor of 2 appears since there are two electrons staying in the same initial orbital with different spin projections [29]. This one-electron result is slightly higher than fully-correlated calculations, but also approaches the same point when $F \to 0$. In other words, they almost converge to $|g_{1s00}|^2$ at $F = 0$. The insight into this situation is somehow revealed in an analysis within the SAEA employing the relevant results and notations from Chapters 2 and 3. The obtained coefficients are given in the last row of Table 6.2, to be compared with their counterpart in the

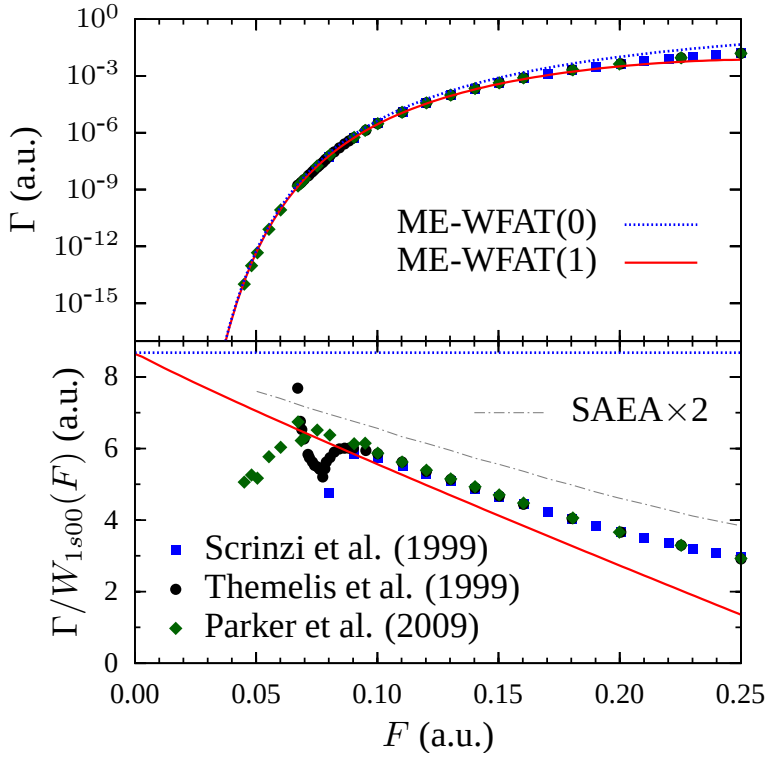

Figure 6.2: Ionization rate of He in the ground state $1s^2\,{}^1S^e$ divided by the field factor $W_{1s00}(F)$ for the dominant channel $\mathrm{He}(1s^2\,{}^1S^e) \to \mathrm{He}^+(1s)$ with $n_\xi = m = 0$.

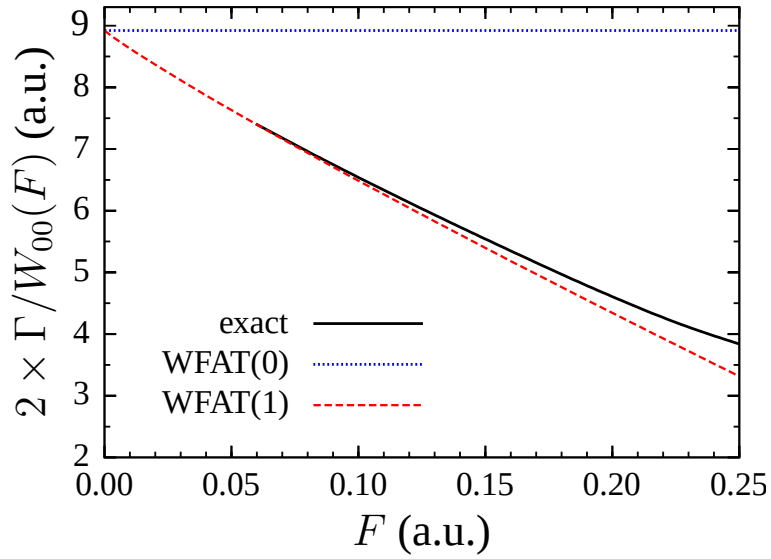

Figure 6.3: SAEA-based results for He atom in the ground state using potential (6.24), multiplied by two and divided by the field factor, Eq. (3.28) for $\nu = (0, 0)$.

ME-WFAT. The values of g_{00} and g_{01} highly accord with those extracted from Dyson orbital, g_{1s00} and g_{1s01}. This can be explained by the very fact that in the SAEA the electron correlations are included only via the wave function of the field-free initial state, whose energy coincides with the exact ionization potential I_n as pointed out above. Coefficients $\varkappa$ and A_{00} characterized by E_{grnd} are in full agreement with $\varkappa_{1s}$ and A_{1s00}, respectively, for the same reason. However, one-electron calculations evidently fail to reproduce correct values of the polarizability α_{1s} and the asymptotic coefficient a_{1s00}, leading to an error in the value of B_{00}. It is where the multi-electron effects, such as correlation, indistinguishability, antisymmetrization, etc., come into play and are indispensable. The implementation of the WFAT for He is shown in Fig. 6.3. The first-order clearly gets the better of the zeroth-order approximation; our formulation within the SAEA is again confirmed, now for He atom.

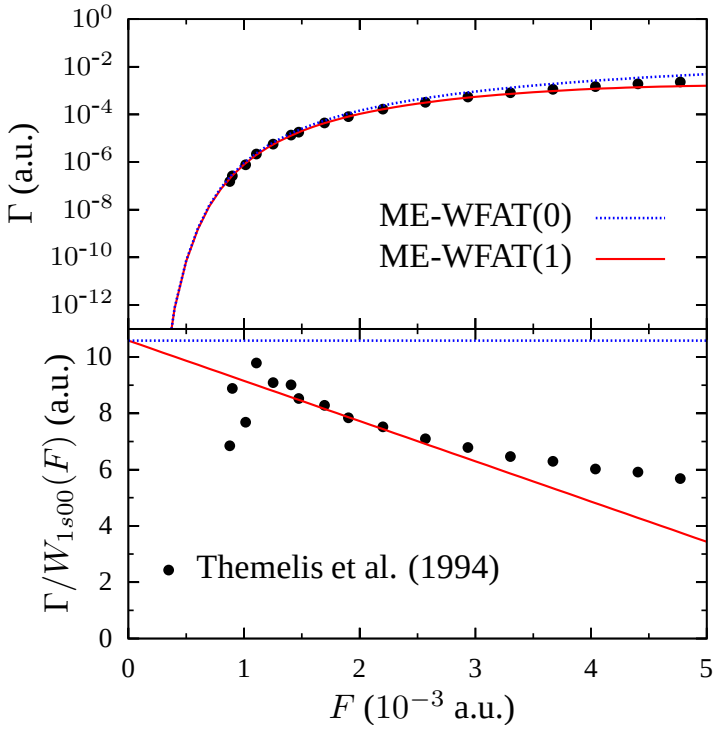

Figure 6.4: Ionization rate of H^- in the ground state $1s^2\,{}^1S^e$ divided by the field factor $W_{1s00}(F)$ for the dominant channel $H^-(1s^2\,{}^1S^e) \to H(1s)$ with $n_\xi = m = 0$.

A verification of the ME-WFAT for the case of H^- ion is carried out in Fig. 6.4. The exact numerical data was calculated from the *ab initio* polyelectronic theory [84, 85], which accounts for electronic structure and electron correlation in the field-dressed states. The calculations for $F < 0.002$ perform a random vibration, and can be singled out. By extrapolating the remaining part, we observe a familiar convergence pattern of the ME-WFAT results where the first-order correction prominently improves the prediction. For example, the relative error is 76% at $F = 4 \times 10^{-3}$ by the ME-WFAT(0), but reduces to only 20% with inclusion of the first-order correction terms. In this case, the asymptotic coefficient A_{1s00} vanished identically, implying a purely linear behavior of the ME-WFAT(1) when $F \to 0$.

Chapter 7

Summary and outlook

In this thesis, the first-order correction terms in the asymptotic expansions of the ionization rate and TMD within the WFAT [23] are obtained. The results apply to any atoms or molecules treated in the single-active-electron and frozen-nuclei approximations. These are one-electron problems. So far, the first-order correction was available only for the ionization rate of hydrogen [46]. The present extension became possible on the basis of the method of Ref. [23], which takes the advantage of the separability of the stationary Schrödinger equation in the asymptotic region, where the potential is dominated by the Coulomb tail. To evaluate the leading-order WFAT results, only the asymptotic charge Z, the energy E_0, dipole moment μ_z, and the asymptotic coefficient g_ν [Eq. (3.11)] for the dominant channel characterizing the unperturbed active orbital are needed. These characteristics define the structure (3.27) and field (3.28) factors. The techniques to calculate them for atoms and molecules based on quantum chemistry codes have been developed in Refs. [51, 52]. To evaluate the first-order correction terms, one additionally needs the ionic dipole moment D_z, coefficients g_ν for several next-to-the-dominant channels, the polarizability α_{zz}, and a new asymptotic coefficient a_ν [Eq. (3.12)] for the dominant channel. The last two

account for the second-order Stark shift and the distortion of the unperturbed orbital by field, respectively.

The WFAT was first illustrated for atomic systems such as hydrogen and noble gas atoms. The results show that inclusion of the first-order correction terms greatly improves the agreement between the rate and the TMD predicted by the WFAT and the results obtained from accurate numerical solution of the SS eigenvalue problem [48]. In practice, the present development extends the region of applicability of the WFAT at the quantitative level up to the boundary between tunneling and over-the-barrier regimes of ionization. Hence, the theory now covers a regime that has been notoriously difficult to describe by previous analytical approaches. We also applied the theory for molecular targets including nonpolar (H_2^+) and polar molecules (HeH^{2+}). The conclusions for atomic cases remain valid here. The first-order corrections are shown to essentially enhance the accuracy of theoretical predictions over not only a wide interval of fields, but also different orientations of the molecules in the field. This demonstrates the good quantitative performance of the WFAT, and confirms the high accuracy of the numerical method [49, 50]. These results establish the WFAT including the first-order correction terms as an appealing alternative to laborious numerical calculations in the tunneling regime $F < F_c$.

Following the streamline of the WFAT, the ME-WFAT originally developed in Ref. [29] was extended to the next order in field for tunneling rate. The tunneling process into a particular channel $\nu = (n, n_\xi, m)$ is described by the working formula in Eq. (6.17). To evaluate the zeroth-order approximation one needs Z, $\varkappa_n$, μ_n, and g_{n00} characterizing the unperturbed system and its subsystem. Invoking the first-order corrections additionally requires g_{n01}, D_n, α_n, and a_{n00}. The last two coefficients are to be calculated from the perturbed system and its subsystem. All of the quantities appearing in the ME-WFAT have the counterparts in the WFAT for one-electron systems, and basically inherit the physical meanings. However, their cal-

culations always require both initial and final systems to be involved. Our derivation recalls the definition of Dyson orbital $\Upsilon_{nM'_S}(q)$ and introduces its first-order correction $\Upsilon'_{nM'_S}(q)$. The implementation of the theory for 2-electron systems including He and H^- indicates an improvement in the ME-WFAT prediction when the first-order correction terms are applied. This conclusion establishes a consistency of the ME-WFAT and a confirmation of the fully-correlated calculations for the systems under consideration.

For future application, it should be mentioned that multi-electron effects (correlation, indistinguishability, antisymmetrization) and characteristics of the systems (dipole moment, polarizability) naturally emerge in our formulation without any *ad hoc* assumption. Moreover, plentiful information on the angular dependence appears not only in the zeroth-order via G_{n00} but also in the first-order terms via G_{n01}, A_{n00} and B_{n00}. The theory thus promises desirable outcomes, and is expected to provide answers to remaining puzzles of current interest in strong field physics. That are the disagreements observed when the experimental measurements on CO_2 [42, 43], CO [44, 45], and OCS [37] are compared with predictions by MO-ADK model and the WFAT of zeroth order, as discussed elsewhere [52]. However, the application of the WFAT and the ME-WFAT of the first order to polyatomic molecules is not straightforward, since the wave functions with proper asymptotic behavior for such large molecular systems are not available. In the single-active-electron approximation, the wave function at the Hartree-Fock (HF) level can be invoked. Therefore, in near future, we will focus on molecules of experimental interest treated in single-active-electron approximation for which virtually exact information can be extracted from HF method. Nevertheless, the Hartree-Fock approximation is not multipurpose [29], feasible predictions for the aforesaid cases based on the ME-WFAT require new techniques. Numerical procedures, which allow us to construct and retrieve neces-

sary quantities from correlated wave functions of many-electron systems, would be an interesting subject for further study.

Being proved to be a fascinating replacement of time-consuming numerical calculations, the WFAT of first order developed in this thesis could provide convenient but fairly accurate tunneling ionization rates and TMDs in tunneling regime. This make the WFAT involved in the adiabatic theory [8], whose implementation requires the SS characteristics to be supplied. So far, we have been working under the framework of stationary Schrödinger equation in adiabatic regime, which corresponds to laser field with sufficiently low frequency at a given intensity. However, there exists an increasing interest in analyzing the interaction between strong ultra-short laser pulses and matter, since it opens new tools to probe electronic dynamics at the spatio-temporal resolution. When the laser parameters fall into category that non-adiabatic effects become important, a representation of tunneling ionization beyond the instantaneous configuration is of fundamental interest. Such a development relied on asymptotic theory to account for frequency dependence of laser-induced ionization would be an attractive direction, and facilitates more applications in strong-field physics.

Appendix A

AN AUXILIARY PROBLEM FOR LAGUERRE BASIC

Here we establish the solutions to a general class of equation having similar form with Eq. (2.9). To this ends, let consider the following eigenvalue problem

$$\left[\frac{d}{dx}x\frac{d}{dx} - \frac{m^2}{4x} - \frac{x}{4} + \epsilon_n\right]\phi_n(x) = 0, \quad m \geqslant 0, \tag{A.1}$$

whose solutions represent the Laguerre basis, and are given by

$$\epsilon_n = \frac{1}{2}(2n + m + 1), \tag{A.2a}$$

$$\phi_n(x) = x^{m/2}e^{-x/2} \times \sqrt{\frac{n!}{(n+m)!}}\, L_n^{(m)}(x), \tag{A.2b}$$

$$\int_0^\infty \phi_n(x)\phi_{n'}(x)\, dx = \delta_{nn'}, \tag{A.2c}$$

where $L_n^{(m)}(x)$ are the generalized Laguerre polynomials [57]. It can be proven that the below recursive relations hold,

$$x\phi_n(x) = \alpha_{n-1}\phi_{n-1}(x) + \beta_n\phi_n(x) + \alpha_n\phi_{n+1}(x), \tag{A.3a}$$

$$x^2\phi_n(x) = \alpha_{n-1}\alpha_{n-2}\phi_{n-2}(x) + \alpha_{n-1}(\beta_{n-1}+\beta_n)\phi_{n-1}(x)$$
$$+\gamma_n\phi_n(x) + \alpha_n(\beta_n+\beta_{n+1})\phi_{n+1}(x) + \alpha_n\alpha_{n+1}\phi_{n+2}(x), \tag{A.3b}$$

where

$$\alpha_n = -\sqrt{(n+1)(n+m+1)}, \quad \beta_n = 2n+m+1, \quad \gamma_n = \alpha_{n-1}^2 + \beta_n^2 + \alpha_n^2. \tag{A.4}$$

On the basic of Laguerre basic, we can construct the solutions to the corresponding eigenvalue problem with the presence of a small parameter $F \to 0$,

$$\left[\frac{d}{dx}x\frac{d}{dx} - \frac{m^2}{4x} - \frac{x}{4} + (a+bx+cx^2)F + O(F^2) + \varepsilon\right]\varphi(x) = 0, \tag{A.5a}$$
$$\int_0^\infty [\varphi(x)]^2 dx = 1, \tag{A.5b}$$

where a, b, and c are constants. Indeed, the solutions can be found using perturbation-theory scheme [10]

$$\varepsilon = \varepsilon_0 + \varepsilon_1 F + O(F^2), \tag{A.6a}$$
$$\varphi(x) = \varphi_0(x) + \varphi_1(x)F + O(F^2). \tag{A.6b}$$

For $F = 0$, the leading-order approximation gives $\varepsilon_0 = \epsilon_n$ and $\varphi_0(x) = \phi_n(x)$. When $F \neq 0$, substituting Eqs. (A.6) into Eq. (A.5a) and using relations (A.3), one ends up with

$$\varepsilon_1 = -\left[a + b(2n+m+1) + c\gamma_n\right], \tag{A.7a}$$
$$\varphi_1(x) = -\frac{c}{2}\,\alpha_{n-1}\alpha_{n-2}\phi_{n-2}(x) - \alpha_{n-1}\left[b + 2c(2n+m)\right]\phi_{n-1}(x)$$
$$+\alpha_n\left[b + 2c(2n+m+2)\right]\phi_{n+1}(x) + \frac{c}{2}\,\alpha_n\alpha_{n+1}\phi_{n+2}(x), \tag{A.7b}$$

which are the first-order corrections to the solutions of Eq. (A.5a).

Appendix B

CONNECTING FORMULA

This section is devoted to considering the solution to Eq. (2.15) established in Chapter 2. Namely, we construct the asymptotics of the outgoing-wave solution of the equation

$$\left[\frac{d^2}{d\eta^2} + \frac{F\eta}{4} + \frac{E}{2} + \frac{\beta}{\eta} + \frac{\gamma}{\eta^2}\right] f(\eta) = 0 \tag{B.1}$$

for

$$F \to 0, \quad E = O(F^0), \quad \beta = O(F^0), \quad \gamma = O(F^0). \tag{B.2}$$

The above equation has the form of one-dimensional Schrödinger equation, whose effective potential is portrayed in Fig. 3.1. The outer turning point for this potential is given by

$$\eta_t = \frac{\kappa^2}{F} + O(F^0) = O(F^{-1}), \tag{B.3}$$

where

$$\kappa = \sqrt{-2E}. \tag{B.4}$$

The goal is to derive the connection formula which expresses the coefficient of the outgoing wave at $\eta \gg \eta_t$ in terms of coefficients appearing in the expansion of the same solution at $1 \ll \eta \ll \eta_t$.

B.1 Perturbation-theory solution in the inner region

Let first consider Eq. (B.1) in the inner region

$$1 \ll \eta \ll F^{-1/2}. \tag{B.5}$$

The term with F in this region can be treated perturbatively. For $F = 0$, one of the two linearly independent solutions to Eq. (B.1) behaves as

$$f_0(\eta) = \eta^{\beta/\kappa} e^{-\kappa\eta/2} \left[1 + \frac{c_1}{\eta} + \frac{c_2}{\eta^2} + O(\eta^{-3})\right]. \tag{B.6}$$

Substituting this expansion into Eq. (B.1), we find

$$c_1 = -\frac{\gamma}{\kappa} + \frac{\beta}{\kappa^2} - \frac{\beta^2}{\kappa^3}. \tag{B.7}$$

The higher coefficients in Eq. (B.6) can be found similarly. The second linearly independent solution diverges $\propto \eta^{-\beta/\kappa} e^{\kappa\eta/2}$ as η grows. In this case, the solution needed is

$$f(\eta) = g f_0(\eta), \tag{B.8}$$

where g is a field-independent coefficient. For $F \neq 0$, the same solution is sought in the form

$$f(\eta) = g\left[f_0(\eta) + f_1(\eta)F + O(F^2)\right]. \tag{B.9}$$

Substituting this into Eq. (B.1) and neglecting terms $O(F^2)$, one obtains an inhomogeneous equation for $f_1(\eta)$,

$$\left[\frac{d^2}{d\eta^2} + \frac{E}{2} + \frac{\beta}{\eta} + \frac{\gamma}{\eta^2}\right] f_1(\eta) = -\frac{\eta}{4} f_0(\eta). \tag{B.10}$$

The solution to this equation that decays as η grows can be sought in the form

$$f_1(\eta) = \eta^{\beta/\kappa} e^{-\kappa\eta/2} \left\{ a_2\eta^2 + a_1\eta + a_0 + \frac{a_{-1}}{\eta} + O(\eta^{-2}) + \left[b_0 + \frac{b_{-1}}{\eta} + O(\eta^{-2}) \right] \ln\eta \right\}. \tag{B.11}$$

Substituting this expansion into Eq. (B.10), we find

$$a_2 = \frac{1}{8\kappa}, \quad a_1 = \frac{1}{4\kappa^2}\left(\frac{2-\gamma}{2} + \frac{5\beta}{2\kappa} - \frac{\beta^2}{2\kappa^2}\right), \tag{B.12a}$$

$$b_0 = \frac{1}{2\kappa^3}\left(\gamma + \frac{3\beta^2}{\kappa^2}\right). \tag{B.12b}$$

One can continue and express a_{-1}, b_{-1}, and the higher coefficients in Eq. (B.11) in terms of the coefficients in Eq. (B.1) and a_0. However, the coefficient a_0 cannot be found in this way. Such an uncertainty is explained by the fact that the solution to Eq. (B.10) is defined up to an admixture of the solution $f_0(\eta)$ to the corresponding homogeneous equation. Summarizing,

$$f(\eta) = g\eta^{\beta/\kappa} e^{-\kappa\eta/2} \left\{ 1 - \left(\frac{\gamma}{\kappa} - \frac{\beta}{\kappa^2} + \frac{\beta^2}{\kappa^3}\right)\frac{1}{\eta} + O\left(\frac{1}{\eta^2}\right) \right.$$
$$\left. + \left[\frac{\eta^2}{8\kappa} + \left(\frac{2-\gamma}{8\kappa^2} + \frac{5\beta}{8\kappa^3} - \frac{\beta^2}{8\kappa^4}\right)\eta + \left(\frac{\gamma}{2\kappa^3} + \frac{3\beta^2}{2\kappa^5}\right)\ln\eta + a_0 + O\left(\frac{\ln\eta}{\eta}\right) \right] F + O(F^2) \right\}. \tag{B.13}$$

This is a perturbation-theory expansion in F for $F \to 0$ and asymptotic expansion in $1/\eta$ for $\eta \to \infty$. The terms $\propto 1/\eta$ and $\propto F$ in the curly brackets represent corrections existing without the field and caused by the field, respectively. The requirement that these terms must be much smaller than unity defines the lower and upper boundaries of the region of validity (B.5) of this expansion. Note that these terms become comparable at $\eta = O(F^{-1/3})$, which belongs to the region (B.5). The coefficients g and a_0 in Eq. (B.13) remain undefined; they are determined by the behavior of $f(\eta)$

to the left of the region (B.5), for example, by the regularity boundary condition at $\eta = 0$.

B.2 Asymptotic solution in the outer region

Let now consider Eq. (B.1) in the outer region

$$\eta = O(F^{-1}). \tag{B.14}$$

Introducing a new variable,

$$y = \frac{F\eta}{\kappa^2} = O(F^0), \tag{B.15}$$

we rewrite Eq. (B.1) as

$$\left[\frac{d^2}{dy^2} + \frac{\kappa^4}{F^2}\, q(y)\right] f(y) = 0, \tag{B.16}$$

where

$$q(y) = q_0(y) + q_1(y)F + q_2(y)F^2, \tag{B.17a}$$

$$q_0(y) = \frac{\kappa^2}{4}(y-1), \quad q_1(y) = \frac{\beta}{\kappa^2 y}, \quad q_2(y) = \frac{\gamma}{\kappa^4 y^2}. \tag{B.17b}$$

The solution to Eq. (B.16) is sought in the form [59, 60]

$$f(y) = f \exp\left\{\frac{i\kappa^2}{F}\left[s_0(y) + s_1(y)F + s_2(y)F^2 + s_3(y)F^3 + O(F^4)\right]\right\}, \tag{B.18}$$

where f is a field-dependent coefficient. Substituting Eq. (B.18) into Eq. (B.16), we obtain equations defining $s_n(y)$,

$$-s_0'^2(y) + q_0(y) = 0, \tag{B.19a}$$

$$-2s_0'(y)s_1'(y) + \frac{is_0''(y)}{\kappa^2} + q_1(y) = 0, \tag{B.19b}$$

$$-s_1'^2(y) - 2s_0'(y)s_2'(y) + \frac{is_1''(y)}{\kappa^2} + q_2(y) = 0, \tag{B.19c}$$

$$-2s_0'(y)s_3'(y) - 2s_1'(y)s_2'(y) + \frac{is_2''(y)}{\kappa^2} = 0. \tag{B.19d}$$

The solutions to these equations are given by

$$s_0(y) = \frac{\kappa}{3}(y-1)^{3/2}, \tag{B.20a}$$

$$s_1(y) = \frac{i}{4\kappa^2}\ln\frac{\kappa^2(y-1)}{4} + \frac{2\beta}{\kappa^3}\left[\arctan(y-1)^{1/2} - \frac{\pi}{2}\right], \tag{B.20b}$$

$$\begin{aligned} s_2(y) = &-\frac{5}{24\kappa^5(y-1)^{3/2}} + \frac{i\beta}{\kappa^6 y(y-1)} + \left[\frac{\gamma}{\kappa^5} + \frac{3\beta^2}{\kappa^7}\right]\frac{1}{(y-1)^{1/2}} \\ &- \left[\frac{\gamma}{\kappa^5} + \frac{\beta^2}{\kappa^7}\right]\frac{1}{y(y-1)^{1/2}} + \left[\frac{\gamma}{\kappa^5} + \frac{3\beta^2}{\kappa^7}\right]\left[\arctan(y-1)^{1/2} - \frac{\pi}{2}\right]. \end{aligned} \tag{B.20c}$$

The choice of the integration constants on the step from Eqs. (B.19) to Eqs. (B.20) is related to the definition of the coefficient f in Eq. (B.18) and is dictated by the wish to arrive at Eq. (B.22). The sign in Eq. (B.20a) is determined by the outgoing-wave boundary condition. We have omitted the tedious expression for $s_3(y)$; in the following, we need this function only at $y \ll 1$ and $y \gg 1$, which can be easily obtained from Eq. (B.19d) and the corresponding expansions for $s_0(y)$, $s_1(y)$, and $s_2(y)$ given below.

For $y \gg 1$, we have

$$s_0(y) = \frac{\kappa}{3}y^{3/2} - \frac{\kappa}{2}y^{1/2} + O(y^{-1/2}), \tag{B.21a}$$

$$s_1(y) = \frac{i}{4\kappa^2}\ln\frac{\kappa^2 y}{4} + O(y^{-1/2}), \tag{B.21b}$$

$$s_2(y) = O(y^{-1/2}), \quad s_3(y) = O(y^{-2}). \tag{B.21c}$$

Thus

$$f(\eta)|_{\eta\gg\eta_t} = \frac{2^{1/2}f}{(F\eta)^{1/4}}\exp\left[\frac{iF^{1/2}\eta^{3/2}}{3} + \frac{iE\eta^{1/2}}{F^{1/2}}\right], \tag{B.22}$$

which agrees with Eq. (2.17). For $y \ll 1$, we find

$$s_0(y) = -i\left[\frac{\kappa}{3} - \frac{\kappa y}{2} + \frac{\kappa y^2}{8} + O(y^3)\right], \tag{B.23a}$$

$$s_1(y) = -i\left[\frac{\beta}{\kappa^3}\ln\frac{y}{4} - \frac{\ln(\kappa/2)}{2\kappa^2} - \frac{i\pi}{4\kappa^2} - \frac{i\pi\beta}{\kappa^3} + \left(\frac{1}{4\kappa^2} + \frac{\beta}{2\kappa^3}\right)y + O(y^2)\right], \tag{B.23b}$$

$$\begin{aligned} s_2(y) = {} & i\left[\frac{\gamma}{\kappa^5} - \frac{\beta}{\kappa^6} + \frac{\beta^2}{\kappa^7}\right]\frac{1}{y} - i\left[\frac{\gamma}{2\kappa^5} + \frac{3\beta^2}{2\kappa^7}\right]\ln\frac{y}{4} \\ & -i\left[\frac{5 + 12(1 - i\pi)\gamma}{24\kappa^5} + \frac{\beta}{\kappa^6} + \frac{(5 - 3i\pi)\beta^2}{2\kappa^7}\right] + O(y^1), \end{aligned} \tag{B.23c}$$

$$s_3(y) = i\left[\frac{\gamma}{\kappa^5} - \frac{\beta}{\kappa^6} + \frac{\beta^2}{\kappa^7}\right]\left(\frac{\beta}{\kappa^4} - \frac{1}{\kappa^3}\right)\frac{1}{y^2} + O(y^{-1}). \tag{B.23d}$$

Substituting these expansions into Eq. (B.18) and considering the region (B.5), where $y^2/F \ll 1$ and $F/y \ll 1$, we obtain

$$\begin{aligned} f(\eta) = f\exp\left[\frac{\kappa^3}{3F} - \frac{i\pi}{4} - \frac{i\pi\beta}{\kappa}\right]\sqrt{\frac{2}{\kappa}}\left(\frac{F\eta}{4\kappa^2}\right)^{\beta/\kappa} e^{-\kappa\eta/2}\Bigg\{1 - \left(\frac{\gamma}{\kappa} - \frac{\beta}{\kappa^2} + \frac{\beta^2}{\kappa^3}\right)\frac{1}{\eta} + O\left(\frac{1}{\eta^2}\right) \\ + \left[\frac{\eta^2}{8\kappa} + \left(\frac{2-\gamma}{8\kappa^2} + \frac{5\beta}{8\kappa^3} - \frac{\beta^2}{8\kappa^4}\right)\eta + \left(\frac{\gamma}{2\kappa^3} + \frac{3\beta^2}{2\kappa^5}\right)\ln\frac{F\eta}{4\kappa^2}\right. \\ + \left(\frac{10 + 18\gamma + 3\gamma^2}{48\kappa^3} + \frac{\beta(9 - 6\gamma)}{8\kappa^4} + \frac{\beta^2(49 + 2\gamma)}{16\kappa^5} - \frac{3\beta^3}{4\kappa^6} + \frac{\beta^4}{16\kappa^7}\right) \\ \left. -i\pi\left(\frac{\gamma}{2\kappa^3} + \frac{3\beta^2}{2\kappa^5}\right) + O\left(\frac{\ln\eta}{\eta}\right)\right]F + O(F^2)\Bigg\}. \end{aligned} \tag{B.24}$$

B.3 Matching

The inner, Eq. (B.13), and outer, Eq. (B.18), solutions can be matched in the region (B.5), where they both apply. Indeed, expansions (B.13) and (B.24) have the same form. By comparing the coefficients in these expansions one haves

$$\begin{aligned} f = g\exp\left[-\frac{\kappa^3}{3F} + \frac{i\pi}{4} + \frac{i\pi\beta}{\kappa}\right]\sqrt{\frac{\kappa}{2}}\left(\frac{4\kappa^2}{F}\right)^{\beta/\kappa}\Bigg\{1 - \Bigg[\left(\frac{\gamma}{2\kappa^3} + \frac{3\beta^2}{2\kappa^5}\right)\ln\frac{F}{4\kappa^2} \\ + \frac{10 + 18\gamma + 3\gamma^2}{48\kappa^3} + \frac{\beta(9 - 6\gamma)}{8\kappa^4} + \frac{\beta^2(49 + 2\gamma)}{16\kappa^5} - \frac{3\beta^3}{4\kappa^6} + \frac{\beta^4}{16\kappa^7} - a_0 \end{aligned}$$

$$-i\pi\left(\frac{\gamma}{2\kappa^3}+\frac{3\beta^2}{2\kappa^5}\right)\Bigg]F+O(F^2)\Bigg\}. \tag{B.25}$$

This is the connection formula expressing the coefficient f in Eq. (B.22) in terms of the field-independent coefficients g and a_0 appearing in Eq. (B.13).

Appendix C

MULTIPLE-PRECISION NUMERICAL PROCEDURE FOR HYDROGEN

The ionization rate is determined by the imaginary part of the SS energy eigenvalue (2.18). In the weak-field limit (3.1) it becomes exponentially small, while the real part of the eigenvalue tends to a constant E_0. Therefore any numerical procedure of calculating Γ with finite-precision arithmetics fails at sufficiently small F, when the ratio $\Gamma/|E_0|$ approaches the value of the roundoff error. For neutral atoms in the ground state $|E_0| \sim 1$, so double-precision calculations [48] fail when $\Gamma \lesssim 10^{-12}$. This impedes extending the exact results shown in Figs. 4.4, 5.3, 5.8, 5.13, 5.19, 6.2, 6.3, and 6.4 to smaller F. However, for hydrogen this fundamental problem can be overcome, at least in principle, for any nonzero F by using multiple-precision arithmetics [98, 99]. We note that although there exist many efficient numerical techniques to calculate the ionization rate of hydrogen [100, 101, 102, 103, 104, 105, 106, 107, 108], the problem mentioned above, as far as we know, has never been addressed in the literature.

The peculiarity of hydrogen stems from the fact that the algorithm to calculate Γ can be formulated in a very simple form involving only basic arithmetic operations, which is required for the application of the multiple-precision package described in Refs. [98, 99]. For $V(\mathbf{r}) = -1/r$, the variables in Eq. (2.1) can be separated in parabolic coordinates [10]. The solutions to the separated equations in ξ and η are then sought as expansions in a Laguerre basis similar to the one defined by Eq. (3.4b). To impose the outgoing-wave boundary condition (2.17) in such an L^2-integrable basis expansion approach, we rotate the ray $\eta \in [0, \infty)$ into the upper half of the complex plane by an angle $\sim \pi/3$ whose precise value for each state and field is found empirically. In this way the differential equations are turned into algebraic eigenvalue problems with five-diagonal symmetric matrices. The determinant of these matrices can be efficiently calculated by means of the recursive relations presented in Ref. [109]. For any given generally complex energy E, the eigenvalues of the equations in ξ and η can be found by the Newton-Raphson method [110]. The energy E is then adjusted to satisfy a relation for the eigenvalues [10]. The entire procedure can be relatively simply embedded in multiple-precision arithmetics [98] and works very fast. We thus could reproduce all significant digits in the available results for $\mathcal{E}$ and Γ obtained by other methods [100, 101, 102, 103, 104, 105, 106, 107, 108]. But the present procedure works also for very weak fields, when Γ attains extremely small values. The smallest F that can be treated is determined by the available computer memory. For example, with our computational resources we could obtain for the ground state $\Gamma = 0.694\,773\,113\,409\,051 \times 10^{-575}$ at $F = 5 \times 10^{-4}$, which is in full agreement with the WFAT(5) results [47].

Appendix D

IMPLEMENTATION OF PERTURBATION THEORY FOR σ AND $\pi^{\pm}$ STATES

To implement formulas of Chapter 5, we solve Eq. (2.1) for $F = 0$ by employing a single-center expansion in the molecular frame. A similar procedure is outlined in Ref. [49]. However, here we use the direct product of two discrete-variable representation (DVR) basis sets in r' and θ' constructed from the Laguerre and Gegenbauer polynomials [68], respectively. The use of the Laguerre-DVR basis in r' eliminates the issue of convergence with respect to the radius of a finite spherical box used in Ref. [49]. Instead, there appears a 'soft boundary' controlled by a scaling factor relating r' to the argument of the basis functions. A proper choice of this factor accelerates convergence. This basis is also more suitable for extracting the asymptotic coefficients from the wave functions at $\eta \to \infty$ needed to implement the WFAT. This procedure yields a complete set of eigenstates with energies $E_{n|M|}$ and wave functions (5.2). Then it is straightforward to calculate the matrix elements in Eqs. (5.6) for the different symmetries by replacing ψ_0 with the corresponding function of the form

(5.3). For all symmetries we have

$$\mu_{z'} = -\langle f_n^{|M|} | r' \cos\theta' | f_n^{|M|} \rangle. \tag{D.1}$$

For a σ state ψ_{n0}, the other quantities needed are given by

$$\alpha_{x'} = \sum_{n'} \frac{|\langle f_{n'}^1 | r' \sin\theta' | f_n^0 \rangle|^2}{E_{n'1} - E_{n0}}, \tag{D.2a}$$

$$\alpha_{z'} = 2 \sum_{n' \neq n} \frac{|\langle f_{n'}^0 | r' \cos\theta' | f_n^0 \rangle|^2}{E_{n'0} - E_{n0}}, \tag{D.2b}$$

$$\chi_{x'}(\mathbf{r}') = \sum_{n'} \frac{\langle f_{n'}^1 | r' \sin\theta' | f_n^0 \rangle}{E_{n0} - E_{n'1}} f_{n'}^1(r', \theta') \frac{\cos\varphi'}{\sqrt{2\pi}}, \tag{D.2c}$$

$$\chi_{z'}(\mathbf{r}') = \sum_{n' \neq n} \frac{\langle f_{n'}^0 | r' \cos\theta' | f_n^0 \rangle}{E_{n0} - E_{n'0}} f_{n'}^0(r', \theta') \frac{1}{\sqrt{2\pi}}. \tag{D.2d}$$

For an even π state ψ_{n1}^+, we find

$$\alpha_{x'} = \sum_{n'} \frac{|\langle f_{n'}^0 | r' \sin\theta' | f_n^1 \rangle|^2}{E_{n'0} - E_{n1}} + \frac{1}{2} \sum_{n'} \frac{|\langle f_{n'}^2 | r' \sin\theta' | f_n^1 \rangle|^2}{E_{n'2} - E_{n1}}, \tag{D.3a}$$

$$\alpha_{z'} = 2 \sum_{n' \neq n} \frac{|\langle f_{n'}^1 | r' \cos\theta' | f_n^1 \rangle|^2}{E_{n'1} - E_{n1}}, \tag{D.3b}$$

$$\begin{aligned} \chi_{x'}(\mathbf{r}') = &\sum_{n'} \frac{\langle f_{n'}^0 | r' \sin\theta' | f_n^1 \rangle}{E_{n1} - E_{n'0}} f_{n'}^0(r', \theta') \frac{1}{2\sqrt{\pi}} \\ &+ \sum_{n'} \frac{\langle f_{n'}^2 | r' \sin\theta' | f_n^1 \rangle}{E_{n1} - E_{n'2}} f_{n'}^2(r', \theta') \frac{\cos 2\varphi'}{2\sqrt{\pi}}, \end{aligned} \tag{D.3c}$$

$$\chi_{z'}(\mathbf{r}') = \sum_{n' \neq n} \frac{\langle f_{n'}^1 | r' \cos\theta' | f_n^1 \rangle}{E_{n1} - E_{n'1}} f_{n'}^1(r', \theta') \frac{\cos\varphi'}{\sqrt{\pi}}. \tag{D.3d}$$

Similarly, for an odd π state ψ_{n1}^-, we obtain

$$\alpha_{x'} = \frac{1}{2} \sum_{n'} \frac{|\langle f_{n'}^2 | r' \sin\theta' | f_n^1 \rangle|^2}{E_{n'2} - E_{n1}}, \tag{D.4a}$$

$$\alpha_{z'} = 2 \sum_{n' \neq n} \frac{|\langle f_{n'}^1 | r' \cos\theta' | f_n^1 \rangle|^2}{E_{n'1} - E_{n1}}, \tag{D.4b}$$

$$\chi_{x'}(\mathbf{r}') = \sum_{n'} \frac{\langle f^2_{n'}|r' \sin\theta'|f^1_n\rangle}{E_{n1} - E_{n'2}} f^2_{n'}(r', \theta') \frac{\sin 2\varphi'}{2\sqrt{\pi}}, \tag{D.4c}$$

$$\chi_{z'}(\mathbf{r}') = \sum_{n' \neq n} \frac{\langle f^1_{n'}|r' \cos\theta'|f^1_n\rangle}{E_{n1} - E_{n'1}} f^1_{n'}(r', \theta') \frac{\sin \varphi'}{\sqrt{\pi}}. \tag{D.4d}$$

The summations in these formulas run over all n', including the discretized continuum states with $E_{n'|M|} > 0$.

Bibliography

[1] P. B. Corkum, Phys. Rev. Lett. **71**, 1994 (1993).

[2] T. Morishita, A.-T. Le, Z. Chen, and C. D. Lin, Phys. Rev. Lett. **100**, 013903 (2008).

[3] G. G. Paulus, W. Becker, W. Nicklich, and H. Walther, J. Phys. B **27**, L703 (1994).

[4] F. Fabre,G. Petite,P. Agostini, and M. Clement, J. Phys. B: At. Mol. Phys. **15**, 1353 (1982)

[5] G. Petite,F. Fabre,P. Agostini,M. Crance, and M. Aymar, Phys. Rev. A. **29**, 2677 (1984)

[6] L. V. Keldysh, Zh. Eksp. Teor. Fiz. **47**, 1945 (1964) [Sov. Phys. JETP **20**, 1307 (1965)].

[7] O. I. Tolstikhin, T. Morishita, and S. Watanabe, Phys. Rev. A. **81**, 033415 (2010).

[8] O. I. Tolstikhin and T. Morishita, Phys. Rev. A. **86**, 043417 (2012).

[9] L. I. Schiff, *Quantum Mechanics* (McGraw-Hill, 1949).

[10] L. D. Landau and E. M. Lifshitz, *Quantum Mechanics (Non-relativistic Theory)* (Pergamon Press, Oxford, 1977).

[11] S. Yu. Slavyanov, Problemy Matematicheskoi Fiziki No. 4, 125 (1970). (English translation in: Topics in Mathematical Physics, Vol. 4, Consultants Bureau, New York – London, 1971).

[12] J. R. Oppenheimer, Phys. Rev. **31**, 66 (1928).

[13] C. Lanczos, Z. Phys. **62**, 518 (1930); **65**, 431 (1930); **68**, 204 (1931).

[14] Yu. N. Demkov and G. F. Drukarev, Zh. Eksp. Teor. Fiz. **47**, 918 (1964) [Sov. Phys.JETP **20**, 614 (1964)].

[15] B. M. Smirnov and M. I. Chibisov, Zh. Eksp. Teor. Fiz. **49**, 841 (1965) [Sov. Phys. JETP **22**, 585 (1966)].

[16] A. M. Perelomov, V. S. Popov, and M. V. Terent'ev, Zh. Eksp. Teor. Fiz. **50**, 1393 (1966) [Sov. Phys. JETP **23**, 924 (1966)]; Zh. Eksp. Teor. Fiz. **51**, 309 (1966) [Sov. Phys. JETP **24**, 207 (1967)].

[17] S. Yu. Slavyanov, Probl. Mat. Fiz. **4**, 125 (1970). English translation in Topics in Mathematical Physics, Vol. 4 (Consultants Bureau, New York, 1971)

[18] T. Yamabe, A. Tachibana, and H. J. Silverstone, Phys. Rev. A. **16**, 877 (1977).

[19] M.V. Ammosov, N.B. Delone, V.P. Krainov, Sov. Phys. JETP **64**, 1191 (1986).

[20] F. I. Dalidchik and V. Z. Slonim, Zh. Eksp. Teor. Fiz. **70**, 47 (1976) [Sov. Phys.JETP **43**, 25 (1976)].

[21] S. V. Borzunov, N. L. Manakov, A. F. Starace, and M. V. Frolov, Zh. Eksp. Teor. Fiz. **139**, 835 (2011) [Sov. Phys.JETP **112**, 725 (2011)].

[22] X. M. Tong, Z. X. Zhao, and C. D. Lin, Phys. Rev. A. **66**, 033402 (2002).

[23] O. I. Tolstikhin, T. Morishita, and L. B. Madsen, Phys. Rev. A. **84**, 053423 (2011).

[24] L. Holmegaard, J. L. Hansen, L. Kalhoj, S. L. Kragh, H. Stapelfeldt, F. Filsinger, J. Küpper, G. Meijer, D. Dimitrovski, M. Abu-samha, C. P. J. Martiny, and L. B. Madsen, Nature Physics **6**, 428 (2010).

[25] M. Abu-samha and L. B. Madsen, Phys. Rev. A. **82**, 043413 (2010).

[26] J. L. Hansen et al.,Phys. Rev. A. **83**, 023406 (2011).

[27] H. Ohmura, N. Saito, and T.Morishita, Phys. Rev. A. **83**, 063407 (2011).

[28] A. Etches, M. B. Gaarde, and L. B. Madsen, Phys. Rev. A. **84**, 023418 (2011).

[29] O. I. Tolstikhin, L. B. Madsen, and T. Morishita, Phys. Rev. A. **89**, 013421 (2014).

[30] O. I. Tolstikhin, H. J. Wörner, and T. Morishita, Phys. Rev. A. (2013), accepted.

[31] D. Dimitrovski, C. P. J. Martiny, and L. B. Madsen, Phys. Rev. A. **82**, 053404 (2010).

[32] H. Li, D. Ray, S. De, I. Znakovskaya, W. Cao, G. Laurent, Z. Wang, M. F. Kling, A. T. Le, and C. L. Cocke Phys. Rev. A. **84**, 043429 (2011).

[33] C. Wang, M. Okunishi, R. R. Lucchese, T. Morishita, O. I. Tolstikhin, L. B. Madsen, K. Shimada, D. Ding, and K. Ueda, J. Phys. B **45**, 131001 (2012).

[34] J. Maurer, D. Dimitrovski, L. Christensen, L. B. Madsen, and H. Stapelfeldt, Phys. Rev. Lett. **109**, 123001 (2012).

[35] M. Uiberacker, T. Uphues, M. Schultze, A. J. Verhoef, V. Yakovlev, M. F. Kling, J. Rauschenberger, N. M. Kabachnik, H. Schröder, M. Lezius, K. L. Kompa, H.-G. Muller, M. J. J. Vrakking, S. Hendel, U. Kleineberg, U. Heinzmann, M. Drescher, and F. Krausz, Nature (London) **446**, 627 (2007).

[36] A. N. Pfeiffer, C. Cirelli, M. Smolarski, D. Dimitrovski, M. Abu-samha, L. B. Madsen, and U. Keller, Nature Physics **8**, 76 (2012).

[37] J. L. Hansen, L. Holmegaard, J. H. Nielsen, H. Stapelfeldt, D. Dimitrovski, and L. B. Madsen, J. Phys. B **45**, 015101 (2012).

[38] B. Zhang, J. Yuan, and Z. Zhao, Phys. Rev. Lett. **111**, 163001 (2013).

[39] J. Itatani, J. Levesque, D. Zeidler, H. Niikura, H. Pepin, J. Kieffer, P. Corkum, and D. Villeneuve, Nature (London) **432**, 867 (2004).

[40] H. Niikura, H. J. Wörner, D. M. Villeneuve, and P. B. Corkum, Phys. Rev. Lett. **107**, 093004 (2011).

[41] Y. Okajima, O. I. Tolstikhin, and T. Morishita, Phys. Rev. A. **85**, 063406 (2012).

[42] D. Pavičić, K. F. Lee, D. M. Rayner, P. B. Corkum, and D. M. Villeneuve, Phys. Rev. Lett. **98**, 243001 (2007).

[43] I. Thomann, R. Lock, V. Sharma, E. Gagnon, S. T. Pratt, H. C. Kapteyn, M. M. Murnane, and W. Li, J. Phys. Chem. A **112**, 9382 (2008).

[44] H. Ohmura, N. Saito, and T. Morishita, Phys. Rev. A. **83**, 063407 (2011).

[45] J. Wu, L. P. H. Schmidt, M. Kunitski, M. Meckel, S. Voss, H. Sann, H. Kim, T. Jahnke, A. Czasch, and R. Dörner, Phys. Rev. Lett. **108**, 183001 (2012).

[46] R. J. Damburg and V. V. Kolosov, J. Phys. B **11**, 1921 (1978); *ibid.* **12**, 2637 (1979).

[47] H J. Silverstone, E. Harrell, and C. Grot, Phys. Rev. A. **24**, 1925 (1981).

[48] P. A. Batishchev, O. I. Tolstikhin, and T. Morishita, Phys. Rev. A. **82**, 023416 (2010).

[49] L. Hamonou, T. Morishita, and O. I. Tolstikhin, Phys. Rev. A. **86**, 013412 (2012).

[50] V. N. T. Pham, O. I. Tolstikhin, and T. Morishita, Phys. Rev. A. **89**, 033426 (2014).

[51] L. B. Madsen, O. I. Tolstikhin, and T. Morishita, Phys. Rev. A. **85**, 053404 (2012).

[52] L. B. Madsen, F. Jensen, O. I. Tolstikhin, and T. Morishita, Phys. Rev. A. **87**, 013406 (2013).

[53] V. H. Trinh, O. I. Tolstikhin, L. B. Madsen, and T. Morishita, Phys. Rev. A. **87**, 043426 (2013).

[54] V. H. Trinh, V. N. T. Pham, O. I. Tolstikhin, and T. Morishita, (submitted).

[55] V. H. Trinh, O. I. Tolstikhin, and T. Morishita, (in preparation).

[56] A. J. F. Siegert, Phys. Rev. **56**, 750 (1939).

[57] *Handbook of Mathematical Functions*, edited by M. Abramowitz and I. A. Stegun (Dover Publications Inc., New York, 1972).

[58] É. É. Shnol, Teor. Mat. Fiz. **8**, 140 (1971).

[59] F. W. J. Olver, *Asymptotics and Special Functions* (Academic Press, New York, 1974).

[60] M. V. Fedoryuk, *Asymptotic Analysis: Linear Ordinary Differential Equations* (Springer-Verlag, Berlin, 1993).

[61] R. S. Johnson, *Singular Perturbation Theory* (Springer Science + Business Media, Boston, 2005)

[62] A. I. Nikishov and V. I. Ritus, Zh. Eksp. Teor. Fiz. **50**, 255 (1966) [Sov. Phys. JETP **23**, 162 (1966)].

[63] N. B. Delone and V. P. Krainov, J. Opt. Soc. Am. B **8**, 1207 (1991).

[64] C. Bracher, W. Becker, S. A. Gurvitz, M. Kleber, and M. S. Marinov, Am. J. Phys. **66**, 38 (1998).

[65] H. J. Silverstone, Phys. Rev. A. **18**, 1858 (1978).

[66] A. E. S. Green, D. L. Sellin, and A. S. Zachor, Phys. Rev. **184**, 1 (1969).

[67] R. H. Garvey, C. H. Jackman, and A. E. S. Green, Phys. Rev. A. **12**, 1144 (1975).

[68] O. I. Tolstikhin and C. Namba, *CTBC — A Program to Solve the Collinear Three-Body Coulomb Problem: Bound States and Scattering Below the Three-Body Disintegration Threshold, Research Report NIFS-779* (National Institute for Fusion Science, Toki, Japan, 2003), available at: [`http://www.nifs.ac.jp/report/nifs779.html`].

[69] A. R. Edmonds, Angular Momentum in Quantum Mechanics (Princeton University Press, Princeton, 1957)

[70] D. A. Telnov, and S. I. Chu, Phys. Rev. A. **76**, 043421 (2007).

[71] G. L. Kamta, and A. D. Bandrauk, Phys. Rev. A. **74**, 033415 (2006).

[72] T. K. Kjeldsen, L. A. A. Nikolopoulos, and L. B. Madsen, Phys. Rev. A. **75**, 063427 (2007).

[73] B. Zhang, J. M. Yuan, and Z. X. Zhao, Phys. Rev. A. **85**, 033421 (2012).

[74] T. Zuo, and A. D. Bandrauk, Phys. Rev. A. **52**, R2511 (1995).

[75] T. Seideman, M. Y. Ivanov, and P. B. Corkum, Phys. Rev. Lett. **75**, 2819 (1995).

[76] I. Ben Itzhak, I. Gertner, O. Heber, and B. Rosner, Phys. Rev. Lett. **71**, 1347 (1993).

[77] X. B. Bian, and A. D Bandrauk, Phys. Rev. A. **83**, 023414 (2011).

[78] D Fisher, Y. Maron, and L. P. Pitaevskii, Phys. Rev. A. **58**, 2214 (1998).

[79] T Brabec, M. Côté, P. Boulanger, and L. Ramunno, Phys. Rev. Lett. **95**, 073001 (2005).

[80] R. Wildt, Astrophys. J. **89**, 295 (1939).

[81] R. Wildt, Astrophys. J. **93**, 47 (1941); A. Wheeler and R. Wildt, Astrophys. J. **95**, 281 (1942).

[82] H. C. Bryant, A. Mohagheghi, J. E. Stewart, J. B. Bonahue, C. R. Quick, R. A. Reeder, V. Yuan, C. R. Hummer, W. W. Smith, S. Cohen, W. P. Reinhardt, and L. Overman, Phy. Rev. Lett. **58**, 2412 (1987).

[83] S. Cohen, H. C. Bryant, C. J. Harvey, J. E. Stewart, K. B. Butterfield, D. A. Clark, J. B. Donahue, D. W. MacArthur, G. Comtet, W. W. Smith, Phys. Rev. A. **36**, 4728 (1987).

[84] S. I. Themelis, and C. A. Nicolaides, Phys. Rev. A. **49**, 3089 (1994).

[85] C. A. Nicolaides, and S. I. Themelis, Phys. Rev. A. **47**, 3122 (1993).

[86] A. Scrinzi, Phys. Rev. A. **61**, 041402(R) (2000).

[87] A. Scrinzi, M. Geissler, and T. Brabec, Phys. Rev. Lett. **83**, 706 (1999).

[88] S. I. Themelis, T. Mercouris, and C. A. Nicolaides, Phys. Rev. A. **61**, 024101 (1999).

[89] J. S. Parker, G. S. J. Armstrong, M. Boca, and K. T. Taylor, J. Phys. B **42**, 134011 (2009).

[90] J. Macek, J. Phys. B **1**, 831 (1968).

[91] O. I. Tolstikhin, S. Watanabe, and M. Matsuzawa, J. Phys. B **29**, L389 (1996).

[92] B. Zhou, C. D. Lin, J. Tang, S. Watanabe, and M. Matsuzawa, J. Phys. B: At. Mol. Opt Phys. **26** 2555-2573 (1993).

[93] T. Morishita, C. D. Lin, Phys. Rev. A. **57**, 4268 (1998).

[94] G. W. F. Drake, Nucl. Instr. Meth. B **31**, 7 (1988).

[95] R. M. Glover and F. Weinhold, J. Chem. Phys. **65**, 4913 (1976).

[96] C. H. Park, A. F. Starace, J. Tan, and C. D. Lin, Phys. Rev. A. **33**, 1000 (1986).

[97] M. Masili, J. J. De Groote, and J. E. Hornos, J. Phys. B: At. Mol. Opt. Phys. **33** 2641 (2000).

[98] D. M. Smith, Computing in Science and Engineering, **5**, 88 (2003).

[99] http://myweb.lmu.edu/dmsmith/FMLIB.html

[100] M. H. Alexander, Phys. Rev. **178**, 34 (1969).

[101] M. Hehenberger, H. V. McIntosh, and E. Brändas, Phys. Rev. A. **10**, 1494 (1974).

[102] N. A. Guschina and V. K. Nikulin, Chem. Phys. **10**, 23 (1975).

[103] R. J. Damburg and V. V. Kolosov, J. Phys. B **9**, 3149 (1976).

[104] H. J. Silverstone, B. G. Adams, J. Cizek, and P. Otto, Phys. Rev. Lett. **43**, 1498 (1979).

[105] L. Benassi and V. Grecchi, J. Phys. B **13**, 911 (1980).

[106] A. Maquet, S.-I Chu, and W. P. Reinhardt, Phys. Rev. A. **27**, 2946 (1983).

[107] V. Franceschini, V. Grecchi, and H. J. Silverstone, Phys. Rev. A. **32**, 1338 (1985).

[108] C. A. Nicolaides and S. I. Themelis, Phys. Rev. A. **45**, 349 (1992).

[109] I. Kátai and E. Rahmy, Ann. Univ. Sci. Budapest. Sect. Comput. **2**, 13 (1979).

[110] W. H. Press, S. A. Teukolsky, W. T. Vetterling, and B. P. Flannery, *Numerical Recipes in FORTRAN* (Cambridge University Press, Cambridge, 1992).